LUAN PERONI VENANCIO

REMOTE SENSING APPROACHES FOR EVAPOTRANSPIRATION AND YIELD ESTIMATIONS ON IRRIGATED CORN FIELDS

Thesis submitted to the Agricultural Engineering Graduate Program of the Universidade Federal de Viçosa in partial fulfillment of the requirements for the degree of *Doctor Scientiae*.

VIÇOSA
MINAS GERAIS – BRAZIL
2019

Ficha catalográfica preparada pela Biblioteca Central da Universidade Federal de Viçosa - Câmpus Viçosa

T
V448r
2019

Venancio, Luan Peroni, 1990-
Remote sensing approaches for evapotranspiration and yield estimations on irrigated corn fields / Luan Peroni Venancio. – Viçosa, MG, 2019.
xvi, 155 f. : il. (algumas color.) ; 29 cm.

Orientador: Everardo Chartuni Mantovani.
Tese (doutorado) - Universidade Federal de Viçosa.
Inclui bibliografia.

1. Vegetação - Mapeamento. 2. Milho - Rendimento. 3. Evapotranspiração. 4. Sensoriamento remoto. I. Universidade Federal de Viçosa. Departamento de Engenharia Agrícola. Programa de Pós-Graduação em Engenharia Agrícola. II. Título.

CDD 22. ed. 621.3678

LUAN PERONI VENANCIO

REMOTE SENSING APPROACHES FOR EVAPOTRANSPIRATION AND YIELD ESTIMATIONS ON IRRIGATED CORN FIELDS

Thesis submitted to the Agricultural Engineering Graduate Program of the Universidade Federal de Viçosa in partial fulfillment of the requirements for the degree of *Doctor Scientiae*.

APPROVED: February 25, 2019.

Fernando Coelho Eugenio

Thomé Simpliciano Almeida

Cibele Hummel do Amaral
(Co-advisor)

Christopher Michael Usher Neale
(Co-advisor)

Everardo Chartuni Mantovani
(President)

This thesis is dedicated to...

My great parents, Rosa Angela and Francisco,
My dear maternal grandparents, Assunta (*in memoriam*) and Paulo,
To my beloved sister, Luana,
To my best friend and love, Mariana,
To all professors, friends and family.

“*A fé na vitória tem que ser inabalável*”.

(Marcos Fernandes de Omena)

ACKNOWLEDGMENTS

First and foremost, I would like to thank God for giving me the health, knowledge, ability and opportunity to conduct this thesis.

I am extremely thankful to my parents, Rosa Angela and Francisco. They are the basis of everything, and I have only reached this moment because of their teachings, support and dedication to my professional and personal formation.

To my maternal grandparents, Assunta (*in memoriam*) and Paulo, examples of humility, respect and perseverance, especially my grandmother, who despite being illiterate always supported me to study, without ever measuring efforts.

To my lovely sister Luana, for always listening to me, supporting me in all my decisions.

To my beloved girlfriend, Mariana, the person who is always with me for everything, believing in me, giving me love, peace and confidence to win.

I would like to express my heartfelt gratitude towards my advisor, professor Everardo Chartuni Mantovani, who has always been a friendly mentor and has supported my study and research continuously with great patience and transparence.

I want to thank my co-advisors, Cibele Hummel do Amaral and Christopher Michael Usher Neale, who along with my advisor were my basis of knowledge for writing this thesis.

I would like to take this opportunity to thank the Universidade Federal de Viçosa (UFV), Departamento de Engenharia Agrícola (DEA) and the Programa de Pós-Graduação em Engenharia Agrícola (PPGEA) for the immensurable opportunity of study. They provided me with a unique and wonderful experience, with opportunities for career development, exploration, and discovery.

The completion of this thesis would not be possible without the financial support from National Council for Scientific and Technological Development (CNPq) and Coordination for Improvement of Higher Education Personnel (CAPES).

To Daugherty Water for Food Global Institute at the University of Nebraska for all the support during my doctoral internship. Special thanks to PhD Christopher Neale and PhD Ivo Zution Gonçalves, for all their attention and important teachings.

To all Daugherty Water for Food Global Institute staff, specially: Ivo Zution Gonçalves, Christopher Neale, Mesfin Mekonnen, John Burdette Barker, Babak Safa, Molly Nance, Peter McCornick, Amber Poythress, Jesse Starita, and Janet Means. Thanks for the help and for sharing with me good moments during my internship. I am so glad to have met all of you.

To all friends from my research group in Brazil, in particular: Catariny Cabral Aleman, Enoque Pereira da Silva, Francisco Cássio Gomes Alvino, Gláucio Luciano Araújo, Gustavo Henrique da Silva, Igor Silva Santos, Jannaylton Éverton Oliveira Santos, Lucas Borges Ferreira, Rafael Gomes Martins, Roberto Filgueiras, Robson Argolo, Rodrigo Dal Sasso Lourenço, Santos Henrique Brant Dias, and Vinicius Mendes Rodrigues de Oliveira.

To professor Fernando França da Cunha, for always giving me valuable ideas and to my great friend Roberto Filgueiras, a person that helped me a lot with the use of remote sensing software programs, essential for conducting this thesis.

To longtime friends André Thomazini, Paulo César da Silva Pereira Júnior, Vitor Zuim, Elder Felipe Silva Roncheti and Luciano Bertollo Rusciolelli for the friendship and partnership during those years. To the friends from the city of Alegre, who are the best.

To the company IRRIGER - Irrigation Management and Engineering and the Triflora farm for making available the field data used in this work.

Lastly, I would like to thank all my colleagues, friends, professors, and family members who directly or indirectly contributed to the accomplishment of this work.

Thank you everyone!

BIOGRAPHY

LUAN PERONI VENANCIO, son of Rosa Angela Peroni Venancio and Francisco de Paula Venancio, was born in Rio Bananal – ES, Brazil, on May 27, 1990.

In December of 2007 finished high school along with the course of agricultural technician at the former Escola Agrotécnica Federal de Colatina (EAFCOL), now called Instituto Federal do Espírito Santo (IFES), in Colatina – ES.

In March of 2008 started an undergraduate course in Agronomy at the Universidade Federal do Espírito Santo (UFES), located in the city of Alegre - ES, finishing it in January of 2013.

In March of 2013 started his master's degree studies in the Postgraduate Program in Plant Production at UFES, also in Alegre – ES, finishing it in February of 2015.

In March of 2015 started his doctorate in the Agricultural Engineering Graduate Program at Universidade Federal de Viçosa (UFV). From April to August 2017, he was a doctoral intern at Daugherty Water for Food Global Institute at the University of Nebraska (UNL), United States. The thesis has been submitted to defense in February of 2019, to obtain the Doctor Scientiae degree in Agricultural Engineering.

SUMMARY

LIST OF ABREVIATIONS AND SYMBOLS

AGB	Aboveground Dry Biomass
APAR	Absorbed Photosynthetically Active Radiation
Bio	Biomass production
Chl	Chlorophyll Content
CI_{green}	Green Chlorophyll Index
CLS	Constrained Least Squares
CSWS	Current Soil Water Storage
CVI	Chlorophyll Vegetation Index
DAS	Days After Sowing
DC	Duration of the Cycle
DN	Digital Numbers
DOS1	Dark-Object Subtraction
ET	Actual Crop Evapotranspiration
ETM+	Enhanced Thematic Mapper Plus
ET_{MFAO}	ET Estimated by the Modified FAO Method
ETo	Reference Evapotranspiration
ET_{SAFER}	ET Estimated by SAFER with Original Coefficients
EVI	Enhanced Vegetation Index
FAO	Food and Agriculture Organization of the United Nations
fPV	Fraction of Photosynthetically Active Vegetation
fS	Fraction of Soil
fSh	Fraction of Shade
GDD	Growing Degree Day
gNDVI	Green Normalized Difference Vegetative Index
GS	Growing Season
HD	Harvest Date
HI	Harvest Index
IE	Image Endmember
IFOV	Instantaneous Field of View
Irr	Applied Irrigation
Kc	Crop Coefficient

Kcb	Basal Crop Coefficient
Kcb_{adj}	Basal Crop Coefficient Adjusted
K_L	Localized Water Application Coefficient
Ks	Water Stress Coefficient
K_{ST}	Temperature Stress Coefficient
K_{SW}	Water Stress Coefficient
LAI	Leaf Area Index
LaSRC	Landsat Surface Reflectance Code
MAE	Mean Absolute Error
MBE	Mean Bias Error
METRIC	Mapping EvapoTranspiration at high Resolution with Internalized Calibration
MFAO	Modified FAO Method
MSE	Mean Square Error
MSI	MultiSpectral Instrument
MSWD	Maximum Soil Water Deficit
NAVI	Normalized Area Vegetation Index
NDVI	Normalized Difference Vegetative Index
NIR	Near Infrared
fNPV	Fraction of Non-photosynthetically Active Vegetation
NSE	Nash-Sutcliffe Efficiency
OLI	Operational Land Imager
OSAVI	Optimized Soil-Adjusted Vegetation Index
PCA	Principal Component Analysis
r^2	Coefficient of Determination
Ra	Extraterrestrial Radiation
RH	Relative Humidity
RMSE	Root Mean Square Error
ROI	Region of Interest
RRMSE	Relative Root Mean Square Error
RS	Remote Sensing
SAFER	Simple Algorithm for Evapotranspiration Retrieving
SAVI	Soil-Adjusted Vegetation Index

SD	Sowing Date
SEBAL	Surface Energy Balance Algorithms for Land
SMA	Spectral Mixture Analysis
SR	Simple Ratio
SRe	Surface Reflectance
S_{relT}	Relative Water Stress Level
SWIR	Shortwave Infrared
SWS	Total Soil Water Storage
T_0	Surface Temperature
T_1	Maximum or Lethal Temperature
T_b	Basal Temperature
T_B	Satellite Brightness Temperature
TIRS	Thermal Infrared Sensor
Tm	Daily Mean Air Temperature
T_o	Optimum Temperature
TOA	Top of Atmosphere Reflectance
$TONI_{pbp}$	Tool for Numerical Integration pixel by pixel
U_2	Wind Speed at 2 m Height
USGS	United States Geological Survey
UTM	Universal Transverse Mercator
VI	Vegetation Indices
VIPER	Tools Visualization and Image Processing for Environmental Research
VIS	Visible
WGS84	World Geodetic System 1984
WLS	Weighted Least Square
WP	Water Productivity
WP*	Normalized Water Productivity
WUE^*_B	Water Use Efficiency for Biomass Production
α_0	Surface Albedo

ABSTRACT

VENANCIO, Luan Peroni, D.Sc., Universidade Federal de Viçosa, February, 2019. **Remote sensing approaches for evapotranspiration and yield estimations on irrigated corn fields**. Advisor: Everardo Chartuni Mantovani. Co-advisors: Christopher Michael Usher Neale and Cibele Hummel do Amaral.

Remote sensing data and applications have been experiencing a revolutionary advancement in various areas in the last fifteen years, including agriculture. These advancements are boosted by a large amount of the satellite sensors in orbit obtaining a large number of images of the Earth's surface every day in different temporal, spatial, spectral and radiometric resolutions. This dynamism is very useful to agriculture, since it is also a very dynamic system. Besides that, faced with the global problems of water and food shortages, climate change, environmental pollution, among others, high-efficiency agriculture will be increasingly required, which can be achieved more easily by means of the remote sensing data and applications. This thesis is divided into three chapters, making use of different satellites (Landsat 7, Landsat 8, Sentinel 2A and Sentinel 2B) with focus on the corn crop plantations irrigated by center pivot system in the western region of Bahia state, Brazil. The general focus was the estimation of evapotranspiration and yield along with vegetation spectral indices and spectral mixture analysis in irrigated corn fields using remote sensing approaches. The first study (chapter one) aimed to evaluate, calibrate and validate the SAFER algorithm for evapotranspiration estimation in irrigated corn fields. Meteorological and crop data were used to calculate corn evapotranspiration by means of the modified FAO method. In order to use SAFER algorithm, images of the sensors ETM+ and OLI/TIRS were acquired. SAFER algorithm with original regression coefficients has low accuracy for corn ET estimation, and after calibration with empirical data it showed a good performance, being a very useful tool for estimating water consumption by corn crop. Chapter two focused on corn yield estimation at farm level in Brazil using a new and simplified remote sensing approach, initially validated for North American corn production conditions. The

formulation combines the methodology for biomass determination presented in the FAO-66 manual and a basal crop coefficient based on reflectance data adjusted by water and cold temperature stress. Data of 52 center pivots fields, collected during growing season of 2013 to 2016, were used. ETM+ and OLI surface reflectance images were used for the calculation of SAVI. The difference between predicted yield values and actual ones ranged between 12.2% and 18.8%, but with the majority of estimates between -10 and 10%, considering a single harvest index for all hybrids. After the reanalysis (grouping of similar hybrids and use of a specific HI) the performance of predictions increased, especially for Pioneer hybrids, with the majority of the differences, between predicted yield values and measured, remaining between -5 and 5%. Chapter three had as general objective to investigate the performance of vegetation indices for corn aboveground biomass estimation by means of their comparison with the fraction of photosynthetically active vegetation estimated from Spectral Mixture, defining the three best ones. Nine vegetation indices were calculated using the near infrared and visible bands of OLI sensor. Among the analyzed, VI, EVI, SAVI and OSAVI were considered the first, second and third best ones, respectively, for corn aboveground biomass estimation, based on their comparison with fraction of photosynthetically active vegetation. A second objective of this chapter was to find the best interval of VI accumulation (days) for corn grain yield estimation, using the three best classified in the general objective. For this purpose, field data of center pivots grown with irrigated corn during the season of 2018 were used along with Sentinel 2 images. The intervals that extended up to 120 days after sowing were the best. Finally, this work was a great challenge, mainly due to the use of data belonging to a commercial farm with a large number of cultivated corn hybrids. But, on the other hand, it brings very interesting results, showing the great potential of the remote sensing in agriculture. In turn, these results are useful for both the scientific community and farmers in Brazil, who are constantly being pressured by improvements in production processes, especially in water use.

RESUMO

VENANCIO, Luan Peroni, D.Sc., Universidade Federal de Viçosa, fevereiro de 2019. **Abordagens de sensoriamento remoto para estimativas de evapotranspiração e produtividade em plantios de milho irrigado**. Orientador: Everardo Chartuni Mantovani. Coorientadores: Christopher Michael Usher Neale e Cibele Hummel do Amaral.

Dados e aplicações de sensoriamento remoto têm tido um avanço revolucionário em várias áreas nos últimos quinze anos, incluindo na agricultura. Esses avanços são estimulados pela grande quantidade de satélites em órbita obtendo uma grande quantidade de imagens da superfície da Terra em diferentes resoluções temporais, espaciais, espectrais e radiométricas. Todo esse dinamismo é muito útil para a agricultura, já que esta é também um sistema muito dinâmico. Além disso, diante dos problemas globais de escassez de água e alimentos, mudanças climáticas, poluição ambiental, entre outros, será demandada a cada vez mais uma agricultura de alta eficiência, a qual pode ser mais facilmente alcançada através de dados e abordagens de sensoriamento remoto. Essa tese está dividia em três capítulos, fazendo o uso de diferentes satélites (Landsat 7, Landsat 8, Sentinel 2A e Sentinel 2B) com foco em plantações de milho irrigadas por pivô central na região Oeste do estado da Bahia, Brasil. O foco geral foi a estimativa de evapotranspiração e produtividade juntamente com índices espectrais de vegetação e análise de mistura espectral em campos de milho irrigado utilizando abordagens de sensoriamento remoto. O primeiro estudo (capítulo um) objetivou avaliar, calibrar e validar o algoritmo SAFER para a estimativa de evapotranspiração em campos de milho irrigado. Foram utilizados dados meteorológicos e da cultura para calcular a evapotranspiração do milho utilizando o método FAO modificado. Para a utilização do algoritmo SAFER, foram obtidas imagens dos sensores ETM+ e OLI/TIRS. O algoritmo SAFER com os coeficientes originais de regressão tem baixa acurácia para estimar ET de milho e, após a calibração com dados empíricos, este algoritmo demonstrou bom desempenho, sendo uma ferramenta

muito útil para estimar o uso consumo de água pela cultura milho. O capítulo dois focou em estimar a produtividade do milho ao nível de fazenda no Brasil usando uma nova e simplificada abordagem de sensoriamento remoto, inicialmente validada para condições Norte Americanas de produção de milho. A formulação combina a metodologia para determinação de biomassa apresentada no manual 66 da FAO e um coeficiente basal da cultura baseado nos dados de reflectância ajustados pelos estresses hídrico e de baixa temperatura. Foram utilizados dados de 52 campos de pivôs centrais, coletados durante as safras de 2013 a 2016. Imagens de reflectância dos sensores ETM+ e OLI foram usadas para calcular o SAVI. A diferença entre os valores de produtividade preditos e reais variou entre -12,2% e 18,8%, mas com a maioria das estimativas entre -10 e 10%, considerando somente um índice de colheita para todos os híbridos. Depois da reanálise, considerando o grupamento de híbridos semelhantes e utilização de um índice específico de colheita, o desempenho das predições aumentou, especialmente para o híbrido Pioneer, com a maioria das diferenças, entre os valores de produtividade previstos e medidos, permanecendo entre -5 e 5%. O capítulo três teve como objetivo geral investigar o desempenho de índices de vegetação para estimativa de biomassa seca acima do solo do milho, comparando-os com a fração da vegetação fotossintética derivada da Análise de Mistura Espectral, definindo os três melhores. Foram calculados nove índices de vegetação, utilizando as bandas do vermelho próximo e visível do sensor OLI. Dentro os índices analisados, o EVI, SAVI e OSAVI foram considerados o primeiro, segundo e terceiro melhores, respectivamente, para a estimativa de biomassa seca acima, baseado em sua comparação com a fração de vegetação fotossintética. Um segundo objetivo desse capítulo foi encontrar o melhor intervalo de acúmulo de índice de vegetação (dias) para a estimativa da produtividade de grãos de milho, usando os três melhores classificados no objetivo geral. Para este propósito, foram utilizados dados de campo de pivôs centrais cultivados com milho irrigado durante a safra de 2018, juntamente com imagens do sensor MSI. Os intervalos que se estenderam até 120 dias após a semeadura foram os melhores. Por fim, este trabalho foi um grande desafio, principalmente pelo uso de dados pertencente a uma fazenda comercial com um grande número de híbridos de milho cultivados. Mas por outro lado, ela traz

resultados muito interessantes, mostrando o grande potencial do sensoriamento remoto na agricultura. Por sua vez, esses resultados são úteis tanto para a comunidade científica quanto para os agricultores do Brasil, que são constantemente pressionados por melhorias nos processos de produção, principalmente no uso da água.

GENERAL INTRODUCTION

Remote sensing (RS) involves the measurement or acquisition of information of some property of an object or phenomenon, by a recording device that is not in physical or intimate contact with the object or phenomenon under study (Cowell, 1983). The advancement in satellite sensor technology in terms of spatial, temporal, spectral and radiometric resolutions leads, successfully, to more specific and intensified research on agriculture (Mondal et al., 2014). Besides these advantages, there are actually more than a thousand active satellites orbiting the Earth and quite a number of the satellites are for remote sensing applications (Huang et al., 2018). These advancement in satellite technology along with the number of instruments available will continue to be an indispensable way to help understand and solve the problems which have been affecting the planet in recent decades, such as water and food shortages, population growth and climate changes, mainly.

In respect to agricultural environment, RS data are widely used and necessary, because the main variables related to this production sector (e.g. climate, soil, rainfall) are highly variable in space or time, or both. Moreover, a very important factor in agriculture, such as the yield, can change within short time periods, due to unfavorable growing conditions. Thus, agricultural monitoring need to be frequent. Therefore, RS data can significantly contribute to providing a timely and accurate picture of the agricultural sector, as it is very suitable for gathering information over large areas with high revisit frequency (Atzberger, 2013). According to Khanal et al. (2017), RS is the most cost-effective method for large-scale monitoring and analyses in agriculture.

Assessing the spatial-temporal distribution of actual crop evapotranspiration (ET) of agricultural crops is essential for an optimal water use in irrigated agriculture, and it can be estimated from remote sensing-based models. Currently there are several models and algorithms for this purpose, some widely known such as Surface Energy Balance Algorithm – SEBAL (Bastiaanssen et al., 1998a, 1998b) and Mapping EvapoTranspiration at high Resolution with Internalized Calibration – METRIC (Allen et al., 2007b, 2007a). On the other hand, there are those which are little known and whose performance

needs to be assessed, such as the Simple Algorithm For Evapotranspiration Retrieving – SAFER (Teixeira 2010, 2012), which will be tested in the present study. This algorithm uses the Normalized Difference Vegetation Index (NDVI), (Rouse et al., 1973) surface albedo and land surface temperature derived from RS along with reference evapotranspiration to assess the ET of crops, being developed and validated for Brazilian semi-arid conditions involving irrigated crops and natural vegetation.

Like ET, grain yield estimation prior to harvest is very important to help in the decision-making inside the farm, mainly regarding harvest scheduling, storage, and sales of production, and also for the decision-making in a broader context, involving national food policy (Li et al., 2014; Mokhtari et al., 2018). RS coupled with crop growth models have been shown to be a promising alternative for crop yield estimation, as observed in some works with corn (Li et al., 2014), soybean (Gusso et al., 2017), and wheat (Li et al., 2015). A recent example of this combination (i.e. crop growth models and RS data) can be found in the work of Campos et al. (2018). These authors proposed the assessment of aboveground dry biomass (AGB) and yield production from the incorporation of the reflectance-based basal crop coefficient (Kcb) (Campos et al., 2017; Neale et al., 1989) into the AQUACROP crop growth and yield partitioning model (Steduto et al., 2009) popularized by the FAO-66 manual (Steduto et al., 2012).

The Kcb is estimated from soil-adjustment vegetation index (SAVI) (Huete, 1988). The potential AGB is estimated as the product of the summation of Kcb over season times the parameter of water use efficiency for biomass production (WUE*B). For real AGB production, Kcb needs to be multiplied by a water stress coefficient and cold temperature stress coefficient (Campos et al., 2018). Lastly, for grain yield estimation, the use of harvest index is necessary.

Most remote sensing applications in agriculture involve the use of vegetation indices (VI), which can be defined as optical measures of vegetation canopy “greenness”, a composite property of leaf chlorophyll, leaf area, canopy cover, and canopy architecture (Jiang et al., 2008). A range of VI formulations have been developed to estimate biophysical parameters of vegetation. The group of the most well-known VI includes simple ratio - SR (Jordan, 1969), normalized difference vegetation index – NDVI (Rouse et al., 1973), soil-adjusted

vegetation index - SAVI (Huete, 1988), green NDVI - gNDVI (Gitelson et al., 1996), enhanced vegetation index - EVI (Huete et al., 2002), etc.

Each spectral VI has its own merits and limitations (Ji and Peters, 2007), and also a biophysical meaning (i.e., what is its applicability?), that is, which make it more or less related to certain biophysical parameter of vegetation. Considering as biophysical parameter the AGB, several vegetation indices can be used to assess it, for example, those used for estimation of absorbed photosynthetically active radiation (APAR), leaf area index (LAI) and chlorophyll content (Chl). These VIs can be used because they are closely related to AGB. For example, if a plant has higher chlorophyll content, it also has a greater photosynthetic capacity and consequently a higher APAR, culminating in a higher production of biomass.

Thus, several VIs can be listed for the estimation of APAR, LAI and Chl, and consequently AGB, so each one needs to be evaluated to identify the best for such purpose. The fraction of photosynthetically active vegetation (fPV), derived from Spectral Mixture Analysis - SMA (Adams et al., 1986), is a great option. Since the fPV is the class of vegetation of a plant responsible for photosynthesis, mainly by means of the leaf area (Li and Guo, 2015), thus, VIs well-related to it are also strongly related to AGB. Besides that, the fPV, when compared to VI, is subject to less variations in factors, such as scene lighting conditions and atmospheric variations (Shimabukuro et al., 1998).

The corn crop (*Zea mays* L.) as well as the western region of Bahia state were the focus of this study. Brazil currently occupies the third position in the global corn production ranking, behind United States and China, first and second, respectively (USDA, 2018). In Brazil, corn is the second largest crop produced after soybean (CONAB, 2019). In the western region of Bahia, corn is considered the third most important crop and occupied 7% of the area of the main crops in the 2016/17 harvest, which resulted in a cultivated area of 180,000 ha and a production of 1,404,000 tons (AIBA, 2017).

The adoption of RS data in agriculture is increasingly necessary, especially with the scenarios presented by the Food and Agriculture Organization of the United Nations (FAO). This institution cites that the world's population is expected to grow to almost 10 billion by 2050, boosting agricultural demand, in a

scenario of modest economic growth, by some 50 percent compared to 2013 (FAO, 2017). To face this boosting agricultural demand high-efficiency agriculture will be necessary, especially in the use of water, because, at global level, the water withdrawal in agriculture correspond to around 69 percent (FAO, 2016).

Given the potential of RS data in agriculture and the need for agriculture to become more efficient, studies focusing on the connection between these two parts are very useful, which motivated the accomplishment of three chapters in the present thesis. The first study involved the aspect of water in agriculture and aimed to evaluate, calibrate and validate the SAFER algorithm to estimate corn crop evapotranspiration. In the second study, the focus was on corn grain yield estimation using RS data along with the crop growth model available in AQUACROP. As the second study, the last one focused on biomass and yield estimation, and its aim was defined as investigation of the performance of nine vegetation indices for AGB estimation in irrigated corn fields by means of their comparison with the fraction of photosynthetically active vegetation estimated from Spectral Mixture. All three studies were performed in corn fields irrigated by center pivot systems, in the western region of Bahia state, Brazil.

REFERENCES

Adams, J.B., Smith, M.O., Johnson, P.E., 1986. Spectral mixture modeling: A new analysis of rock and soil types at the Viking Lander 1 Site. Journal of Geophysical Research 91, 8098–8112.

AIBA - Associação de Agricultores e Irrigantes da Bahia, 2017. anuário da região oeste da Bahia: safra 2016/2017. Barreiras: Bahia, Brazil.

Allen, R.G., Tasumi, M., Morse, A., Trezza, R., Wright, J.L., Bastiaanssen, W., Kramber, W., Lorite, I.J., Robison, C. w., Tasumi, M., Trezza, R., 2007a. Satellite-based energy balance for Mapping Evapotranspiration with Internalized Calibration (METRIC) – Applications. Journal of Irrigation and Drainage Engineering 133, 395–406.

Allen, R.G., Tasumi, M., Trezza, R., 2007b. Satellite-based energy balance for mapping evapotranspiration with internalized calibration (METRIC) – Model. Journal of irrigation and drainage engineering 133, 380–394.

Atzberger, C., 2013. Advances in remote sensing of agriculture: Context description, existing operational monitoring systems and major information needs. Remote Sensing 5, 949–981.

Bastiaanssen, W.G.M., Menenti, M., Feddes, R.A., Holtslag, A.A.M., 1998a. A remote sensing surface energy balance algorithm for land (SEBAL): 1. Formulation. Journal of Hydrology 212–213, 198–212.

Bastiaanssen, W.G.M., Pelgrum, H., Wang, J., Ma, Y., Moreno, J.F., Roerink, G.J., Van Der Wal, T., 1998b. A remote sensing surface energy balance algorithm for land (SEBAL): 2. Validation. Journal of Hydrology 212–213, 213–229.

Campos, I., Neale, C.M.U., Arkebauer, T.J., Suyker, A.E., Gonçalves, I.Z., 2018. Water productivity and crop yield: A simplified remote sensing driven operational approach. Agricultural and Forest Meteorology 249, 501–511.

Campos, I., Neale, C.M.U., Suyker, A.E., Arkebauer, T.J., Gonçalves, I.Z., 2017. Reflectance-based crop coefficients REDUX: For operational evapotranspiration estimates in the age of high producing hybrid varieties. Agricultural Water Management 187, 140–153.

CONAB - Companhia Nacional de Abastecimento, 2019. Acompanhamento da safra brasileira de grãos: v.6 - safra 2018/19 - n. 4 - Quarto levantamento, janeiro 2019. http://www.conab.gov.br (accessed 1.20.19).

FAO - Food and Agriculture Organization of the United Nations, 2017. The future of food and agriculture, trends and challenges, channels. https://doi.org/10.1155/2010/178034 (accessed 1.22.19).

FAO - Food and Agriculture Organization of the United Nations , 2016. Water uses: Thematic discussion. http://www.fao.org/nr/water/aquastat/water_use/index.stm (accessed 1.22.19).

Gitelson, A.A., Kaufman, Y.J., Merzlyak, M.N., 1996. Use of a green channel in remote sensing of global vegetation from EOS- MODIS. Remote Sensing of Environment 58, 289–298.

Gusso, A., Arvor, D., Ducati, J.R., 2017. Model for soybean production forecast based on prevailing physical conditions. Pesquisa Agropecuária Brasileira 52, 95–103.

Huang, Y., Chen, Z. xin, Yu, T., Huang, X. zhi, Gu, X. fa, 2018. Agricultural remote sensing big data: Management and applications. Journal of Integrative Agriculture 17, 1915–1931.

Huete, A., Didan, K., Miura, T., Rodriguez, E.P., Gao, X., Ferreira, L.G., 2002. Overview of the radiometric and biophysical performance of the MODIS vegetation indices. Remote Sensing of Environment 83, 195–213.

Huete, A.R., 1988. A soil-adjusted vegetation index (SAVI). Remote Sensing of Environment 25, 295–309.

Ji, L., Peters, A.J., 2007. Performance evaluation of spectral vegetation indices using a statistical sensitivity function. Remote Sensing of Environment 106, 59–65.

Jiang, Z., Huete, A.R., Didan, K., Miura, T., 2008. Development of a two-band enhanced vegetation index without a blue band. Remote Sensing of Environment 112, 3833–3845.

Jordan, C.F., 1969. Derivation of Leaf-Area Index from Quality of Light on the Forest Floor. Ecology 50, 663–666.

Khanal, S., Fulton, J., Shearer, S., 2017. An overview of current and potential applications of thermal remote sensing in precision agriculture. Computers and Electronics in Agriculture 139, 22–32.

Li, Y., Zhou, Q., Zhou, J., Zhang, G., Chen, C., Wang, J., 2014. Assimilating remote sensing information into a coupled hydrology-crop growth model to estimate regional maize yield in arid regions. Ecological Modelling 291, 15–27.

Li, Z., Guo, X., 2015. Remote sensing of terrestrial non-photosynthetic vegetation using hyperspectral, multispectral, SAR, and LiDAR data. Progress in Physical Geography 40, 276–304.

Li, Z., Jin, X., Zhao, C., Wang, J., Xu, X., Yang, G., Li, C., Shen, J., 2015.

Estimating wheat yield and quality by coupling the DSSAT-CERES model and proximal remote sensing. European Journal of Agronomy 71, 53–62.

Mokhtari, A., Noory, H., Vazifedoust, M., 2018. Improving crop yield estimation by assimilating LAI and inputting satellite-based surface incoming solar radiation into SWAP model. Agricultural and Forest Meteorology 250–251, 159–170.

Mondal, S., Jeganathan, C., Sinha, N.K., Rajan, H., Roy, T., Kumar, P., 2014. Extracting seasonal cropping patterns using multi-temporal vegetation indices from IRS LISS-III data in Muzaffarpur District of Bihar, India. The Egyptian Journal of Remote Sensing and Space SciencesEgyptian Journal of Remote Sensing and Space Science 17, 123–134.

Neale, C.M.U., Bausch, W.C., Heerman, D.F., 1989. Development of reflectance-based crop coefficients for corn. Transactions of the ASAE 32, 1891–1899.

Rouse, J.W., Hass, R.H., Schell, J.A., Deering, D.W., 1973. Monitoring vegetation systems in the great plains with ERTS, in: Third ERTS Symposium. NASA, Washington, DC, pp. 309-317.

Shimabukuro, Y.E., Novo, E.M., Ponzoni, F.J., 1998. Índice de vegetação e modelo linear de mistura espectral no monitoramento da região do pantanal. Pesquisa Agropecuaria Brasileira 33, 1729–1737.

Steduto, P., Hsiao, T.C., Fereres, E., Raes, D., 2012. Crop yield response to water, FAO Irrigation and Drainage Paper 66. FAO, Rome.

Steduto, P., Raes, D., Hsiao, T.C., Fereres, E., Heng, L.K., Howell, T.A., Evett, S.R., Rojas-Lara, B.A., Farahani, H.J., Izzi, G., Oweist, T.Y., Wani, S.P., Hoogeveen, J., Geerts, S., 2009. Concepts and Applications of AquaCrop: The FAO Crop Water Productivity Model, in: Cao, W., White, J.W., Wang, E. (Eds.), Crop Modeling and Decision Support. Springer, Berlin, Germany, pp. 175–191.

Teixeira, A.H.C., 2012. Modelling evapotranspiration by remote sensing parameters and agro-meteorological stations, in: Neale, C.M.U., Cosh, M.H. (Eds.), Remote Sensing and Hydrology 2010 Symposium. International Association of Hydrological Sciences, Jackson Hole, Wyoming, pp. 154–157.

Teixeira, A.H.C., 2010. Determining regional actual evapotranspiration of irrigated crops and natural vegetation in the São Francisco river basin (Brazil) using remote sensing and Penman-Monteith equation. Remote Sensing 2, 1287–1319.

USDA - United States Department of Agriculture, 2018. Grain: World markets and trade, p. 12-44. https://apps.fas.usda.gov/psdonline/circulars/grain.pdf (accessed 1.22.19).

CHAPTER 1

Evapotranspiration estimation using SAFER algorithm in irrigated corn fields in western Bahia state, Brazil: assessment, calibration and validation

ABSTRACT

Crop evapotranspiration is an important element of the water cycle, and its estimation is essential for the analysis of irrigation management efficiency and planning of water resources. The Simple Algorithm for Evapotranspiration Retrieving (SAFER) is an algorithm relatively new to crop evapotranspiration estimates and, since its development, has been constantly applied at different spatial scales and for different crops. However, its application in irrigated corn areas is scarce and needs to be further investigated. Thus, the aim of this study was to evaluate, calibrate and validate the SAFER algorithm to estimate evapotranspiration in corn irrigated by center pivot systems, in the western region of Bahia state, Brazil. For this purpose, meteorological and crop data were acquired to calculate actual crop evapotranspiration (ET) of corn by means of the modified FAO method in commercial fields in the western region of Bahia state, Brazil. In order to use the SAFER algorithm, Landsat 7 and 8 surface reflectance images were acquired. The SAFER algorithm with original parameters was tested during the growing seasons of 2014, 2015 and 2016, involving 42 plots (center pivots). In order to make the SAFER algorithm more accurate for corn ET estimation, it was calibrated (2014 and 2015 data) and validated (2016 data). SAFER estimation performance was assessed using the following statistical parameters: RMSE, MBE, MAE, NSE and r^2. SAFER algorithm with original regression coefficients has low accuracy for corn ET estimation. Conversely, the results show good agreement between ET/ETo estimated by calibrated SAFER and ET/ETo estimated by the modified FAO method (r^2 and NSE = 0.75). The SAFER algorithm showed good performance (r^2 = 0.86) after validation using ET

data of 2016, with lowest RMSE (0.58 mm d^{-1}), MBE (0.18 mm d^{-1}) and MAE (0.47mm d^{-1}) values, for the set of 14 center pivots cultivated in this growing season. Results from the study support the applicability of the calibrated SAFER algorithm in irrigated corn fields in western Bahia state, Brazil, as a tool for estimating consumptive water use via remotely sensed methods.
Keywords: *Zea mays* L., remote sensing, irrigation, evapotranspiration models.

1. INTRODUCTION

Evapotranspiration is one of the most important parameters of the hydrological cycle, affecting water availability on the Earth's surface (Olivera-Guerra et al., 2017). On average, it accounts for 60-90% of rainfall water returning back to the atmosphere (Rawat et al., 2017). Regarding crops, knowing the evapotranspiration has long been a critical requirement for a range of applications, such as irrigation management (Gheysari et al., 2017; Li et al., 2008; Singh et al., 2016), hydrological studies (Dias et al., 2015; Gonzalez-Ollauri and Mickovski, 2017) and climate change scenarios (Croitoru et al., 2013; Li et al., 2017). At field level, information on ET can be a powerful tool to farmers and other users, helping them in the decision-making and promoting better water use.

Although ET is a process of fundamental importance in many applications, it cannot be directly measured, so it has to be estimated by monitoring the exchange of energy/water above the vegetated surface (micrometeorological methods), or as a residual term of the hydrological balance (lysimeters, soil water budget). The techniques to be adopted are often complex, costly and require specific equipment, thus they are generally applied only in scientific research (Gharsallah et al., 2013). Considering that satellites usually acquire images of the Earth's surface unceasingly at different spatial and temporal resolutions (Huang et al., 2018), ET models based on remote sensing data appear as an important tool for ET estimation. Because they will allow obtaining ET estimates for larger and more heterogeneous areas (Sun et al., 2011; Teixeira et al., 2013), knowing about spatial-temporal distribution of evapotranspiration (Cao et al., 2018;

Christou et al., 2017; Liaqat et al., 2015; Zhang et al., 2017) and, in addition, the operating costs are relatively lower compared to the other methods.

In the last decades, several methods to estimate ET using remote sensing data have been developed, validated and applied in different vegetation and climate types, such as Surface Energy Balance Algorithm for Land (SEBAL) (Bastiaanssen et al., 1998b, 1998a) and Mapping ET at High Resolution with Internalized Calibration (METRIC) (Allen et al., 2007a, 2007b). These applications in different edaphoclimatic scenarios are very important for consolidating the methods, identifying their limitations, and proposing improvements. In this context, the Simple Algorithm for Evapotranspiration Retrieving (SAFER) (Teixeira 2010, 2012), still needs to be further investigated, in order to become a consolidated algorithm, since it is a relatively recent algorithm with few studies validating it.

SAFER was developed and validated for Brazilian semi-arid conditions involving irrigated crops and natural vegetation under different meteorological and hydrological conditions, based on simultaneous field data from four flux towers and Landsat images (Teixeira, 2010). The algorithm is based on the modeling of ET/ETo ratio at the satellite overpass time, calculated using the following remote sensing data: Normalized Difference Vegetation Index (NDVI) (Rouse et al., 1973), surface albedo (α_0) and surface temperature (T_0). This ratio in conjunction with reference evapotranspiration data (ETo) estimated through meteorological station, allows the ET estimation (Teixeira, 2010; Teixeira et al., 2013, 2012). These authors cite that the simplicity of application is the main advantage of the algorithm, because: (i) it does not require either crop classification or extreme conditions identification; (ii) it does not require energy balance, like most methods do (e.g., SEBAL, METRIC and T-SEB) and, (iii) it can be applied with meteorological data from different types of stations, that is, agrometeorological, conventional and automatic stations.

Corn (*Zea mays* L.) is grown throughout the world, with the United States, China, and Brazil being the top three corn-producing countries on the planet (Ranum et al., 2014). This cereal represents the largest global crop in production with 1,036.07 million metric tons produced in the 2017/18 harvest (Statista, 2018). This study was conducted in Western Bahia state, Brazil, a region which stands

out from the others for being the largest producer of soybeans, cotton and corn in the state. Corn is considered as the third most important crop of the western region of Bahia and, in 2015/16, it occupied 31% of the planted area in the state, but was responsible for 77% of the total harvested area (AIBA (Association of Farmers and Irrigators of Bahia), 2016). Another highlight for the region is its concentration of central pivots. In 1985 there were only 9 central pivots in the region and in 2016 there were more than 1,550 (ANA (Agência Nacional de Águas), 2017), responsible for the irrigation of 120 thousand hectares, which correspond to 62% of total irrigated area of the Bahia state (AIBA, 2016).

The general objective of this research was to assess the performance of the SAFER algorithm to estimate the ET of corn irrigated by center pivot systems in the western region of Bahia state, Brazil, using Landsat 7 and 8 satellite images. The specific objective was to calibrate and validate the original regression coefficients of the algorithm for application in irrigated corn fields.

2. MATERIAL AND METHODS

2.1. Study area

The study area belongs to a commercial farm, located at the municipality of São Desidério, in the western region of Bahia state, Brazil (Figure 1a). The area is located in the rectangle bounded by the coordinate pairs: lower left 12°28'08"S; 45°45'12"W and upper right 12°25'40"S; 45°34'55"W, reference system of geographic coordinates, Datum SIRGAS 2000, with an average altitude of 750 m above the sea level (Figure 1b). According to Köppen's climatic classification (Alvares et al., 2013), the climate of the region is Aw, tropical climate, with rainy season in the summer and dry winter, with an annual normal precipitation in the region of 1003.4 mm (INMET (Instituto Nacional de Meteorologia), 2018), concentrated in the rainy season (October to April). The predominant soil type in the region of the fields is Yellow Latosol (Santos et al., 2011). The farm has 17 center pivots, 16 of them towable, indicated by the letters A and B in Figure 1b, occupying an area of 1598 hectares. Due to phytosanitary

issues, the same center pivot is not cultivated in two consecutive seasons with the same crop.

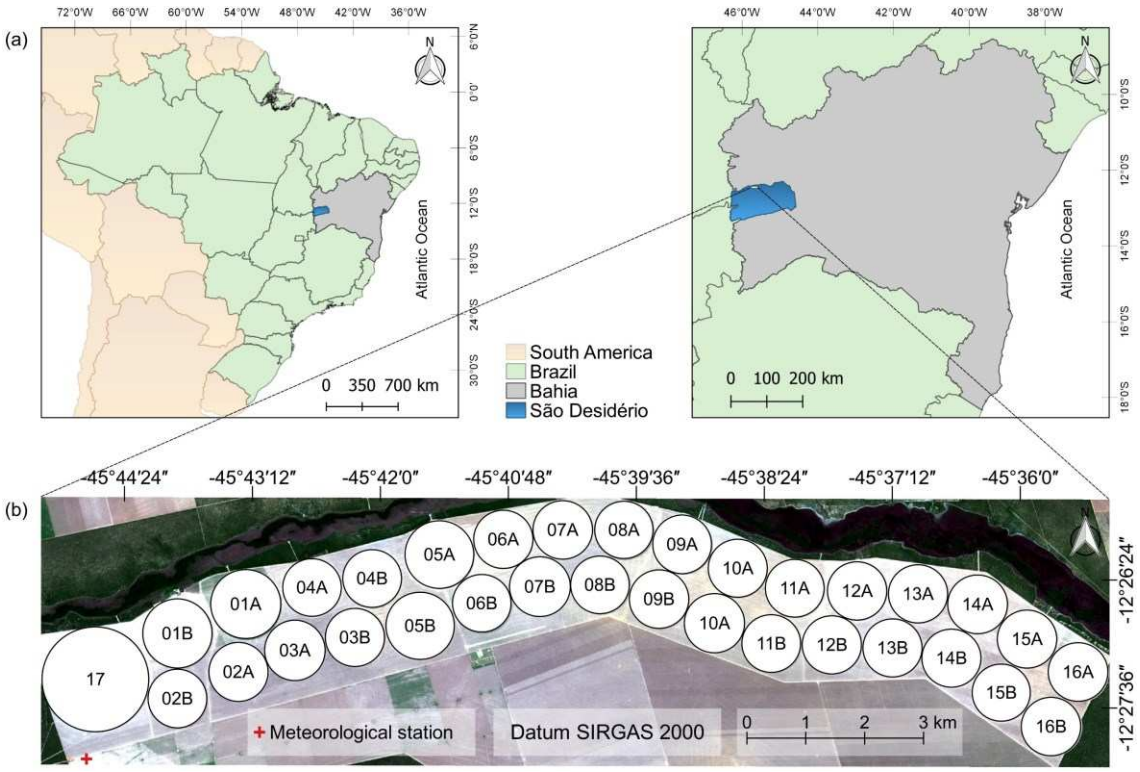

Figure 1. Location of study area (a), nomenclature and distribution of the center pivots in the fields (b), and meteorological station position (in red).

2.2. Meteorological, crop and irrigation management data

Field data used in this work refer to the corn crop (*Zea mays* L.) and were collected during the growing seasons of 2014, 2015 and 2016 by the company IRRIGER - Irrigation management and engineering (http://www.irriger.com.br/en-US/). The IRRIGER company was founded in 2005 and is a market leader in Brazil in its area of expertise. Since its foundation, it has already monitored more than 690 farms, which corresponds to more than 2.5 million hectares. Currently, this company monitors more than 4,123 center pivots and lateral move machines, and the center pivots are the great majority. One important point about the company refers to the field data. Since the foundation, it provides its field data for

universities and research institutions to carry out several studies on irrigation, mainly involving the crops of corn, bean, soybean, arabica coffee, cotton, sugarcane, wheat and potato (IRRIGER (Irrigation management and engineering), 2018).

Meteorological data such as air temperature (Tm, °C), wind speed at 2 m height (U_2, m s^{-1}), radiation (Ra, MJ m^2 dia^{-1}), relative humidity (RH, %) and rainfall (P, mm), were obtained from the automated meteorological station (Davis, Vantage Pro Plus, Hayward - CA), located near the center pivots (Figure 1b). The meteorological station provided meteorological data throughout the years on hourly basis, which were used to estimate the daily reference evapotranspiration (ETo) using the Penman-Monteith equation (Allen et al., 1998).Regarding the crop, the acquired data were the sowing and harvest dates, duration of the cycle, hybrid planted, and center pivot cultivated (Table 1). In relation to irrigation management, the following data were acquired: reference evapotranspiration (ETo), corn ET, applied irrigation (Irr) and rainfall.

Table 1. Sowing date (SD), harvest date (HD), duration of the cycle (DC) and cultivated hybrid name for each center pivot (CP) analyzed in the growing seasons of 2014, 2015, and 2016

CP	SD	HD	DC, days	Hybrid	CP	SD	HD	DC, days	Hybrid	CP	SD	HD	DC, days	Hybrid
2014					2015					2016				
01B	04/23	09/05	140	H8	01A	05/20	10/17	150	H1	03B	05/06	09/25	142	H2
02B	04/29	09/05	137	H9	04A	05/21	10/17	149	H7	04B	05/05	10/04	152	H9
03B	04/27	09/05	147	H9	05A	04/25	09/16	144	H9	05B	05/04	10/04	153	H9
04B	04/25	09/05	143	H9	06B	05/28	10/19	144	H9	06A	05/02	09/18	139	H6
05B	04/26	09/05	145	H3	07B	05/27	10/18	144	H9	07A	04/29	09/14	138	H6
06A	05/10	09/16	145	H3	08B	05/26	10/17	144	H9	08A	04/27	09/09	135	H7
07A	05/10	09/16	144	H3	09B	05/25	10/16	144	H9	09A	04/25	09/25	153	H3
08A	05/09	09/16	143	H3	10B	05/24	10/15	144	H9	10A	04/22	09/25	156	H3
09A	05/08	09/16	141	H7	11B	05/23	10/14	144	H9	11A	04/20	09/08	141	H10
10A	05/05	09/16	142	H7	12A	05/09	10/04	148	H9	12B	04/04	08/31	149	H9
11A	05/03	09/16	139	H7	13A	05/13	10/05	145	H9	13B	04/06	08/31	147	H9
12A	05/01	09/16	134	H6	14A	05/14	10/08	147	H9	14B	04/12	09/05	146	H9
-	-	-	-	-	15A	05/15	10/08	146	H9	15B	04/14	09/25	144	H9
-	-	-	-	-	16A	05/16	10/08	145	H9	16B	04/18	09/24	159	H9

*The row spacing adopted at the farm is 0.5 m. *Hybrids names:* Dekalb DKB 390 Pro (H1), Dow AgroSciences 2B810 (H2), Pioneer 30F35 (H3), Pioneer 30F53 (H4), Pioneer 3431 (H5), Pioneer P2830 (H6), Pioneer P3646 (H7), Maximus Viptera 3 (H8), Status Viptera 3 (H9) and Supremo Viptera (H10).

2.3. Satellite Images - Landsat 8 OLI/TIRS and Landsat 7 ETM+ data

The present study used images of the Landsat 7 and 8 satellites, which allowed a good temporal resolution (8 days). The combined use of Landsat 7 and 8 data is common (Barker et al., 2018; Qin et al., 2015) and correct, since previous studies have demonstrated that Enhanced Thematic Mapper Plus (ETM+) and Operational Land Imager (OLI) imagery can be used as complementary data (Li et al., 2013). Besides that, pre-tests showed that differences in performance were small between different sensor inputs. Images of ETM+ sensor onboard the Landsat 7 and images of OLI and Thermal Infrared Sensor (TIRS) sensors onboard the Landsat 8 satellite (patch 220 and row 69) were downloaded from the United States Geological Survey (USGS) EarthExplore (https://earthexplorer.usgs.gov/). For both satellites, the surface reflectance (SRe, top of atmosphere reflectance (TOA) corrected for atmospheric effect) products, generated by the USGS on-demand processing system EROS Science Processing Architecture (ESPA) (https://espa.cr.usgs.gov/), were used.

For the ETM+ sensor, the multispectral bands 1 to 5 with spatial resolution of 30 m and thermal band 6 with a spatial resolution of 60 m, resampled at 30 m, were used. The surface reflectance images of Landsat 7 were obtained by applying the Landsat Ecosystem Disturbance Adaptive Processing System (LEDAPS) algorithm (Masek et al., 2006; Schmidt et al., 2013). LEDAPS operates from the Level 1 terrain corrected (L1T) TOA products, which include radiometric correction, systematic geometric correction, precision correction using ground control chips, and the use of a digital elevation model to correct parallax error due to local topographic relief (Claverie et al., 2015). The products are delivered in 8-bit unsigned integer format and the output coordinate system assigned is the UTM with WGS84 (USGS (United States Geological Survey), 2018a).

Regarding Landsat 8, for the OLI sensor, the multispectral bands 2 to 7 with spatial resolution of 30 m were used and, for TIRS sensor, the thermal band 10 with a spatial resolution of 100 m, resampled at 30 m, was used. Landsat 8 Surface Reflectance data are generated from the Landsat Surface Reflectance Code (LaSRC). LaSRC makes use of the coastal aerosol band to perform aerosol inversion tests, uses auxiliary climate data from Moderate-Resolution Imaging

Spectroradiometer (MODIS) and uses a radiative transfer model. Details about LaSRC and Landsat 8 Surface Reflectance data products can be found in the Landsat 8 Surface Reflectance Product Guide (USGS (United States Geological Survey), 2018b). The images of Landsat 8 satellite are originally distributed as Level 1 terrain corrected (L1T) products, which means that images have systematic radiometric and geometric accuracy, orthorectification with a digital elevation model (DEM) and precision correction assisted by ground control chips. The products are delivered in 16-bit unsigned integer format and the output coordinate system assigned is the Universal Transverse Mercator (UTM) with World Geodetic System 1984 (WGS84) datum (Peña and Brenning, 2015; Roy et al., 2014; USGS (United States Geological Survey), 2016).

We acquired 46 cloud-free images including the OLI/TIRS sensors and ETM+ sensor for the crop seasons of 2014, 2015 and 2016 (Figure 2). The number of images used for corn ET estimation varied by center pivot and by year, according to different sowing and harvest dates. It is important to point out that the area where the center pivots are located are not affected by the gaps problem of Landsat 7, which results in about 22% of the pixels per scene not being scanned (Chen et al., 2011), except the center pivots 01A, 01B and 02B in some periods of the growing season. However, gaps when present in these three center pivots were converted to no data values in order not to influence the statistical analysis.

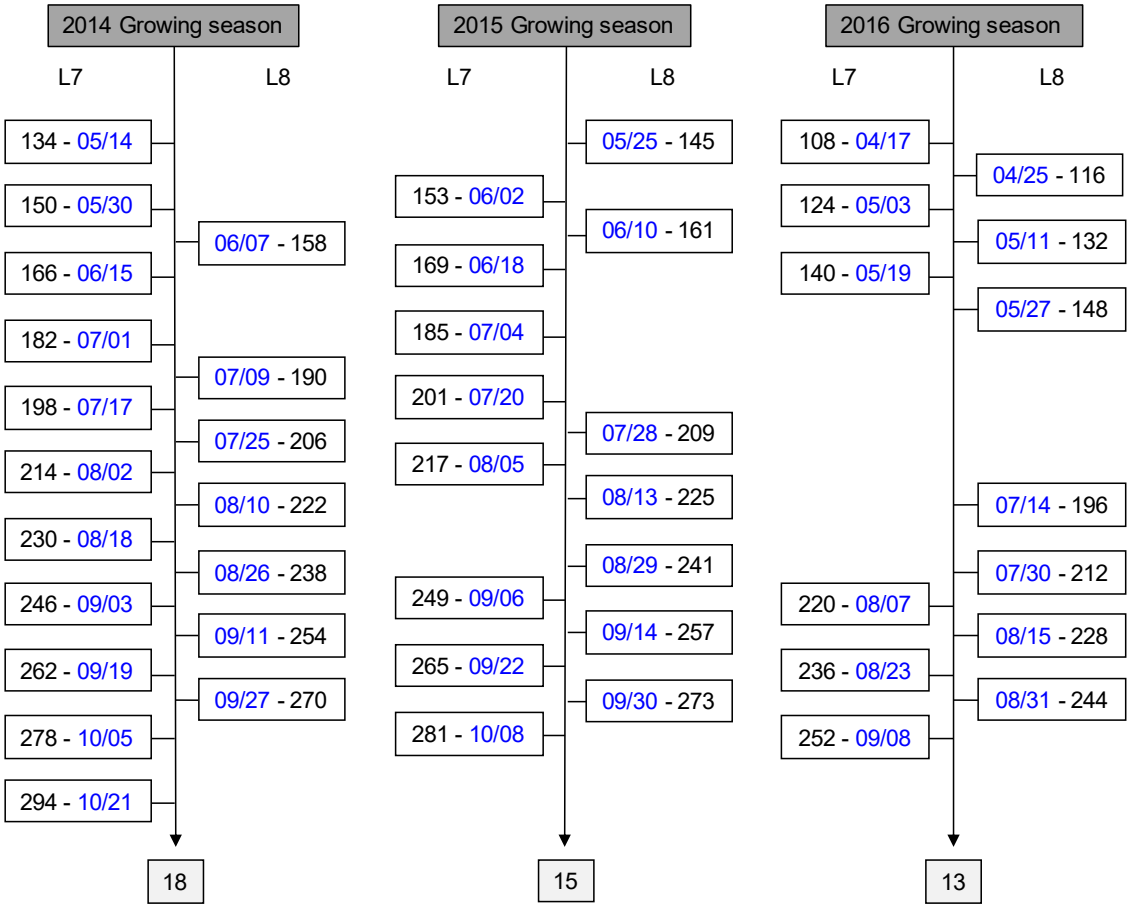

Figure 2. Day of year (black) with respective date (blue) of Landsat 7 (L7) and Landsat 8 (L8) images, with the respective number of total images.

2.4. Actual crop evapotranspiration (ET) estimation

2.4.1. Modified FAO method

Corn ET is estimated by means of the method called modified FAO method (MFAO) (Mantovani and Costa, 1998). The methodology of these authors is based on method proposed by Doorenbos and Pruitt (1977). Doorenbos and Pruitt's method is simple and widely used in the potential evapotranspiration estimation and for practical irrigation water management. To increase the performance of Doorenbos and Pruitt (1977) method without so much complexity, as in the FAO-56 dual Kc approach (Allen et al., 1998), Mantovani and Costa

(1998) added the water stress coefficient (K_S) and localized water application coefficient (K_L) (Equation 1).

$$ET = ETo \times K_c \times K_S \times K_L \qquad (1)$$

where ET is the actual crop evapotranspiration (mm d^{-1}), ETo is the reference evapotranspiration according to Allen et al. (1998) (mm d^{-1}), Kc is the crop coefficient, K_S is the water stress coefficient (Bernardo, 1989) and K_L is the localized water application coefficient (Keller and Bliesner, 1990); for center pivots, K_L value is 1 (100% of cultivated area receives irrigation water).

MFAO has been applied and validated by many researchers in Brazil with different crops and irrigation systems (Figueiredo et al., 2006; Mantovani et al., 2013; Medeiros et al., 2003; Souza et al., 2005a; Vieira et al., 2014). In terms of practical application, this method is used for crop ET estimation in irrigated plantations in Brazil, Paraguay, Argentina, Chile, Bolivia, Peru, Nicaragua, Venezuela, Mexico, United States, Nigeria, Sudan, Turkey, Ukraine, Russia and Laos (IRRIGER (Irrigation management and engineering), 2018). Another point is that to check the efficiency of this method in crop ET estimation, the IRRIGER company periodically collects soil samples during the irrigation management period for soil moisture determination and then compares the values to estimated soil moisture based on MFAO method. If large differences are found, modifications are made (e.g., change in Kc value) to adjust the ET estimates (*Everardo Chartuni Mantovani, Personal Communication*).

The crop coefficient varies according to growth stage and is also affected by the growth stage length. The Kc values used by the IRRIGER company for corn ET determination are the ones recommend by the FAO-56 approach (Allen et al., 1998) and are presented in Figure 3. These values have been adjusted by the company over the years in order to obtain the best performance of irrigation scheduling and, normally, the recommended values are 0.5, 1.2 and 0.6 for initial, mid-season and late-season stages (Allen et al., 1998).

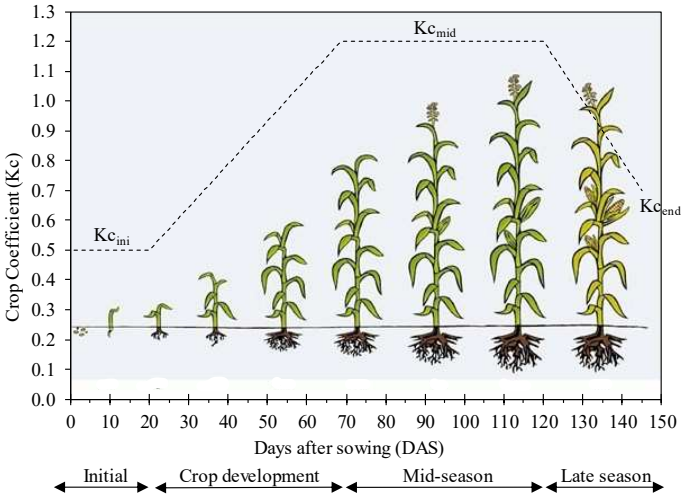

Figure 3. Crop coefficient curve for corn with the respective values used in ET estimation.

Source: Adapted by the author from Allen et al. (1998) and Conceito Agrícola (2017).

The K_S used in the MFAO method (Equation 1) is less complex than described in the FAO-56 dual Kc approach (Allen et al., 1998) and has been widely used in several scientific studies (Freitas et al., 2017; Santos et al., 2018; G. H. Silva et al., 2018; Vicente et al., 2017), and in several irrigated farms in Brazil by the IRRIGER company, which is a market leader in the field of irrigation engineering and management in Brazil. K_s calculation is performed according to Equation 2.

$$K_S = \frac{\ln (1 + CSWS)}{\ln (1 + SWS)} \qquad (2)$$

where SWS is the total soil water storage (mm), and CSWS is the current soil water storage (mm) at a given time.

Irrigation management is based on ET (water output) and on the maximum soil water deficit (MSWD), which represents the maximum amount of moisture that can be removed from the soil before irrigation is required. From the relationship between these two variables it is possible to define the irrigation

interval and the irrigation depth to be applied. The data presented in Table 2 were used in the calculation of K_S and MSWD.

Table 2. Values and units for the parameters used in K_S and MSWD determination

Parameter	Center pivot numbers						
	1	2	3	4	5	6	7 to 16
FC, $cm^3\ cm^{-3}$	0.133	0.125	0.137	0.131	0.146	0.149	0.129
PWP, $cm^3\ cm^{-3}$	0.070	0.070	0.070	0.070	0.070	0.070	0.680
BD, $g\ cm^{-3}$	1.50	1.50	1.50	1.50	1.50	1.55	1.55
AC*, %	35, 50, 40 and 50						
Z*, m	0.1, 0.25, 0.3 and 0.3						

Field capacity (FC), permanent wilting point (PWP), bulk density (BD), availability coefficient (AC) and effective rooting depth (Z); * values relative to the initial, crop development, mid-season and late-season stages, respectively.

2.4.2. Simple Algorithm for Evapotranspiration Retrieving (SAFER)

The SAFER algorithm allows the estimation of ET without requiring energy balance, as occurs in most methods (e.g., SEBAL). Besides that, it does not require either crop classification or extreme conditions identification in the images. SAFER combines remote sensing data, namely, Normalized Difference Vegetation Index (NDVI) (Rouse et al., 1973), surface albedo (α_0), and surface temperature (T_0), with the ETo (Allen et al. 1998) calculated using data from weather station (automatic or conventional). A summary of ET calculation using SAFER can be seen in Figure 4, and the steps for SAFER application are described in sequence, according to Teixeira (2012, 2010).

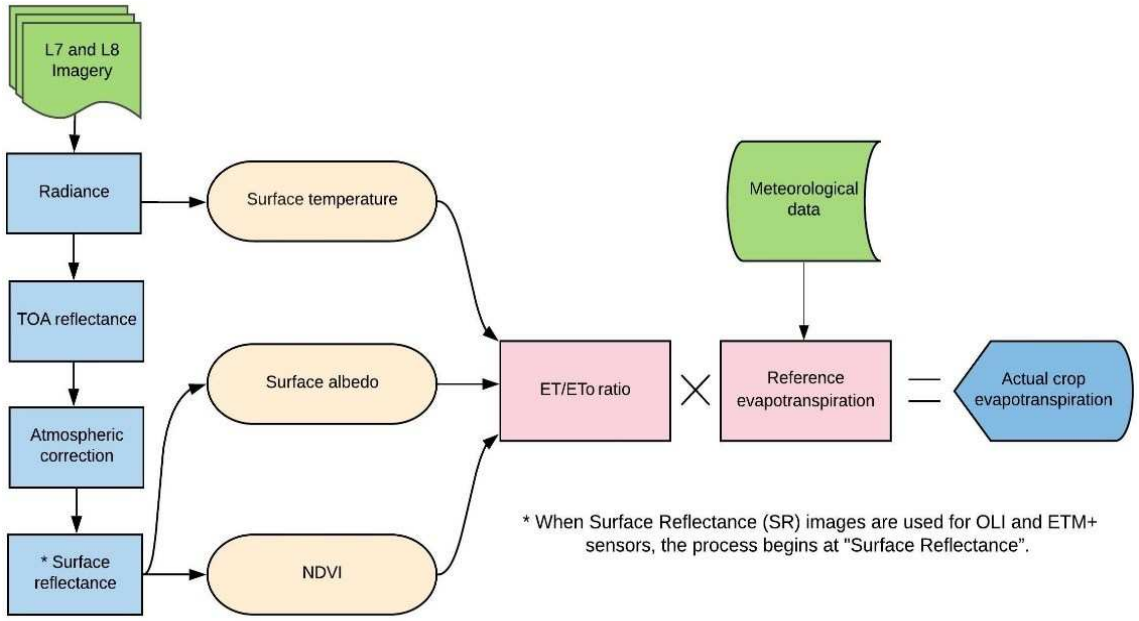

Figure 4. Flowchart with step-by-step calculation of actual crop evapotranspiration (ET) using SAFER algorithm.
Source: Adapted by the author from Teixeira (2010).

2.4.2.1. Radiometric calibration

The present work used surface reflectance images for both sensors (ETM+ and OLI), so the radiometric calibration was applied to band 6 and 10 of ETM+ and TIRS sensors, respectively. The digital numbers (DN) of this band (6 and 10) were converted to radiance on top of atmosphere (TOA) using the radiance rescaling factors provided in the metadata file. Equation 3 was used for Landsat 7, while Equation 4 was used for Landsat 8 (USGS (United States Geological Survey), 2016).

$$L_\lambda = \left(\frac{L_{max\lambda} - L_{min\lambda}}{Q_{calmax} - Q_{calmin}}\right) \times \left(Q_{calmax} - Q_{calmin}\right) + L_{min\lambda} \qquad (3)$$

$$L_\lambda = M_L \times Q_{cal} + A_L \qquad (4)$$

where L_λ is the T_{OA} spectral radiance (W m^{-2} sr^{-1} μm^{-1}); Q_{cal} the quantized and calibrated standard product pixel values (DN); Q_{calmin} the minimum quantized calibrated pixel value corresponding to $L_{min\lambda}$ (DN); Q_{calmax} the maximum quantized calibrated pixel value corresponding to $L_{max\lambda}$ (DN); $L_{min\lambda}$ the spectral at-sensor radiance that is scaled to Q_{calmin} (W m^{-2} sr^{-1} μm^{-1}); $L_{max\lambda}$ the spectral at-sensor radiance that is scaled to Q_{calmax} (W m^{-2} sr^{-1} μm^{-1}); ML the band-specific multiplicative rescaling factor from the metadata; A_L the band-specific additive rescaling factor from the metadata.

Subsequently, the bands 6 and 10 were converted from spectral radiance to brightness temperature using Planck's function. Brightness temperature is calculated by applying the inverse of the Planck's function to the estimated radiation. Equation 5 was used to obtain brightness temperature (USGS (United States Geological Survey), 2016; Wukelic et al., 1989).

$$T_B = \frac{K_2}{\ln\left(\frac{K_1}{L_\lambda} + 1\right)} \qquad (5)$$

where T_B is the satellite brightness temperature (K); L_λ is the T_{OA} is spectral radiance (W m^{-2} sr^{-1} μm^{-1}) for the thermal bands (6 and 10); and K_1 and K_2 are the band-specific thermal conversion constants from the metadata (specific for each sensor).

2.4.2.2. SAFER input parameters: Surface albedo (α_0), normalized difference vegetation index (NDVI) and surface temperature (T_0)

Surface albedo, surface temperature and the NDVI are the only input parameters for estimating the instantaneous values of the ET/ETo ratio (Equation 10). The instantaneous values of this ratio are multiplied by the daily value of ETo to estimate the ET value daily (Equation 1). Regarding α_0 calculation, firstly the top-of-atmosphere (TOA) albedo data were obtained by means of Equation 6.

$$\alpha_{TOA} = \sum(\omega_p \times \rho_\lambda) \qquad (6)$$

where ω_ρ is the weight coefficients for each band and ρ_λ is the surface reflectance of bands 1, 2, 3, 4, 5 and 7 (ETM+) and of bands 2, 3, 4, 5, 6 and 7 (OLI). The weight coefficients for ETM+ (Allen et al., 2002a) and OLI (Silva et al., 2016) sensors are presented in Table 3.

Table 3. Albedo weight coefficients for each band of ETM+ and OLI sensors

Sensor	B1	B2	B3	B4	B5	B6	B7
ETM+	0.293	0.274	0.231	0.156	0.034	-	0.012
OLI	-	0.300	0.277	0.233	0.143	0.036	0.012

The data of α_{TOA} were transformed to surface albedo data using Equation 7 (Teixeira, 2010).

$$\alpha_0 = 0.7 \times \alpha_{TOA} + 0.06 \quad (7)$$

Surface temperature of bands 6 and 10 was obtained according to Equation 8 (Teixeira, 2010).

$$T_0 = 1.11 \times T_b - 31.89 \qquad (8)$$

where T_0 is the surface temperature (K) and T_B is satellite brightness temperature (K). Then, the temperature was converted from Kelvin to Celsius.

The last remote sensing input of SAFER, the NDVI, was obtained by Equation 9 (Rouse et al., 1973).

$$NDVI = \frac{\rho_{NIR} - \rho_{red}}{\rho_{NIR} + \rho_{red}} \qquad (9)$$

where ρ_{NIR} and ρ_{red} are the reflectance of near-infrared band and red band, respectively.

2.4.2.3. Actual crop evapotranspiration (ET)

After SAFER input parameters were calculated, the relationship between ET and ETo, denominated ET/ETo ratio, was calculated according to Equation 10 (Teixeira, 2010; Teixeira et al., 2013, 2012). ET/ETo ratio values are related to crop development and to soil moisture conditions (Teixeira, 2010) and conceptually correspond to the crop coefficient (Kc) multiplied by water stress coefficient (K_S).

$$\frac{ET}{ET_o} = \exp\left[a + b\left(\frac{T_0}{\alpha_0 \times NDVI}\right)\right] \qquad (10)$$

where “a” and “b” are regression coefficients, which for the Brazilian semi-arid conditions are 1.9 and −0.008, respectively (Teixeira, 2010) or also 1.8 and -0.008 according to Teixeira et al. (2013b). In this work, the coefficients 1.8 and -0.008 were tested.

From the ET/ETo ratio and ETo (Allen et al., 1998), ET was estimated by Equation 11.

$$ET = \left(\frac{ET}{ET_o}\right) \times ETo \qquad (11)$$

where ET is the actual crop evapotranspiration in mm d^{-1}.

2.5. SAFER calibration and validation

Firstly, the SAFER algorithm with the regression coefficients recommended by Teixeira et al. (2013b), a = 1.8 and b = -0.008, was tested during the growing seasons of 2014, 2015 and 2016, involving 42 center pivots,

covering an area of 3,357 hectares. The obtained results were very poor, especially during the first 30 days after sowing (see Results and Discussion section), mainly because of the low values of ET/ETo ratio. Thus, we chose to calibrate and validate the algorithm regression coefficients (a and b), using data of 2014 and 2015 for the first and 2016 for the second procedure. The calibration based on adjustment of the empirical parameters described in Equation 10 (parameters a and b) was performed using the Solver tool from Microsoft Excel, which employs the nonlinear optimization algorithm generalized reduced gradient (GRG) (Lasdon et al., 1978).

The adjustment of empirical parameters of the ET/ETo ratio was performed using data from the modified FAO method as a standard, specifically, Kc x K_S values. According to Teixeira (2010), the ET/ETo ratio values are related to crop development and to soil moisture conditions, as occurs for the values of Kc x K_S. In other words, it is possible to affirm that ET/ETo ratio corresponds (conceptually and numerically) to the crop coefficient (Kc) multiplied by water stress coefficient (K_S), which we will call ET/ETo_{MFAO}.

In the calibration process the original values of the equation parameters, proposed by Teixeira et al. (2013b), were used as initial values for the adjusting process. Thus, through an iterative process, the Solver tool changes the parameters values aiming to reduce the distance between the ET/ETo ratio calculated by SAFER (Equation 10) and ET/ETo_{MFAO}. This distance was measured by the Mean Square Error (MSE) (Equation 12). So, this process aims to find the values of the parameters which lead to the minimum possible MSE.

$$MSE = \frac{\sum_{i=1}^{n} (S_i - O_i)^2}{n} \qquad (12)$$

where O_i is the ET/ETo_{MFAO} value, S_i is ET/ETo_{SAFER}, and n is the total number of data pairs.

In order to facilitate the visualization of the effect of calibrations, scatter plots were elaborated before and after the calibrations.

This study may not be a robust validation study because it does not use field data measured using a lysimeter or eddy covariance system, for example. However, data from the company IRRIGER are of high quality, since this company has used the modified FAO method for more than 13 years (since 2005) and has already made several adjustments to it in order to obtain optimal estimates of ET.

2.6. Statistical analysis

In order to assess the accuracy of the SAFER algorithm in corn ET modelling, the statistical indicators Root Mean Square Error (RMSE), Mean Bias Error (MBE), Mean Absolute Error (MAE), Nash-Sutcliffe efficiency (NSE) (Nash and Sutcliffe, 1970) and Coefficient of Determination (r^2) were calculated according to Equations 13, 14, 15, 16 and 17.

$$RMSE = \sqrt{\frac{\sum_{i=1}^{n}(S_i - O_i)^2}{n}} \qquad (13)$$

$$MBE = \frac{\sum_{i=1}^{n}(S_i - O_i)}{n} \qquad (14)$$

$$MAE = \frac{\sum_{i=1}^{n}(|S_i - O_i|)}{n} \qquad (15)$$

$$NSE = 1 - \frac{\sum(O_i - S_i)^2}{\sum(|O_i - \bar{O}|)^2} \qquad (16)$$

$$r^2 = \left(\frac{\sum_{i=1}^{n}(|O_i - \bar{O}|)(|S_i - \bar{S}|)}{\sqrt{\sum_{i=1}^{n}(O_i - \bar{O})^2 \sum_{i=1}^{n}(S_i - \bar{S})^2}} \right)^2 \qquad (17)$$

where O_i is the observed value, S_i is the estimated value, $\overline{O}$ is the observed mean, $\overline{S}$ is the estimated mean, n is the total number of observations and i is the current observation. NSE ranges from -∞ to 1: (i) NSE ≤ 0 indicates that the mean observed value is a better predictor than the forecasting model; (ii) 0.1 ≤ NSE ≤ 0.4 is classified as useful; (iii) 0.5 ≤ NSE ≤ 0.8 is classified as good, and (iv) NSE ≥ 0.9 is classified as excellent (Richter et al., 2011).

3. RESULTS AND DISCUSSION

3.1. Meteorological conditions

Figure 5 shows the average monthly climatic conditions of daily mean air temperature (Tm), extraterrestrial radiation (Ra), relative humidity (RH), wind speed at 2 m height (U_2), reference evapotranspiration (ETo) and rainfall (P). Air temperatures were very similar in the three growing seasons, approaching the historical average for the region (INMET (Instituto Nacional de Meteorologia), 2018). The coldest days occur in the middle of the growing season, which is not particularly favorable to corn, a C4 plant, with distinct growth advantages particularly under stress conditions, such as high light intensity, high temperature and drought (Singh et al., 2018).

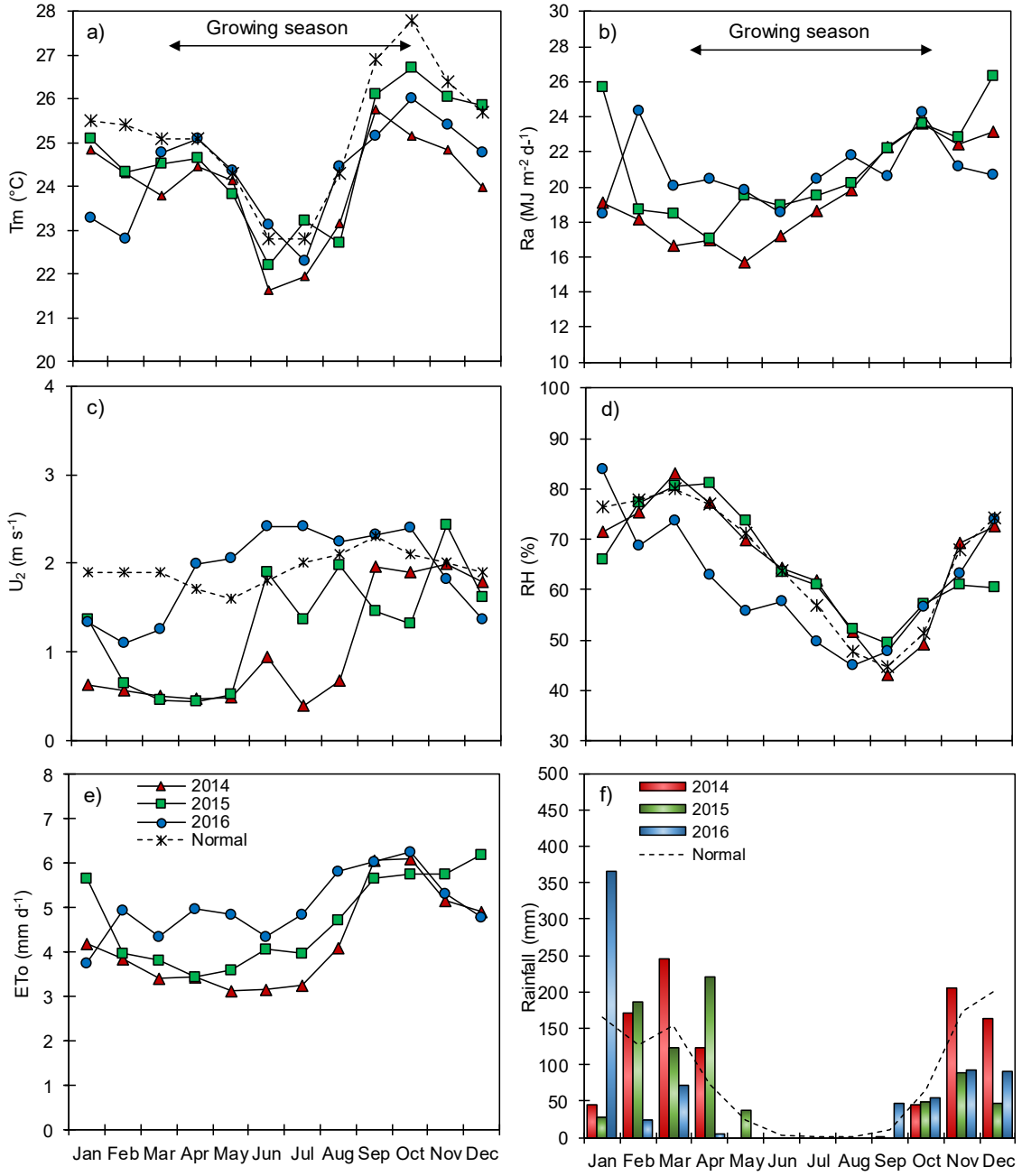

Figure 5. Comparison of monthly climatic conditions between growing seasons of 2014, 2015 and 2016 using averages for: daily mean air temperature air temperature (a); extraterrestrial radiation (b); wind speed at 2 m height (c), relative humidity (d); reference evapotranspiration (e) and rainfall (f).

The wind speed caught the attention regarding the big difference between the values in the growing seasons of 2014 and 2016, with average values around 0.9 and 2.1 m s^{-1}, respectively (Figure 5c). In relation to rainfall, during the corn

growing season (~140 days), there were few rain events (Figure 5f), and in the months of June, July and August rainfall events did not occur in any of the three seasons. For this reason, the corn crop is cultivated in this period under full irrigation. ETo considerably increased after August, and, for sowing in June (e.g., corn season of 2014, Table 1), the flowering period (~9-10 weeks after sowing) may coincide with this increase of ETo; thus, more attention should be given to the irrigation management for sowing in June.

3.2. Irrigation management

Figure 6 shows the cumulative values for Irrigation (Irr), actual crop evapotranspiration (ET) of corn, reference evapotranspiration (ETo) and rainfall (P) for the center pivots cultivated in the growing seasons of 2014, 2015 and 2016. The period of cultivation is characterized by scarce rainfall events, practically none, justifying the large amount of water applied by irrigation, normally between 730 and 800 mm (Figure 6). In other words, corn production in this period is totally dependent on irrigation. Overall, the irrigation applied varied little from season to season and from pivot to pivot, except for the center pivot 05A in 2015, which was planted first than the others (Table 2) and so, may have taken advantage of some rain events occurred close to the sowing date.

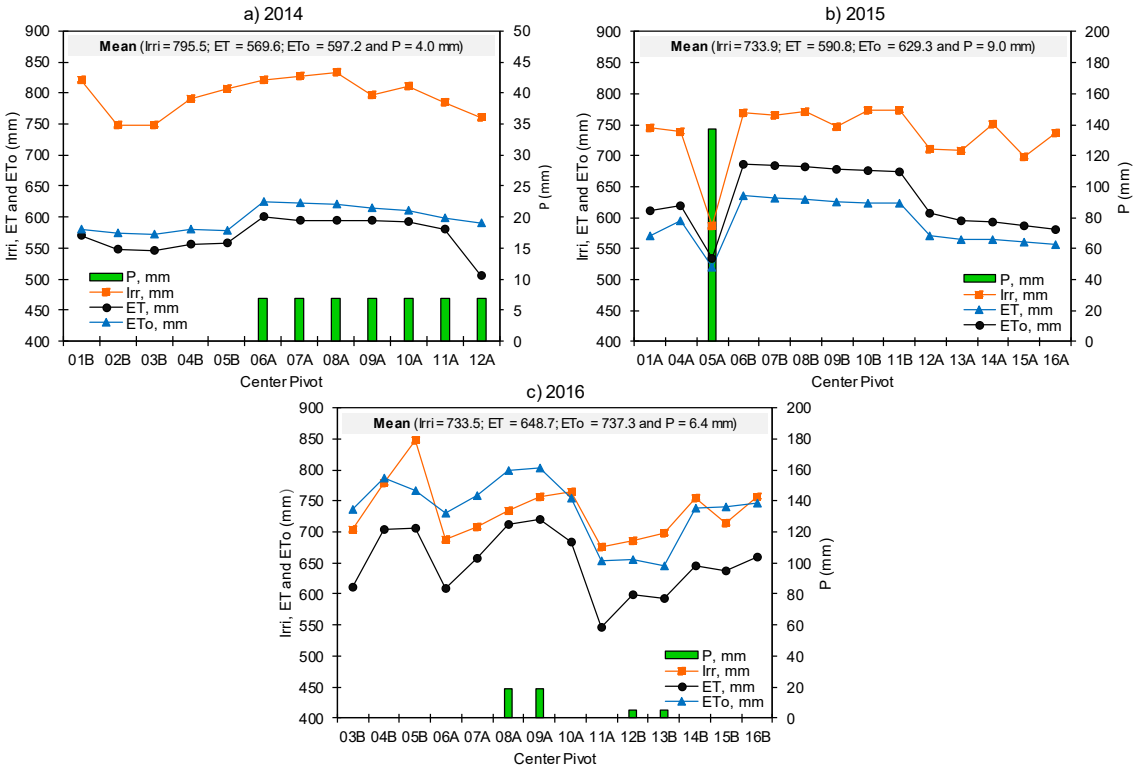

Figure 6. Cumulative values of Irrigation (Irr), actual evapotranspiration (ET) of corn, reference evapotranspiration (ETo) and rainfall (P) for each center pivot cultivated during the growing seasons of 2014 (a), 2015 (b) and 2016 (c).

The mean cumulative values of corn ET for 2014, 2015 and 2016 year were 569.6, 590.8 and 648.7 mm, respectively (Fig 6a, b and c). These data are similar to those found by Piccinni et al. (2009) in Uvalde, Texas (USA), where the climatic conditions during corn growing season were comparable to those of the present study region. Regarding the comparison between ET and ETo, the cumulative amounts were similar, but ETo was greater than ET, because the average Kc for corn during its full cycle is less than one. Normally, the Kc is less than one in the first 72 days after sowing (DAS), great than 1.0 from 72 to 110 DAS, reaching 1.2 between 88 and 98 DAS and, after that, is less than one again until harvest, around 140 DAS (Piccinni et al., 2009).

3.3. SAFER input parameters: Surface albedo (α_0), normalized difference vegetation index (NDVI) and surface temperature (T_0)

Surface albedo, NDVI, and surface temperature are the remote sensing parameters required by SAFER for ET estimation (Teixeira, 2010; Teixeira et al., 2013). Six images which best described the growing seasons (2014, 2015, and 2016) were selected to generate the images of α_0,T_0, and NDVI, shown hereinafter.

The albedo of vegetated land surfaces is a key regulatory factor in atmospheric circulation and plays an important role in mechanistic accounting of many ecological processes (Oguntunde and Van De Giesen, 2004), with direct influence on net radiation flux and, consequently, on the evapotranspiration. Figure 7 shows the spatial and temporal distribution of albedo values for the center pivots cultivated in the growing seasons of 2014, 2015 and 2016. Small variations of albedo throughout the crop cycle were observed. The center pivots were sown on different dates. Thus, in the first images more pronounced differences can be seen in the albedo, for instance, in June 07 of 2014 (Figure 7a) and, after the soil is completely covered, more homogeneity is observed (e. g. July 14, Figure 7a).

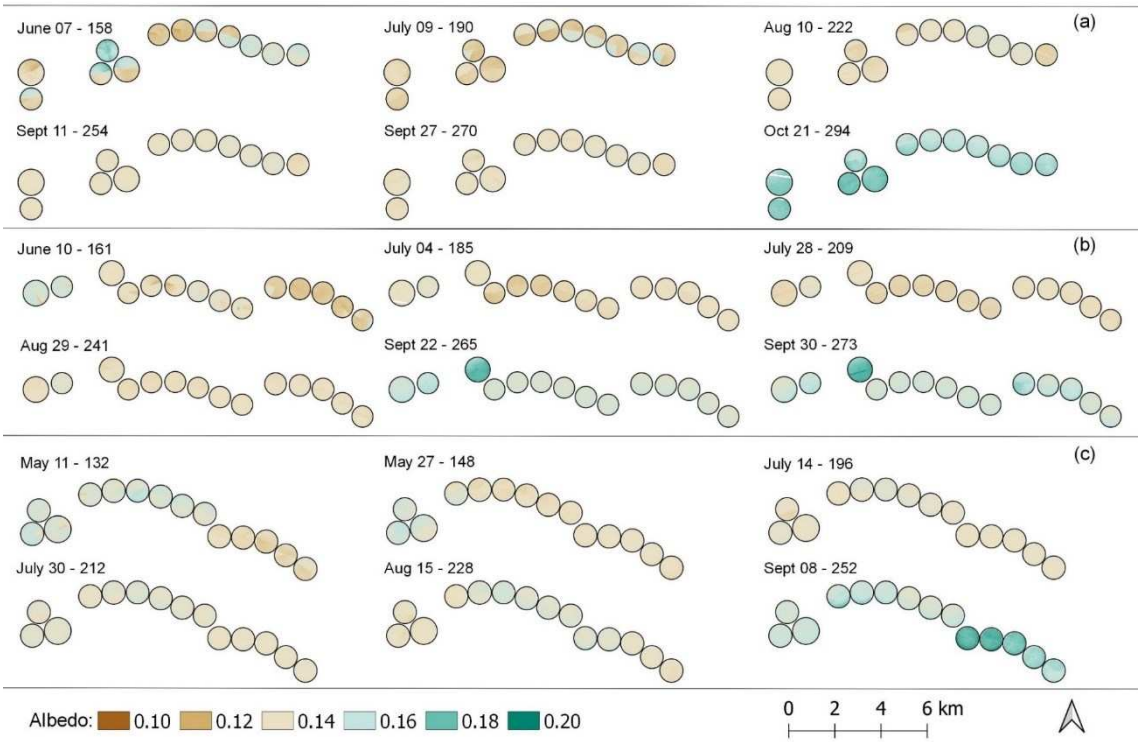

Figure 7. Map of spatial and temporal distribution of albedo values for the center pivots cultivated in the growing seasons of 2014 (a), 2015 (b) and 2016 (c).

Figure 8 shows the distribution of α_0 data based on boxplot for the center pivots cultivated in the growing seasons of 2014, 2015 and 2016. The albedo range was between 0.13 and 0.18, with low variation of the values over the crop cycle. This amplitude agrees with the data reported in the literature for corn fields, 0.14 and 0.22 (Allen et al., 2002b). The average value remained close to 0.15 for three seasons, and it corroborates results reported in the literature for corn (Bsaibes et al., 2009; Eichelmann et al., 2016).

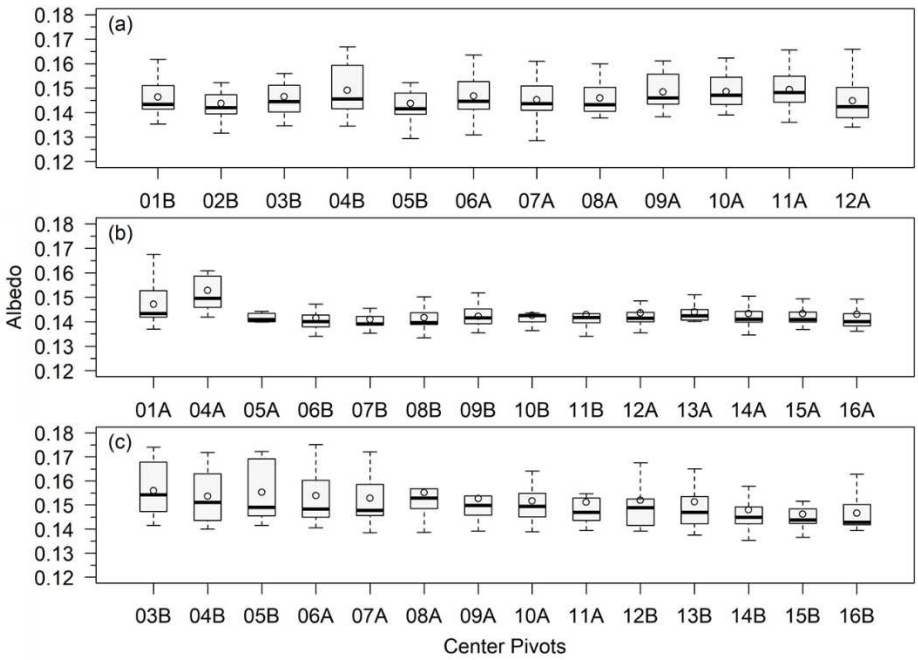

Figure 8. Boxplot of surface albedo values for the center pivots cultivated in the growing seasons of 2014 (a), 2015 (b) and 2016 (c).

During the growing season of 2015, α_0 albedo data had a low amplitude (Figure 8b). This behavior is due to the cultivation of only one corn hybrid in the center pivots 05A to 16A, differently from the seasons of 2014 and 2016, where five different hybrids were planted (see Table 1). As the α_0 value decreases, the surface increases its absorption of solar energy and the local surface temperature increases (Richardson et al., 2013), which in turn can contribute to a greater water consumption. Thus, the use of α_0 in SAFER algorithm is essential for more accuracy in ET estimates.

Variations of crop conditions were described based on the NDVI pattern in Figure 9, which shows that it has a trend of fast increase at the beginning of the growing cycle, with maximum values occurring in July (Figures 9b and c) and August (Figure 9a), when an effective full cover occurs. A declining trend appears at the end of the growing cycle, coinciding with ripening and maturity stages. Thus, understanding these NDVI patterns is critical for crop management.

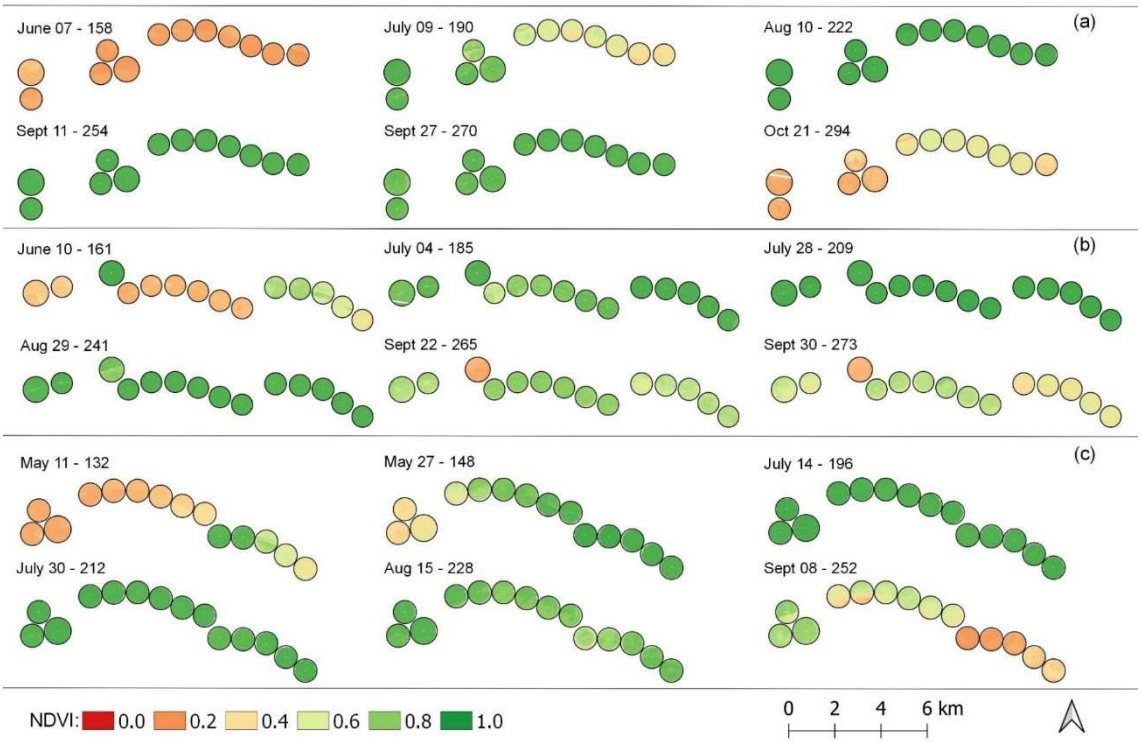

Figure 9. Map of spatial and temporal distribution of NDVI values for the center pivots cultivated in the growing seasons of 2014 (a), 2015 (b) and 2016 (c).

The NDVI values were very similar in the three growing seasons and, during 2014 and 2015 (Figures 10a and b) the median was greater than that of 2016 (Figure 10c), which indicates high NDVI values for a longer time in these first two seasons. The maximum NDVI values remained around 0.9, while the minimum values were close to 0.2, with an average value around 0.7. The minimum value, around 0.2, is commonly observed near the sowing date, while the maximum value is observed in the full cover period. Results similar to the maximum, minimum and mean values verified in the present study have been found by others authors (Nagy et al., 2018; Nguy-Robertson et al., 2013; Wang et al., 2016).

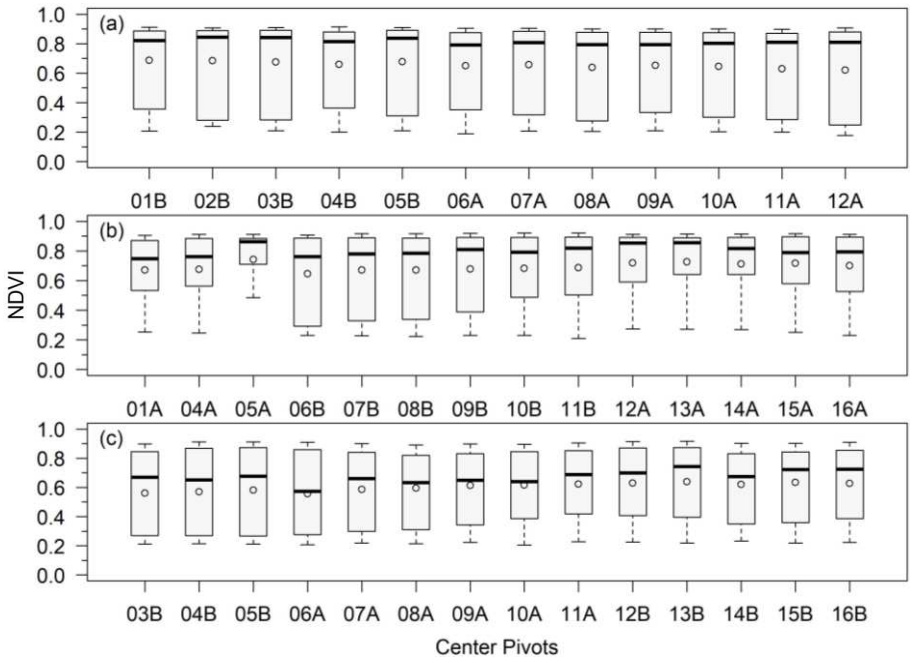

Figure 10. Boxplot of NDVI values for the center pivots cultivated in the growing seasons of 2014 (a), 2015 (b) and 2016 (c).

The spatial and temporal distribution of T_0 based on the images of the 2014, 2015 and 2016 growing seasons is shown in Figure 11. Highest T_0 values are normally observed at the beginning or end of the season, when there is either uncovered soil or reduced cover by plants, due to senescence. In the period from full cover (normally in July) to senescence (normally in late September), few temperature variations were observed among the center pivots for the three growing seasons. These few variations are consequence of full soil cover, low variation in the climatic conditions over three years (Figure 5) and low variation of cultivation system and irrigation management.

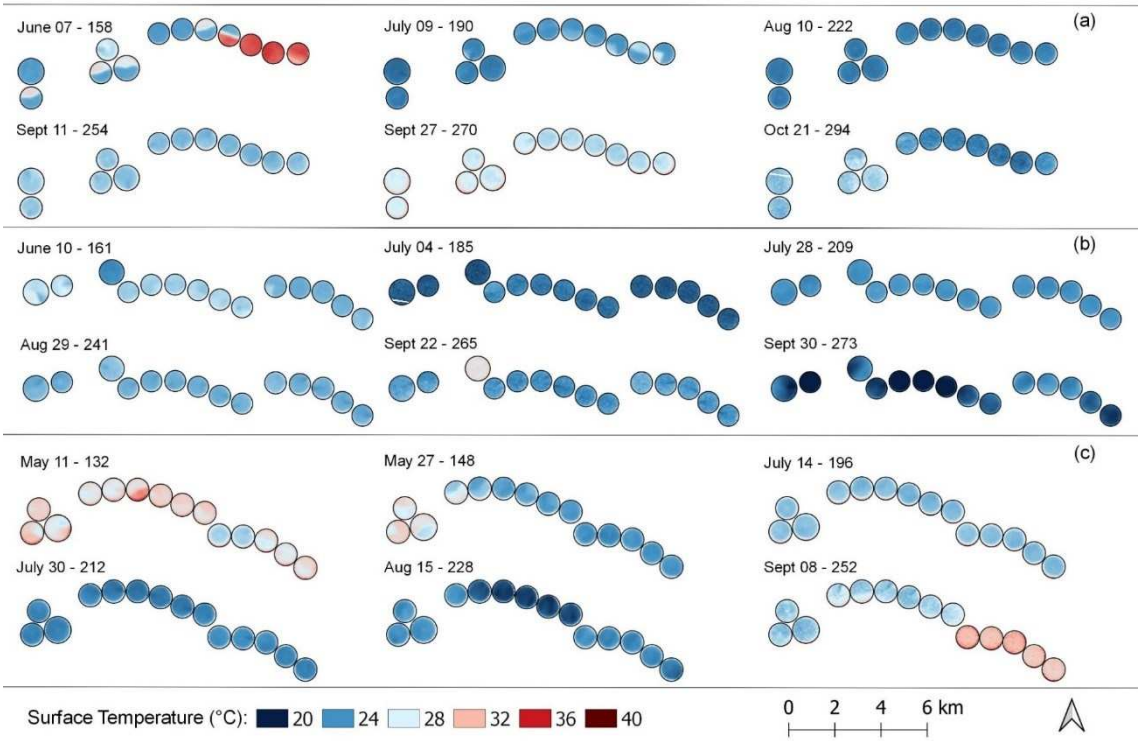

Figure 11. Map of spatial and temporal distribution of surface temperature values for the center pivots cultivated in the growing seasons of 2014 (a), 2015 (b) and 2016 (c).

Surface temperature is one of the most important variables measured by satellite remote sensing (Rozenstein et al., 2014). This metric is valuable to many fields such as weather prediction, climate change research, and agriculture (Laraby and Schott, 2018). In the field of agriculture, it is used for the estimation of several geophysical variables, especially evapotranspiration, vegetation water stress (Bhattarai et al., 2017; Sayago et al., 2017) and soil moisture.

Figure 12 shows the boxplot of surface temperature values for the center pivots cultivated in the growing seasons of 2014, 2015 and 2016. T_0 ranged from 20 to 36 °C. The majority of center pivots had surface temperature around 25 °C. The maximum values for surface temperature are observed during the beginning of the season and also at the border areas (Figure 11). Low pressure is common at the border of the center pivots, which culminates with irrigation deficit, thus leading to higher temperatures. Besides

that, the external areas are normally uncultivated and have high temperatures, influencing the border areas of center pivots.

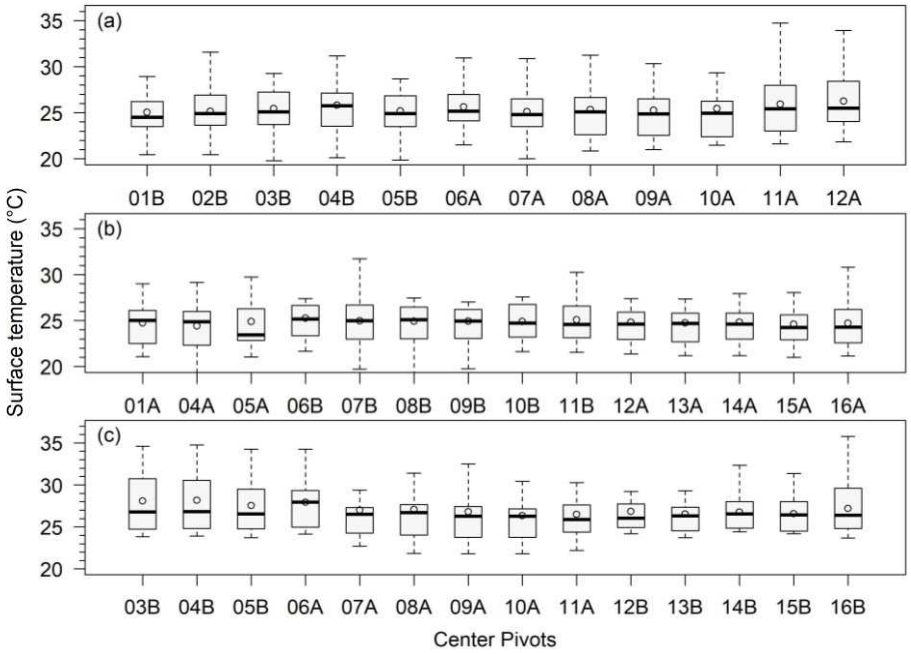

Figure 12. Boxplot of surface temperature values for the center pivots cultivated in the growing seasons of 2014 (a), 2015 (b) and 2016 (c).

Overall, there was very low variability in the surface albedo, NDVI and surface temperature. Our findings are consistent with the investigation of (Teixeira et al., 2017). These authors applied the SAFER algorithm in a semi-arid area composed of irrigated crops and natural vegetation in the municipality of Petrolina, Northeast Brazil and verified small variability in the above-cited parameters for irrigated crops. According to them, as the water is regularly applied, the variations of these remote sensing parameters, besides the global solar radiation levels, are influenced by the different crop stages together with water and fertilization managements.

Calculating ET from remote sensing data has been increasingly common. Overall, ET models based on remote sensing data use the values of surface albedo, ground surface temperature and infrared bands in order to calculate spatial variations of short- and long-wave radiations, which allow calculating ET for each pixel of the images (Kamali and Nazari, 2018). For the SAFER algorithm,

it was not different, since it uses albedo, NDVI and surface temperature as the remote sensing parameters to calculate ET. However, the major point is that, among the models or algorithm based on remote sensing data (e.g., SEBAL), SAFER can be considered as relatively simpler.

Its simplicity comes from the fact that it does not require either identification of extreme conditions in the images or energy balance, so ET can be obtained from remote sensing data (surface albedo, NDVI and surface temperature) and meteorological data (ETo) from different types of stations, that is, agrometeorological, conventional and automatic stations (Andrade et al., 2016; Coaguila et al., 2017; Teixeira et al., 2015; Teixeira, 2010). Another problem in relation to the applicability of some remote sensing radiation and energy balance algorithms, when aiming at the end users, is the need for background knowledge in radiation physics (Teixeira et al., 2017).

3.4. SAFER: ET/ETo ratio and corn ET with original regression coefficients

The ET/ETo ratio values are related to crop development and to soil moisture conditions (Teixeira, 2010) because of their input parameters. Thus, by comparing SAFER algorithm with modified FAO method, it is possible to affirm that ET/ETo ratio corresponds (conceptually and numerically) to the crop coefficient (Kc) multiplied by water stress coefficient (K_S), as presented in Equation 1. The center pivots of this study are very well managed in relation to the water applied, causing K_S values to remain normally within the range from 0.9 to 1.0. Thus, the ET/ETo ratio is expected to be close to the values of Kc recommended for the corn crop (Figure 3). However, values with a different pattern can be seen in Figure 13: (i) during the beginning or at the end of the season, the ET/ETo ratio has very low values, close to zero (underestimates), and (ii) during crop-development and mid-season stages, there is an overestimation. As well as SAFER input parameter, six images which best described the growing seasons (2014, 2015, and 2016) were selected to generate the images of ET/ETo.

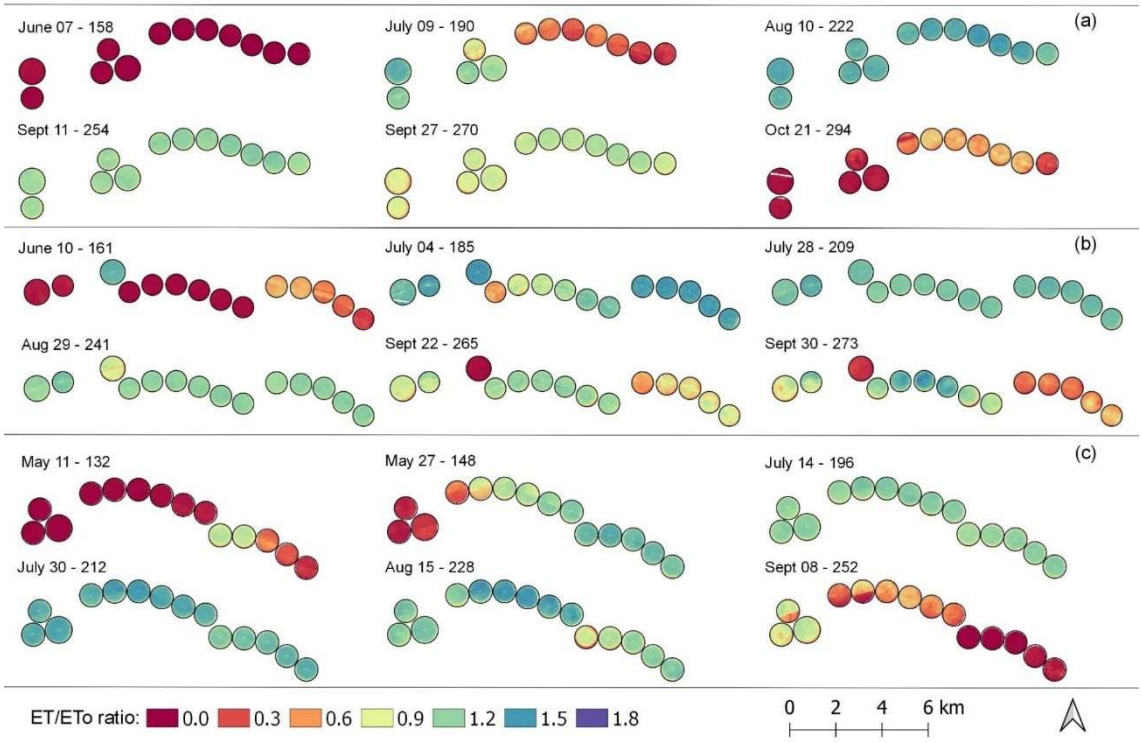

Figure 13. Map of spatial and temporal distribution of ET/ETo ratio values for the center pivots cultivated in the growing seasons of 2014 (a), 2015 (b) and 2016 (c).

Additionally, Figure 14 shows a boxplot for ET/ETo ratio values, demonstrating pixels ranging from 0 to 1.7, with 25% of the data (third quartiles) between 1.3 and 1.7 normally (Figures 14a and b). In 2016 (Figure 14c) the maximum values were lower (~1.4). These values are out of normality, for the corn crop and for the water management adopted in the field. Teixeira et al. (2015) verified in irrigated corn fields some pixels with ET/ETo close to 1.40 and, a value ranging normally between 0.2 and 1.2, but the regression coefficients used in the study were 1.0 and -0.008 for a and b, respectively. These results indicate that the ET/ETo ratio is not adequately sensitive to represent the behavior of the crop coefficient adjusted to water stress in irrigated corn fields. Besides that, the results close to zero evidence the high dependency on soil cover ratio.

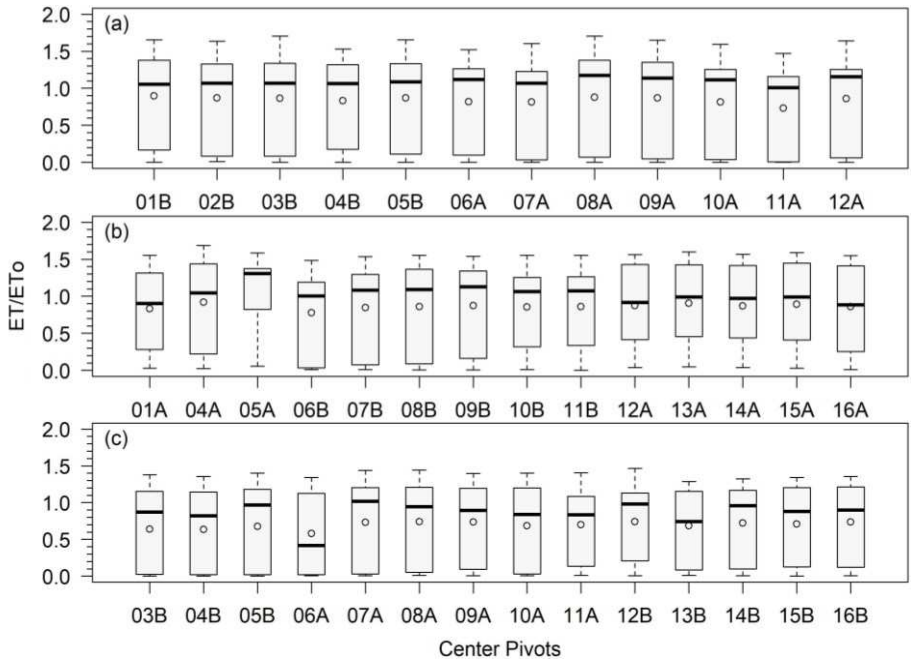

Figure 14. Boxplot of ET/ETo ratio values for the center pivots cultivated in the growing seasons of 2014 (a), 2015 (b) and 2016 (c).

Our first reason to think about calibrating SAFER arose from these results, but our conclusion came from the results presented below, based on statistical parameters. Figure 15 shows scatter plots with statistical metrics between corn ET estimated by the modified FAO method (ET_{MFAO}) and estimated by SAFER with original coefficients (ET_{SAFER}) for four center pivots selected in three growing seasons. The comparison between ET_{SAFER} and ET_{MFAO} shows reasonable agreement, based on r^2, with values higher than 0.8 in some pivots, 08A and 12A in 2014 (Figure 15a) and 03B in 2016 (Figure 15c). In general, r^2 values were good, with the minimum value of 0.59 for the 16A center pivot in 2016 (Figure 15c). In addition, it is important to point out that SAFER algorithm has a major underestimation, values practically equal to zero, when the evapotranspiration from ET_{MFAO} is lower than 3 mm d^{-1} (Figure 15a, b and c), normally in the early season.

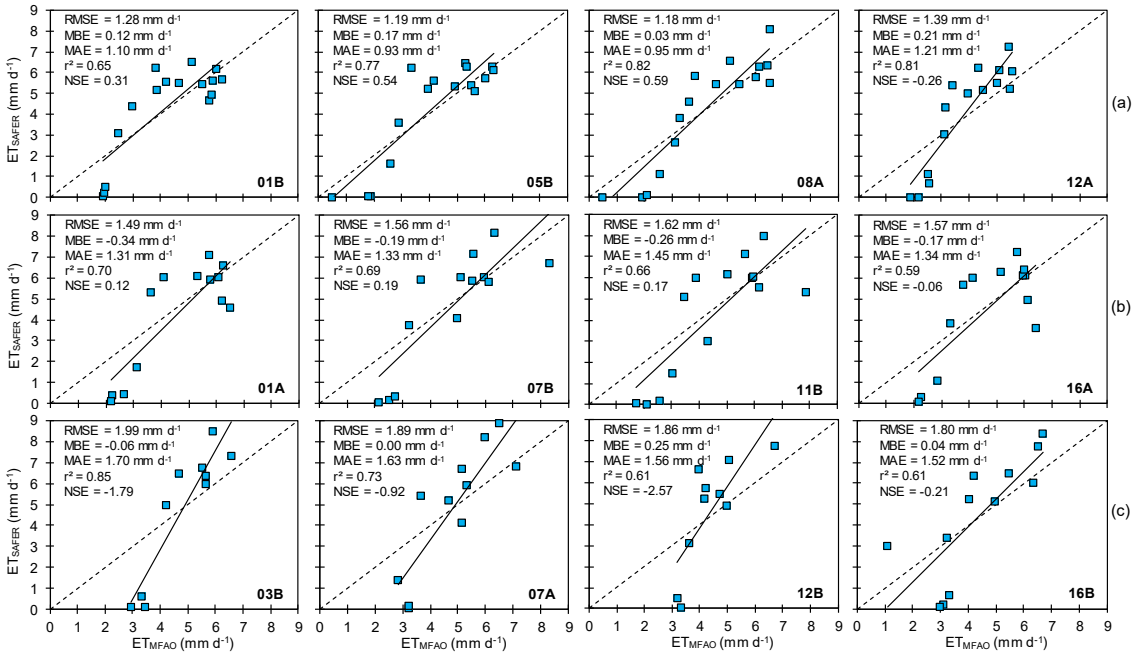

Figure 15. Comparison between daily corn evapotranspiration estimated by SAFER algorithm and modified FAO method at four center pivots selected in the growing seasons of 2014 (a), 2015 (b) and 2016 (c). The dotted lines represent the 1:1 line and the solid black lines represent the linear regressions.

Although the largest losses of corn are observed when the stress occurs in the development phase just before and after flowering (Claassen and Shaw, 1970; Daryanto et al., 2016), when corn plants are exposed to water stress at the early vegetative growth, it normally reduces plant growth and inhibits plant development. This occurs because the water deficit induces stomatal closure and inhibits photosynthesis, which limits carbohydrate synthesis and thus cell division and expansion (Barnabás et al., 2008). Thus, corn ET determination based on SAFER could lead to a deficit irrigation, generating the problems mentioned above.

The statistical parameters show that the SAFER algorithm completely inefficient, with RMSE reaching almost 2.00 mm d^{-1} in the 03B pivot in 2016 (Figure 15c). By analyzing all pivots, it is possible to observe that the RMSE is very high (always greater than 1.18 mm d^{-1}), considering the magnitude for corn ET in the region. In the last years, many authors have worked with the comparison of ET from remote sensing-based methods with other

methodologies, and they often take into account the RMSE value in order to infer on the estimation accuracy. Paço et al. (2014), for example, performed the comparison between METRIC (Allen et al., 2007a, 2007b) and the FAO-56 dual Kc approach, and considered as low a RMSE value less than 0.44 mm d^{-1}. Da Silva et al. (2018) compared SEBAL (Bastiaanssen et al., 1998a, 1998b) and the FAO-56 (single Kc approach), and considered SEBAL results as satisfactory, because the difference in the estimates were less than or equal to 1.00 mm d^{-1}. In general terms, RMSE or differences in the estimate greater than 1 mm d^{-1} are not satisfactory.

Regarding MBE, an equilibrium was verified. SAFER underestimated corn ET for all center pivots in 2015 (Figure 15b) and for 03B in 2016 (Figure 15c) and overestimated it for the rest of the pivots analyzed. As observed for RMSE, the MAE demonstrates that the SAFER algorithm has low efficiency, with MAE reaching up to 1.7 mm d^{-1} in the 03B center pivot (Figure 15c). In comparison with the results obtained by Yi et al. (2018), who estimated corn ET by means of remote sensing models and compared with eddy covariance measurement, our results of MAE and RMSE are high. These authors considered that their methodology had a good agreement, from a RMSE equal to 0.8 and MEA equal to 1.1 mm d^{-1}. For NSE, most values were lower than zero, which means that the mean value of the observed variable would obtain a higher accuracy than the simulated values (Richter et al., 2011). In summary, Figure 15 demonstrates the poorness of the SAFER approach to estimate corn ET with original regression coefficients.

Figure 16 shows the seasonal cycle of daily ET obtained by the SAFER algorithm (ET_{SAFER}) and by modified FAO method (ET_{MFAO}) for the 2014, 2015 and 2016 growing seasons. For both methodologies, the daily ET had a strong seasonal cycle, with low values in the initial stage, high values during crop development and mid-season stages and decrease of these values in late-season stage until harvest, performing normally between 135 and 150 days after sowing in Brazil.

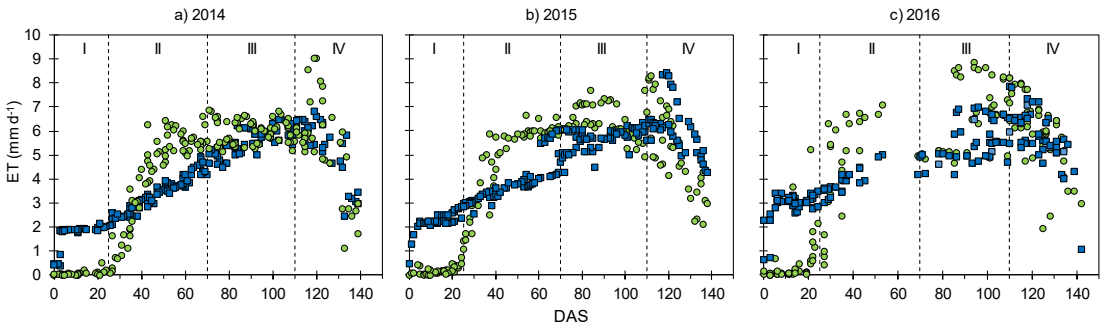

Figure 16. Temporal evolution of daily corn evapotranspiration estimated by SAFER algorithm (green) and modified FAO method (blue) for all center pivots cultivated during the growing seasons of 2014 (a), 2015 (b) and 2016 (c) as a function of days after sowing (DAS). Growth stages: I (initial); II (crop development); III (mid-season), and IV (late season).

When the data are separately analyzed in each phenological phase, more valuable information can be seen (Figure 16). The first point is the very low ET_{SAFER} (close to zero) during the first 30 DAS, while ET_{MFAO} remained between 2 and 3 mm d^{-1}. The main reason for lower ET could be the large area of uncovered soil in this period because, after full soil cover ET values increase quickly. Thus, taking into account that, among the inputs of SAFER (NDVI, surface albedo and surface temperature), NDVI has high positive correlation with soil cover (Barati et al., 2011; Zhang et al., 2006), it is possible to affirm that the SAFER algorithm has high dependence on NDVI values.

During the crop development stage, the opposite of the initial phase was observed, with the SAFER algorithm presenting higher ET values in comparison to modified FAO method (Figure 16). In addition, during the last two stages, more coincidence between data is verified, but with ET values of SAFER a little greater than those of ETo_{MFAO}. In summary, these results indicate that SAFER algorithm does not have the capacity to accurately estimate ET, especially during the initial (underestimates) and crop development stages (overestimates).

In this context, that is, with the results of ET/ETo ratio discussed in Figures 13 and 14, the poor agreement for corn ET based on statistical parameters (15), along with terrible estimation for the first 30 DAS and overestimates during crop development stage (Figure 16), encouraged us to calibrate and validate SAFER

algorithm based on modified FAO method (Equation 1) to increase its performance for ET estimation in irrigated corn fields.

3.5. SAFER calibration

The calibration focused on the adjustment of regression coefficients (a = 1.8 and b = -0.008) of ET/ETo ratio (Equation 10), and not exactly on ET, since the ETo used in SAFER algorithm (Equation 10) to obtain ET is the same used in modified FAO method. After calibration employing the nonlinear optimization algorithm generalized reduced gradient (GRG) of Solver tool from Microsoft Excel, the observed values for “a” and “b” coefficients were 0.32 and -0.0013, respectively, with a final MSE of 0.0105. To assess the calibration, Figure 17 shows the correlations between ET/ETo estimated by SAFER with calibrated regression coefficients (ET/ETo_{SAFERC}) and ET/ETo estimated by modified FAO method (ET/ETo_{MFAO}), along with the statistics for their comparison.

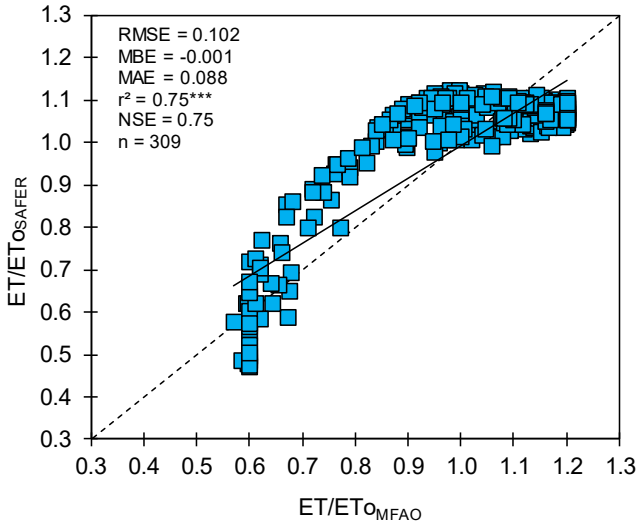

Figure 17. Comparison between ET/ETo estimated by SAFER with calibrated regression coefficients (ET/ETo_{SAFER}) and ET/ETo estimated by modified FAO method (ET/ETo_{MFAO}). The dotted lines represent the 1:1 line and the solid black lines represent the linear regressions. *** indicates significance of regression at p-value < 0.001.

The calibration of SAFER algorithm showed reasonable agreement, with estimates relatively close to the 1:1 line and r^2 and NSE equal to 0.75 (Figure 17). RMSE was low (0.102), as also observed for MAE (0.092). With MBE = -0.001 the calibrated SAFER tends to underestimate the data, but now with an almost insignificant difference. Overall, these results show a good improvement compared to the previous results (without calibration).

In order to show the spatial and temporal distribution of ET/ETo ratio after calibration (2014 and 2015), a center pivot was in each growing season were used to create Figure 18. Note that low values of ET/ETo ratio no longer occur in the first 30 DAS (Figures 18a and b), as verified before calibration (Figure 13). It is possible to clearly observe, in general terms, that the ratio has a behavior similar to that of Kc adjusted to water stress (Kc x K_S) (Figure 18), which is desirable.

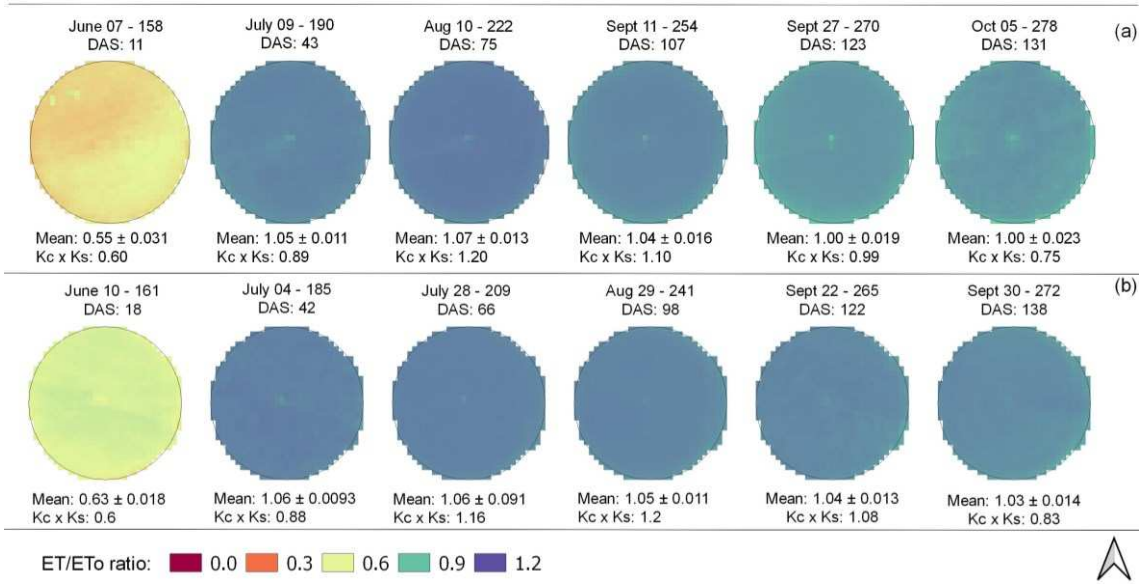

Figure 18. Results of spatial and temporal distribution for ET/ETo ratio values after calibration, referring to the center pivot 03B selected in the growing seasons of 2014 (a) and 2015 (b).

The results was similar for two center pivots, thus, analyzing the pivot 03B as reference, verifies that after 11 DAS, a value of 0.55 was found for ET/ETo

ratio, very close to Kc x K_S (0.60). When corn was at the crop development stage (20 to 70 DAS, see Figure 3) the ratio was 1.05 (43 DAS) and 1.07 (75 DAS), values consistent with those of Kc x K_S (Figure 18a). In the next image, now, in the mid-season stage, the ratio has a mean value of 1.04 (107 DAS), similar to that of adjusted Kc, which was 1.10. Then, in the last stage, late season, the ratio value decreased to 1.00 (Sept 27), whereas Kc x K_S was 0.99. Eight days later (Oct 05), ET/ETo maintained the same value (1.00), but Kc x K_S decreased to 0.75.

3.6. SAFER validation

Figure 19 presents the spatial and temporal distribution of ET/ETo ratio after validation with 2016 data. The main problem in the SAFER algorithm was the very low values of ET/ETo ratio (close to zero) during the entire initial stage and part of the crop development, that is, during the first 30 DAS, and overestimates during the crop development stage. However, after calibration (Figure 18) and validation (Figure 19), it is clearly verified that this problem was well solved. During the initial growth stage (e.g., May 11, Figure 19b) a value around 0.5 can be observed, and during the crop development period (20 to 70 DAS) the ET/ETo ratio reached 1.04 (72 DAS). In the next stage, mid-season, the ET/ETo mean is close to 1.05 (Kc x K_S was 1.2) and, during late season from 120 DAS, it started to decrease and showed a mean value of 0.88 at 128 DAS.

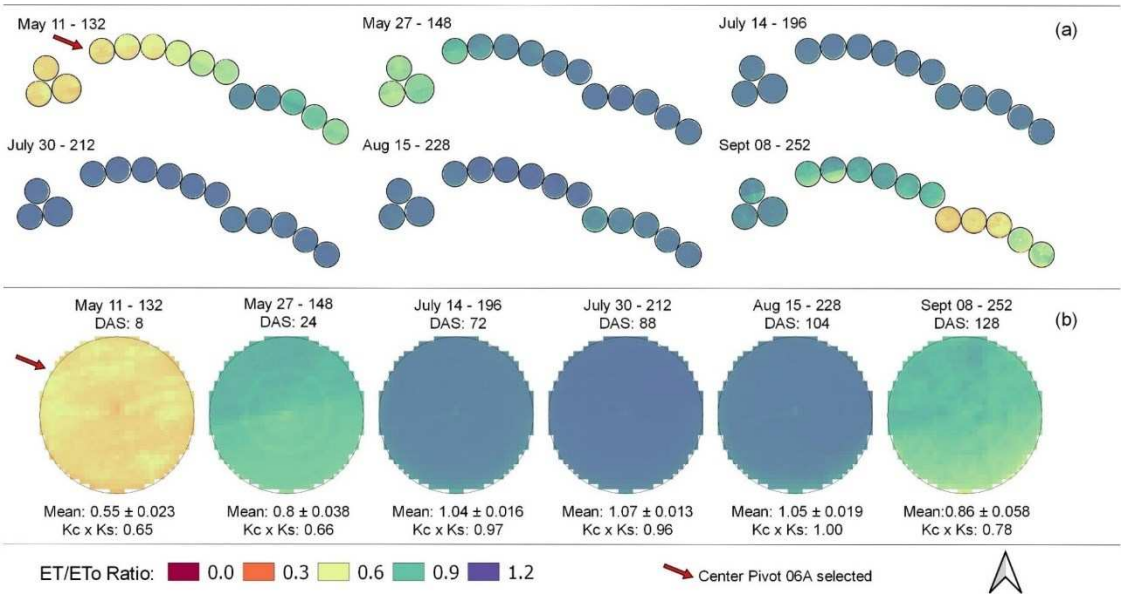

Figure 19. Results of spatial and temporal distribution for ET/ETo ratio values after validation, referring to the center pivots cultivated in the growing seasons of 2016 (a), with highlight to center pivot 06A (b).

From the ET/ETo ratio used in validation, corn ET values were obtained and compared with corn ET estimated by modified FAO method (Figure 20). Individual graphs were created and also one involving all center pivots of the growing season (GS) of 2016 (GS - 2016). The results of validation showed a good agreement, with estimates close to the 1:1 line and, based on r^2, it can be observed that ET values from SAFER explained between 66 and 97% of the variation of data estimated by modified FAO method (Figure 20). Only one field (13B) had a relatively low r^2 ($r^2 = 0.66$), but its r^2 was not significant as well as the field 09A.

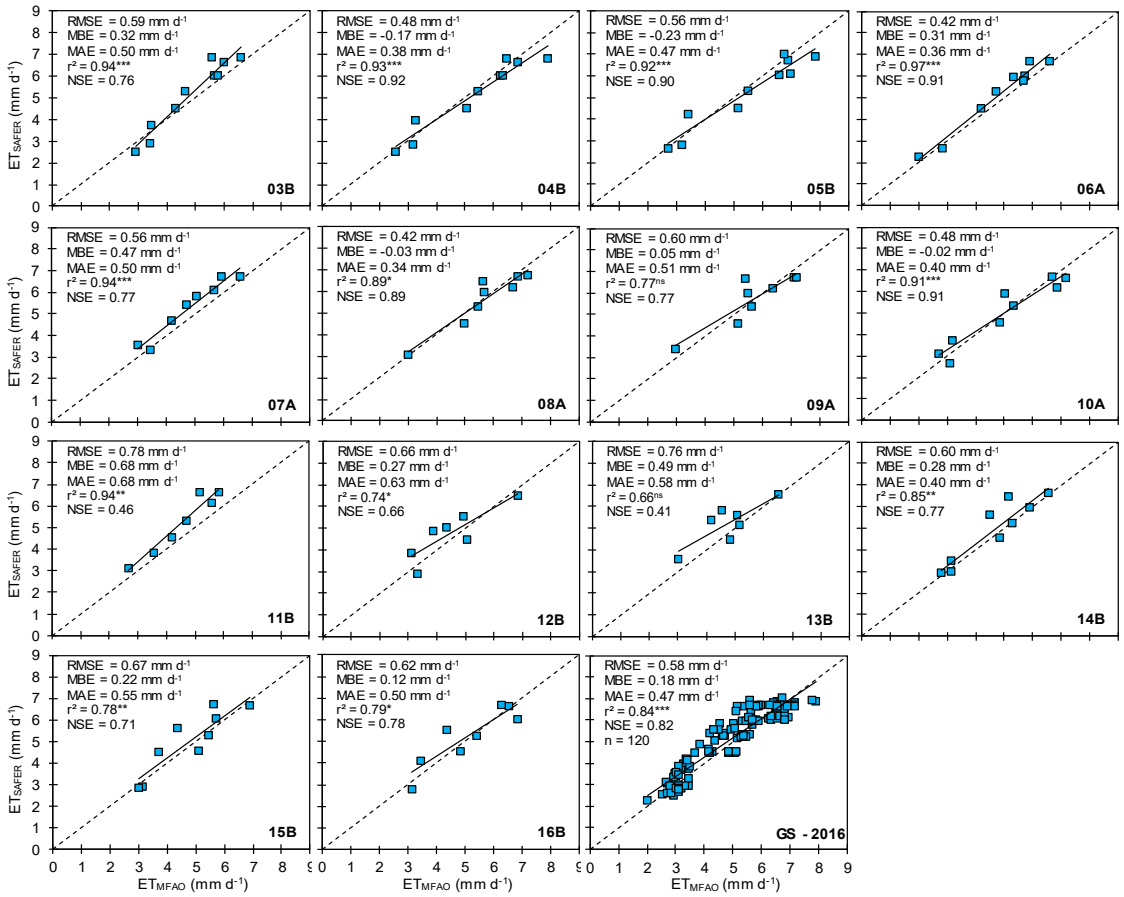

Figure 20. SAFER algorithm validation results using ET data estimated by modified FAO method collected during the growing season of 2016. The dotted lines represent the 1:1 line and the solid black lines represent the linear regressions. ns not significant, * indicates significance of regression at p-value < 0.05, ** indicates significance of regression at p-value < 0.01 and *** indicates significance of regression at p-value < 0.001.

In general terms, the results found for r^2 can be classified as very good and excellent, since most center pivots had r^2 above 0.84 and some had r^2 above 0.9. The NSE values reinforce the very good agreement verified based r^2, with values reaching 0.92 for center pivot 04B and most fields with values above 0.7, allowing the SAFER algorithm to be classified as good ($0.5 \leq NSE \leq 0.8$) or excellent ($NSE \geq 0.8$) (Richter et al., 2011) for ET estimation in irrigated corn crop.

Overall, the SAFER algorithm tends to overestimate corn ET, since MBE was positive for 10 out of the 14 center pivots analyzed. Besides that, positive

value was verified (MBE = 0.18 mm d^{-1}) in the analysis of all pivots together (GS - 2016, Figure 20). Regarding the magnitude, the highest MBE was verified in the 11B pivot (0.68 mm d^{-1}). The MAE was low, close to 0.5, varying between 0.34 and 0.68. Considering that the average value of ET for the corn crop in the region of study in the period from April to October is around 4.2 mm d^{-1}, the MBE and MAE can be considered as low.

The center pivots of the 2016 growing season were also analyzed together and the results were similar to those observed for individual pivots (GS-2016, Figure 20). The NSE was 0.82 and with 83% of the scatter close to the 1:1 line (r^2 = 0.83). The RMSE was 0.58, MBE was 0.18 and, MAE was 0.47 mm d^{-1}. Based on these results, considered as very good, it is possible to confirm the accuracy of calibration and assert that the SAFER algorithm is able to accurately estimate corn ET.

Almost no study was published in scientific literature with SAFER algorithm involving large areas with monoculture under full irrigation (e.g., corn). Most works available to the scientific community were conducted in large areas involving different crops, cultivation systems and edaphoclimatic conditions (Andrade et al., 2016; Coaguila et al., 2017; Hernandez et al., 2014), that is, heterogeneous areas. Thus, our study is something new in terms of field of application, having demonstrated also that SAFER algorithm when applied in irrigated monoculture areas needs to be carefully evaluated before being used, since it showed problems with underestimates (first 30 days after sowing) and overestimates (from this period) (Figure 16) of ET/ETo ratio and, consequently, of ET.

Finally, the authors acknowledge that a more robust validation study could have been conducted, if we had used field data measured by an eddy covariance system, for example. However, we trusted in the amount (42 center pivots used) and quality of the data made available by the company IRRIGER, because it has adopted the modified FAO method for more than 13 years (since 2005) in more than 690 farms involving in a wide range of crops, irrigation systems and edaphoclimatic conditions, and nowadays, this company is a world leader in irrigation management, currently acting in 16 countries (IRRIGER, 2018).

4. CONCLUSIONS

The SAFER algorithm was tested on fully irrigated corn in the western region of Bahia state Brazil, a condition which is slightly different from algorithm validation conditions (larger areas in semi-arid region involving irrigated crops and natural vegetation). For these corn field conditions, SAFER algorithm without calibration performed very poorly in corn ET estimation, with RMSE higher than 1.8 mm d^{-1} in four fields and always greater than 1.18 mm d^{-1} for the 12 fields analyzed, and NSE values lower than zero in most fields.

Regarding the periods, until 30 days after sowing, SAFER was very inconsistent, with ET values close to zero. When the regression coefficients of ET/ETo ratio were calibrated, good agreement was verified (RMSE = 0.012, MBE= -0.001, MAE = 0.008 and r^2 = NSE = 0.85). Validation with ET data of 2016 led to good performance of SAFER algorithm (r^2 = 0.84), with low RMSE (0.58 mm d^{-1}), MBE (0.18 mm d^{-1}) and MAE (0.47 mm d^{-1}) values, for the set of 14 center pivots cultivated in this growing season.

These results suggest that care must be taken in using SAFER to estimate ET in large areas irrigated (e.g., center pivots), because the algorithm was initially validated for large-scale application and in areas involving irrigated crops and natural vegetation. In addition, the integration of SAFER with field observations can be very beneficial for precision irrigation, allowing a better use of water in irrigation management, particularly in environments where water is scarce. However, further research involving different crops, cultivation systems, edaphoclimatic conditions, among other factors, is needed to test and improve SAFER predictions of ET.

5. REFERENCES

AIBA - Associação de Agricultores e Irrigantes da Bahia, 2016. Anuário agropecuário Oeste da Bahia: safra 2015/2016. Barreiras: Bahia, Brazil.

Allen, R., Tasumi, M., Trezza, R., Bastiaanssen, W., Walters, R., Waters, R., Allen, R., Tasumi, M., Trezza, R., Bastiaanssen, W., 2002a. SEBAL Surface Energy Balance Algorithms for Land.

Allen, R.G., Pereira, L.S., Raes, D., Smith, M., 1998. Crop evapotranspiration: Guidelines for computing crop water requirements, FAO Irrigation and Drainage Paper No. 56. FAO, Rome, Italy.

Allen, R.G., Tasumi, M., Morse, A., Trezza, R., Wright, J.L., Bastiaanssen, W., Kramber, W., Lorite, I.J., Robison, C. w., Tasumi, M., Trezza, R., 2007a. Satellite-Based energy balance for Mapping Evapotranspiration with Internalized Calibration (METRIC) – Applications. Journal of Irrigation and Drainage Engineering 133, 395–406.

Allen, R.G., Tasumi, M., Trezza, R., 2007b. Satellite-based energy balance for Mapping Evapotranspiration with Internalized Calibration (METRIC) – Model. Journal of irrigation and drainage engineering 133, 380–394.

Alvares, C.A., Stape, J.L., Sentelhas, P.C., Gonçalves, J.L. De M., Sparovek, G., 2013. Köppen's climate classification map for Brazil. Meteorologische Zeitschrift 22, 711–728.

ANA – Agência Nacional de Águas, 2017. Atlas Irrigação: Uso da Água na Agricultura. ANA, Brasília.

Andrade, R.G., Teixeira, A.H. de C., Leivas, J.F., Nogueira, S.F., 2016. Analysis of evapotranspiration and biomass in pastures with degradation indicatives in the Upper Tocantins River Basin, in Brazilian Savanna. Revista Ceres 63, 754–760.

Barati, S., Rayegani, B., Saati, M., Sharifi, A., Nasri, M., 2011. Comparison the accuracies of different spectral indices for estimation of vegetation cover fraction in sparse vegetated areas. Egyptian Journal of Remote Sensing and Space Science 14, 49–56.

Barker, J.B., Heeren, D.M., Neale, C.M.U., Rudnick, D.R., 2018. Evaluation of variable rate irrigation using a remote-sensing-based model. Agricultural Water Management 203, 63–74.

Barnabás, B., Jäger, K., Fehér, A., 2008. The effect of drought and heat stress on reproductive processes in cereals. Plant, Cell and Environment 31, 11–38.

Bastiaanssen, W.G.M., Menenti, M., Feddes, R.A., Holtslag, A.A.M., 1998a. A remote sensing surface energy balance algorithm for land (SEBAL): 1. Formulation. Journal of Hydrology 212–213, 198–212.

Bastiaanssen, W.G.M., Pelgrum, H., Wang, J., Ma, Y., Moreno, J.F., Roerink, G.J., Van Der Wal, T., 1998b. A remote sensing surface energy balance algorithm for land (SEBAL): 2. Validation. Journal of Hydrology 212–213, 213–229.

Bernardo, S., 1989. Manual de Irrigação, 5th ed. UFV, Viçosa.

Bhattarai, N., Wagle, P., Gowda, P.H., Kakani, V.G., 2017. Utility of remote sensing-based surface energy balance models to track water stress in rain-fed switchgrass under dry and wet conditions. ISPRS Journal of Photogrammetry and Remote Sensing 133, 128–141.

Bsaibes, A., Courault, D., Baret, F., Weiss, M., Olioso, A., Jacob, F., Hagolle, O., Marloie, O., Bertrand, N., Desfond, V., Kzemipour, F., 2009. Albedo and LAI estimates from FORMOSAT-2 data for crop monitoring. Remote Sensing of Environment 113, 716–729.

Cao, X.C., Shu, R., Chen, D., Guo, X.P., Wang, W.G., 2018. Temporal-spatial distributions of water use and productivity of maize in China. Journal of Agricultural Science 156, 528–536.

Chen, J., Zhu, X., Vogelmann, J.E., Gao, F., Jin, S., 2011. A simple and effective method for filling gaps in Landsat ETM+ SLC-off images. Remote Sensing of Environment 115, 1053–1064.

Christou, A., Dalias, P., Neocleous, D., 2017. Spatial and temporal variations in evapotranspiration and net water requirements of typical Mediterranean crops on the island of Cyprus. Journal of Agricultural Science 155, 1311–1323.

Claassen, M., Shaw, R.H., 1970. Water Deficit Effects on Corn. Grain Components. Agronomy Journal 62, 649–652.

Claverie, M., Vermote, E.F., Franch, B., Masek, J.G., 2015. Evaluation of the Landsat-5 TM and Landsat-7 ETM+ surface reflectance products. Remote Sensing of Environment 169, 390–403.

Coaguila, D.N., Hernandez, F.B.T., Teixeira, A.H. de C., Franco, R.A.M., Leivas, J.F., 2017. Water productivity using SAFER - Simple Algorithm for Evapotranspiration Retrieving in watershed. Revista Brasileira de Engenharia Agrícola e Ambiental 21, 524–529.

Conceito Agrícola, C., 2017. Estádios fenológicos da cultura do milho. https://www.conceitoagricola.com.br/noticias/estadios-fenologicos-da-cultura-do-milho/ (accessed 1.8.18).

Croitoru, A.E., Piticar, A., Dragotă, C.S., Burada, D.C., 2013. Recent changes in reference evapotranspiration in Romania. Global and Planetary Change 111, 127–132.

Da Silva, B.B., Mercante, E., Boas, M.A.V., Wrublack, S.C., Oldoni, L.V., 2018. Satellite-based ET estimation using Landsat 8 images and SEBAL model. Revista Ciencia Agronomica 49, 221–227.

Daryanto, S., Wang, L., Jacinthe, P.A., 2016. Global synthesis of drought effects on maize and wheat production. PLoS ONE 11, 1–15.

Dias, L.C.P., Macedo, M.N., Costa, M.H., Coe, M.T., Neill, C., 2015. Effects of land cover change on evapotranspiration and streamflow of small catchments in the Upper Xingu River Basin, Central Brazil. Journal of Hydrology: Regional Studies 4, 108–122.

Doorenbos, J., Pruitt, W.O., 1977. Guidelines for predicting crop water requirements. FAO Irrigation and Drainage Paper No. 24, Rome, Italy.

Eichelmann, E., Wagner-Riddle, C., Warland, J., Deen, B., Voroney, P., 2016. Comparison of carbon budget, evapotranspiration, and albedo effect between the biofuel crops switchgrass and corn. Agriculture, Ecosystems and Environment 231, 271–282.

Figueiredo, F.P. De, Mantovani, E.C., Soares, A.A., Costa, L.C., Ramos, M.M., Oliveira, F.G., 2006. Produtividade e qualidade da banana prata anã, influenciada por lâminas de água, cultivada no Norte de Minas Gerais. Revista Brasileira de Engenharia Agrícola e Ambiental 10, 798–803.

Freitas, E.M., Giovanelli, L.B., Delazari, F.T., Dos Santos, M.L., Pereira, S.B., Da Silva, D.J.H., 2017. Arugula production as a function of irrigation depths and potassium fertilization. Revista Brasileira de Engenharia Agricola e Ambiental 21, 197–202.

Gharsallah, O., Facchi, A., Gandolfi, C., 2013. Comparison of six evapotranspiration models for a surface irrigated maize agro-ecosystem in Northern Italy. Agricultural Water Management 130, 119–130.

Gheysari, M., Sadeghi, S.-H., Loescher, H.W., Amiri, S., Zareian, M.J., Majidi, M.M., Asgarinia, P., Payero, J.O., 2017. Comparison of deficit irrigation management strategies on root, plant growth and biomass productivity of silage maize. Agricultural Water Management 182, 126–138.

Gonzalez-Ollauri, A., Mickovski, S.B., 2017. Hydrological effect of vegetation against rainfall-induced landslides. Journal of Hydrology 549, 374–387.

Hernandez, F.B.T., Neale, C.M.U., Teixeira, A.H.C., Taghvaeian, S., Teixeira, A.H. de C., Taghvaeian, Taghvaeian, S., 2014. Determining large scale actual evapotranspiration using agrometeorological and remote sensing data

in the northwest of Sao Paulo State, Brazil. Acta Horticulturae 1038, 263–270.

Huang, Y., Chen, Z. xin, Yu, T., Huang, X. zhi, Gu, X. fa, 2018. Agricultural remote sensing big data: Management and applications. Journal of Integrative Agriculture 17, 1915–1931.

INMET - Instituto Nacional de Meteorologia, 2018. Brazilian climatological normals 1981-2010. Brasília, Brazil. http://www.inmet.gov.br/portal/ (accessed 12.17.18).

IRRIGER - Irrigation management and engineering, 2018. IRRIGER quem somos http://www.irriger.com.br/en-US/ (accessed 7.27.18).

Kamali, M.I., Nazari, R., 2018. Determination of maize water requirement using remote sensing data and SEBAL algorithm. Agricultural Water Management 209, 197–205.

Laraby, K.G., Schott, J.R., 2018. Uncertainty estimation method and Landsat 7 global validation for the Landsat surface temperature product. Remote Sensing of Environment 216, 472–481.

Lasdon, L., Waren, A.., Jain, A., Ratner, M., 1978. Design and testing of a generalized reduced gradient code for nonlinearprogramming. ACM Transactions on Mathematical Software 4, 34–50.

Li, C., Wu, P., Li, X., Zhou, T., Sun, S., Wang, Y., Luan, X., Yu, X., 2017. Spatial and temporal evolution of climatic factors and its impacts on potential evapotranspiration in Loess Plateau of Northern Shaanxi, China. Science of The Total Environment 589, 165–172.

Li, H., Zheng, L., Lei, Y., Li, C., Liu, Z., Zhang, S., 2008. Estimation of water consumption and crop water productivity of winter wheat in North China Plain using remote sensing technology. Agricultural Water Management 95, 1271–1278.

Li, P., Jiang, L., Feng, Z., 2013. Cross-comparison of vegetation indices derived from landsat-7 enhanced thematic mapper plus (ETM+) and landsat-8 operational land imager (OLI) sensors. Remote Sensing 6, 310–329.

Liaqat, U.W., Choi, M., Awan, U.K., 2015. Spatio-temporal distribution of actual evapotranspiration in the Indus Basin Irrigation System. Hydrological Processes 29, 2613–2627.

Mantovani, E., Delazari, F., Dias, L., Assis, I., Viera, G., Landim, F., 2013. Yield and water use efficiency for two sweet potato cultivars depending on irrigation depths. Horticultura Brasileira 31, 602–606.

Mantovani, E.C., Costa, L.C., 1998. Manual do SISDA 2.0, in: Workshop Internacional Sobre Manejo Integrado Das Culturas e Recursos Hídricos.

SRH/UFV, Brasília, DF, p. 153.

Masek, J.G., Vermote, E.F., Saleous, N.E., Wolfe, R., Hall, F.G., Huemmrich, K.F., Gao, F., Kutler, J., Lim, T., 2006. A Landsat surface reflectance dataset. IEEE Geoscience and Remote Sensing Letters 3, 68–72.

Medeiros, S. de S., Soares, A.A., Ramos, M.M., Mantovani, E.C., Souza, J.A.A. de, 2003. Avaliação do manejo de irrigação no Perímetro Irrigado de Pirapora, MG. Revista Brasileira de Engenharia Agrícola e Ambiental 7, 80–84.

Nagy, A., Fehér, J., Tamás, J., 2018. Wheat and maize yield forecasting for the Tisza river catchment using MODIS NDVI time series and reported crop statistics. Computers and Electronics in Agriculture 151, 41–49.

Nash, J.E., Sutcliffe, J. V, 1970. River flow forecasting through conceptual models part I - A discussion of principles*. Journal of Hydrology 10, 282–290.

Nguy-Robertson, A., Gitelson, A., Peng, Y., Walter-Shea, E., Leavitt, B., Arkebauer, T., 2013. Continuous monitoring of crop reflectance, vegetation fraction, and identification of developmental stages using a four band radiometer. Agronomy Journal 105, 1769–1779.

Oguntunde, P.G., Van De Giesen, N., 2004. Crop growth and development effects on surface albedo for maize and cowpea fields in Ghana, West Africa. International Journal of Biometeorology 49, 106–112.

Olivera-Guerra, L., Mattar, C., Merlin, O., Durán-Alarcón, C., Santamaría-Artigas, A., Fuster, R., 2017. An operational method for the disaggregation of land surface temperature to estimate actual evapotranspiration in the arid region of Chile. ISPRS Journal of Photogrammetry and Remote Sensing 128, 170–181.

Paço, T.A., Pôças, I., Cunha, M., Silvestre, J.C., Santos, F.L., Paredes, P., Pereira, L.S., 2014. Evapotranspiration and crop coefficients for a super intensive olive orchard. An application of SIMDualKc and METRIC models using ground and satellite observations. Journal of Hydrology 519, 2067–2080.

Peña, M.A., Brenning, A., 2015. Assessing fruit-tree crop classification from Landsat-8 time series for the Maipo Valley, Chile. Remote Sensing of Environment 171, 234–244.

Piccinni, G., Ko, J., Marek, T., Howell, T., 2009. Determination of growth-stage-specific crop coefficients (Kc) of maize and sorghum. Agricultural Water Management 96, 1698–1704.

Qin, Y., Xiao, X., Dong, J., Zhou, Y., Zhu, Z., Zhang, G., Du, G., Jin, C., Kou, W., Wang, J., Li, X., 2015. Mapping paddy rice planting area in cold temperate

climate region through analysis of time series Landsat 8 (OLI), Landsat 7 (ETM+) and MODIS imagery. ISPRS Journal of Photogrammetry and Remote Sensing 105, 220–233.

Ranum, P., Peña-Rosas, J.P., Garcia-Casal, M.N., 2014. Global maize production, utilization, and consumption. Annals of the New York Academy of Sciences 1312, 105–112.

Rawat, K.S., Bala, A., Singh, S.K., Pal, R.K., 2017. Quantification of wheat crop evapotranspiration and mapping: A case study from Bhiwani District of Haryana, India. Agricultural Water Management 187, 200–209.

Richardson, A.D., Keenan, T.F., Migliavacca, M., Ryu, Y., Sonnentag, O., Toomey, M., 2013. Climate change, phenology, and phenological control of vegetation feedbacks to the climate system. Agricultural and Forest Meteorology 169, 156–173.

Richter, K., Hank, T.B., Atzberger, C., Mauser, W., 2011. Goodness-of-fit measures: what do they tell about vegetation variable retrieval performance from Earth observation data. Proc. of SPIE: Remote Sensing for Agriculture, Ecosystems, and Hydrology XIII 8174, 81740R–1–81740R–11.

Rouse, J.W., Hass, R.H., Schell, J.A., Deering, D.W., 1973. Monitoring vegetation systems in the great plains with ERTS, in: Third ERTS Symposium. NASA, Washington, DC, pp. 309-317.

Roy, D.P., Wulder, M.A., Loveland, T.R., C.E., W., Allen, R.G., Anderson, M.C., Helder, D., Irons, J.R., Johnson, D.M., Kennedy, R., Scambos, T.A., Schaaf, C.B., Schott, J.R., Sheng, Y., Vermote, E.F., Belward, A.S., Bindschadler, R., Cohen, W.B., Gao, F., Hipple, J.D., Hostert, P., Huntington, J., Justice, C.O., Kilic, A., Kovalskyy, V., Lee, Z.P., Lymburner, L., Masek, J.G., McCorkel, J., Shuai, Y., Trezza, R., Vogelmann, J., Wynne, R.H., Zhu, Z., 2014. Landsat-8: Science and product vision for terrestrial global change research. Remote Sensing of Environment 145, 154–172.

Rozenstein, O., Qin, Z., Derimian, Y., Karnieli, A., 2014. Derivation of land surface temperature for Landsat-8 TIRS using a split window algorithm. Sensors 14, 5768–5780.

Santos, H.G. dos, Carvalho-Júnior, W. de, Dart, R. de O., Áglio, M.L.D., Sousa, J.S. de., Pares, J.G., Fontana, A., Martins, A.L. da S., Oliveira, A.P. de O., 2011. O novo mapa de solos do Brasil: Legenda atualizada, Embrapa. Rio de Janeiro.

Santos, O.F., Cunha, F.F., Taira, T.L., Souza, E.J., Leal, A.J.F., 2018. Increase in pea productivity associated with irrigation management. Horticultura Brasileira 36, 178–183.

Sayago, S., Ovando, G., Bocco, M., 2017. Landsat images and crop model for

evaluating water stress of rainfed soybean. Remote Sensing of Environment 198, 30–39.

Schmidt, G., Jenkerson, C., Masek, J., Vermote, E., Gao, F., 2013. Landsat Ecosystem Disturbance Adaptive Processing System (LEDAPS) Algorithm Description, Open-file Report 2013-1057.

Silva, B.B. da, Braga, A.C., Braga, C.C., Oliveira, L.M.M. de, Montenegro, S.M.G.L., Barbosa Junior, B., de Oliveira, L.M.M., Montenegro, S.M.G.L., Junior, B.B., 2016. Procedures for calculation of the albedo with OLI-Landsat 8 images: Application to the Brazilian semi-arid. Revista Brasileira de Engenharia Agrícola e Ambiental 20, 3–8.

Silva, G.H., Ferreira, M.G., Pereira, S.B., Delazari, F.T., Silva, D.J.H., 2018. Response of bell pepper crop subjected to irrigation depths calculated by different methodologies. Revista Brasileira de Engenharia Agrícola e Ambiental 22, 45–50.

Singh, A.K., Dubey, O.P., Ghosh, S.K., 2016. Irrigation scheduling using intervention of Geomatics tools - A case study of Khedli minor. Agricultural Water Management 177, 454–460.

Singh, A.K., Singh, R.M., Velmurugan, A., Kumar, R.R., Biswas, U., 2018. Harnessing Genetic Resources in Field Crops for Developing Resilience to Climate Change, in: Biodiversity and Climate Change Adaptation in Tropical Islands. Elsevier Inc., pp. 597–621.

Souza, J. de, Ramos, M., Soares, A., 2005. Effects of the fertirrigation with urban wastewater on coffee yield. Revista Brasileira de Engenharia Agrícola e Ambiental 128–132.

Statista – The portal for statistics, 2018. Worldwide production of grain in 2017/18, by type (in million metric tons) .https://www.statista.com/statistics/263977/world-grain-production-by-type/ (accessed 7.27.18).

Sun, Z., Wei, B., Su, W., Shen, W., Wang, C., You, D., Liu, Z., 2011. Evapotranspiration estimation based on the SEBAL model in the Nansi Lake Wetland of China. Mathematical and Computer Modelling 54, 1086–1092.

Teixeira, A., Hernandez, F., Lopes, H., 2012. Application of Landsat images for quantifying the energy balance under conditions of land use changes in the semi-arid region of Brazil, in: SPIE Remote Sensing. pp. 1–9.

Teixeira, A.H. de C., Hernandez, F.B.T., Andrade, R.G., Leivas, J.F., Victoria, D. de C., Bolfe, E.L., 2015. Corn water variables assessments from earth observation data in the São Paulo state, southeast Brazil. Journal of Hydraulic Engineering 1, 1–11.

Teixeira, A.H. de C., Hernandez, F.B.T., Lopes, H.L., Scherer-Warren, M., Bassoi, L.H., 2013a. Modelagem espaçotemporal dos componentes dos balanços de energia e de água no Semiárido brasileiro. Campinas. 32p. (Documents, 99)

Teixeira, A.H. de C., Leivas, J.F., Andrade, R.G., Hernandez, F.B.T., Momesso, F.R.A., 2015. Modelling radiation and energy balances with Landsat 8 images under different thermohydrological conditions in the Brazilian semi-arid region, in: Remote Sensing for Agriculture, Ecosystems, and Hydrology. p. 96370U.

Teixeira, A.H. de C., Leivas, J.F., Hernandez, F.B.T., Franco, R.A.M., 2017. Large-scale radiation and energy balances with Landsat 8 images and agrometeorological data in the Brazilian semiarid region. Journal of Applied Remote Sensing 11, 016030.

Teixeira, A.H. de C., Scherer-Warren, M., Hernandez, F.B.T., Andrade, R.G., Leivas, J.F., 2013b. Large-scale water productivity assessments with MODIS images in a changing semi-arid environment: A brazilian case study. Remote Sensing 5, 5783–5804.

Teixeira, A.H.C. de C., 2010. Determining regional actual evapotranspiration of irrigated crops and natural vegetation in the São Francisco river basin (Brazil) using remote sensing and Penman-Monteith equation. Remote Sensing 2, 1287–1319.

Teixeira, A.H.C., 2012. Modelling evapotranspiration by remote sensing parameters and agro-meteorological stations, in: Neale, C.M.U., Cosh, M.H. (Eds.), Remote Sensing and Hydrology 2010 Symposium. International Association of Hydrological Sciences, Jackson Hole, Wyoming, pp. 154–157.

USGS - United States Geological Survey, 2016. Landsat 8 (L8): Data Users Handbook, USGS. https://landsat.usgs.gov/sites/default/files/documents/Landsat8DataUsersHandbook.pdf (accessed 1.12.18).

USGS - United States Geological Survey, 2018a. Landsat 7 (L7) data users handbook Version 1.0 June 2018. https://landsat.usgs.gov/sites/default/files/documents/LSDS-1927_L7_Data_Users_Handbook.pdf (accessed 10.17.18).

USGS - United States Geological Survey, 2018b. Landsat8 Surface Reflectance code (LaSRC) Version 4.3 PRODUCT: Product Guide. https://landsat.usgs.gov/sites/default/files/documents/lasrc_product_guide.pdf (accessed 1.12.18).

Vicente, M.R., Mantovani, E.C., Fernandes, A.L.T., Neves, J.C.L., Figueredo, E.M., Delazari, F.T., 2017. Spacial distribution of fertigated coffee root system. Ciencia e Agrotecnologia 41, 72–80.

Vieira, G.H.S., Mantovani, E.C., Sediyama, G.C., Delazari, F.T., 2014. Produtividade e rendimento industrial da cana-de-açúcar em função de lâminas de irrigação. Bioscience Journal 30, 55–64.

Wang, R., Cherkauer, K., Bowling, L., 2016. Corn response to climate stress detected with satellite-based NDVI time series. Remote Sensing 8, 1–22.

Wukelic, G.E., Gibbons, D.E., Martucci, L.M., Foote, H.P., 1989. Radiometric calibration of Landsat Thematic Mapper thermal band. Remote Sensing of Environment 28, 339–347.

Yi, Z., Zhao, H., Jiang, Y., 2018. Continuous daily evapotranspiration estimation at the field-scale over heterogeneous agricultural areas by fusing ASTER and MODIS data. Remote Sensing 10, 1694.

Zhang, H., Sun, J., Xiong, J., 2017. Spatial-temporal patterns and controls of evapotranspiration across the Tibetan Plateau (2000-2012). Advances in Meteorology 2017.

Zhang, X., Yan, G., Li, Q., Li, Z.L., Wan, H., Guo, Z., 2006. Evaluating the fraction of vegetation cover based on NDVI spatial scale correction model. International Journal of Remote Sensing 27, 5359–5372.

CHAPTER 2

Corn yield estimation at farm level in Brazil using a new and simplified remote sensing approach

ABSTRACT

The forecast of crop yield at field-level is of great interest to farmers, essential for decision-making and agricultural economic return prediction. Thus, the aim of this study was to evaluate the performance of a methodology for corn yield prediction, initially validated for North American corn production conditions, in an irrigated plantation in the western region of Bahia, Brazil. This methodology integrate a time series of basal crop coefficient (Kcb) estimated from Soil Adjusted Vegetation Index (SAVI) into a simple model based on the water productivity, presented in the FAO-66 manual. For this purpose, was used an extensive field-level data set of 52 center pivots cultivated with corn (*Zea mays* L.) for four consecutive growing seasons (2013 to 2016). Landsat 7 ETM+ and Landsat 8 OLI surface reflectance images acquired during the corn growth development (normally April-October) were used. Soil-adjusted Vegetation Index (SAVI) was generated from the images to determine Kcb. The estimation performance was assessed using RMSE, RRMSE, MBE, MAE, and r^2. Results of the study revealed that the difference between predicted yield values and actual ones ranged between -12.2% and 18.8%, but with the majority of estimates remaining between -10 and 10%, considering a single harvest index (HI) for the hybrids cultivated in the growing season of 2014, 2015 and 2016. After the reanalysis

(grouping of similar hybrids and use of a specific HI for each one) the performance of predictions increased, especially for Pioneer hybrids, with the majority of the differences, between predicted yield values and measured, remained between -5 and 5%. The results of this research showed that it is essential to work with different harvest indices when different hybrids are studied. Lastly, the identification of the beginning and the end of the growing cycle is the key point of this approach.

Keywords: Corn yield, biomass, remote sensing data, basal crop coefficient, SAVI.

1. INTRODUCTION

Estimation prior to harvest plays a vital role in agricultural development worldwide (Jin et al., 2018), being fundamental to informing world food security, decision-making, and crop yield management (Mokhtari et al., 2018; Xie et al., 2017). So, it is necessary to accurately estimate crop yields before harvest (Jin et al., 2018). Pre-harvest estimates of the aboveground dry biomass (AGB) and/or yield are usually based on experimental evidence and little is known about the yield gap between biologically obtainable and actual achievable on-farm AGB yields (Richter et al., 2016). Another way to estimate AGB and yield is through the use of agrohydrological models (Mokhtari et al., 2018), which works very well at field scales, but input data and boundary conditions uncertainties increase with the increase in scale (Huang et al., 2013).

To overcome these problems, remotely sensed data have been used. Orbital remote sensing allows obtaining data at large scales and can provide temporally and spatially continuous information regarding crop biophysical variables and estimates of their final productivities (Battude et al., 2016; Frampton et al., 2013; Lin et al., 2009; Veloso et al., 2017). Remote sensing (RS) data, if coupled with crop growth models, as in the FAO 66 Manual, can be more effective

to estimate crop yield. Crop growth models primarily simulate the growth and development of crops, and they encompass the primary biophysical and biochemical processes in the soil-crop-atmosphere system, such as photosynthesis, respiration, transpiration, dry matter partitioning and senescence (Wang et al., 2013). Thus, crop growth models can be powerful tools for assessing the impacts of environmental conditions and genetic potential on crop production (Campos et al., 2018).

Given the great potential for yield estimation from the combination of crop growth models with RS data, several authors have sought to develop their models, a recent example is a model developed by Campos et al. (2018). These authors proposed a model based on the use of optical RS to estimate crop biomass production and grain yield of corn and soybean. The model uses the relationship between basal crop coefficient (Kcb) accumulated and dry biomass production, where Kcb accumulated is estimated from Soil-adjusted vegetation index (SAVI) (Huete, 1988), by means of a linear equation (Campos et al., 2017) and numerical integration.

The potential AGB was obtained from the Kcb accumulated in certain period of time (e.g., using a growing degree days value as reference), multiplied by a parameter of water use efficiency for biomass production (WUE_B*, in gm^{-2}). However, this AGB value is potential and not real, because water stress affects biomass production by reducing the rate of increase in canopy cover and limiting plant transpiration (Steduto et al., 2012). The first effect (i.e., reducing the rate of increase in canopy cover) is computed in SAVI values, so it is already included in the actual value of Kcb. However, the effect of water stress on canopy transpiration should be considered using a water stress coefficient, which in the model of Campos et al. (2018) refers to FAO 56 methodology (Allen et al., 1998).

Another possible impact on biomass is related to air temperature. Thus, in the same way as in water stress, the air temperature stress is included based on temperature stress coefficient. Only the cold stress is considered in the formulation, because the effect of high temperatures on crop development is already included in the parameterization of the water stress coefficient (Campos et al., 2018). These two coefficients, along with potential AGB values, allow the

real AGB to be obtained. The yield is estimated by multiplying the real AGB by a harvest index (HI).

Regarding the corn crop (*Zea mays* L.), it is the largest global cereal crop in production, with 1,036.07 million metric tons produced in the 2017/18 harvest (Statista, 2018). This crop is grown throughout the world, with the United States, China and Brazil being the top three corn-producing countries in the world, and it can be processed into a variety of food and industrial products, including starch, sweeteners, oil, beverages, glue, industrial alcohol, and fuel ethanol (Ranum et al., 2014). That is why corn is one of the most important cereal crops in the world (Przybylska et al., 2018).

The study was conducted in western Bahia, Brazil. Corn is considered as the third most important crop of the western region, and in the 2016/17 harvest it occupied an area corresponding to 180,000 ha, with a production of 1,404,000 tons and yield of 130 t ha^{-1} (AIBA, 2017). This region in the 2015/16 harvest occupied 31% of the area planted in the state but was responsible for 77% of what was harvested (AIBA (Association of Farmers and Irrigators of Bahia), 2016).

The use of orbital RS data in agriculture, especially in large-scale agriculture (e.g., farms with many central pivots) is essential to decision-making, crop development monitoring, identification of biotic and abiotic stresses, and obviously for AGB and yield estimation. However, little research has been conducted in Brazil with corn yield estimation using data from large areas, most of it is focused on small experimental plots and, when extrapolated to real situations, has low efficiency.

Considering these aspects, the main objective was to estimate corn yield at farm-level in Brazil using a new and simplified RS approach, based on FAO-66 approach and SAVI, initially validated for North American corn production conditions (Campos et al., 2018). Specific objectives refers to the changes made in the original model, namely: (i) use of a different methodology for water stress coefficient determination instead of FAO-56 approach, (ii) definition of Kcb accumulation interval based on growing degree days (GDD) instead of SAVI values and, (iii) use of an empirical HI based on previous harvests and considering the possible effect of the corn variety in the actual values of HI.

2. MATERIALS AND METHODS

2.1. Study area

This study focused on an agricultural area belonging to a commercial farm, located in the municipality of São Desidério, in the western region of Bahia state, Brazil (Figure 1a). The area is located in the rectangle bounded by the coordinate pairs: lower left 12°28'08"S; 45°45'12"W and upper right 12°25'40"S; 45°34'55"W, reference system of geographic coordinates, Datum WGS-84, with an average altitude of 750 m above the sea level (Figure 1b).

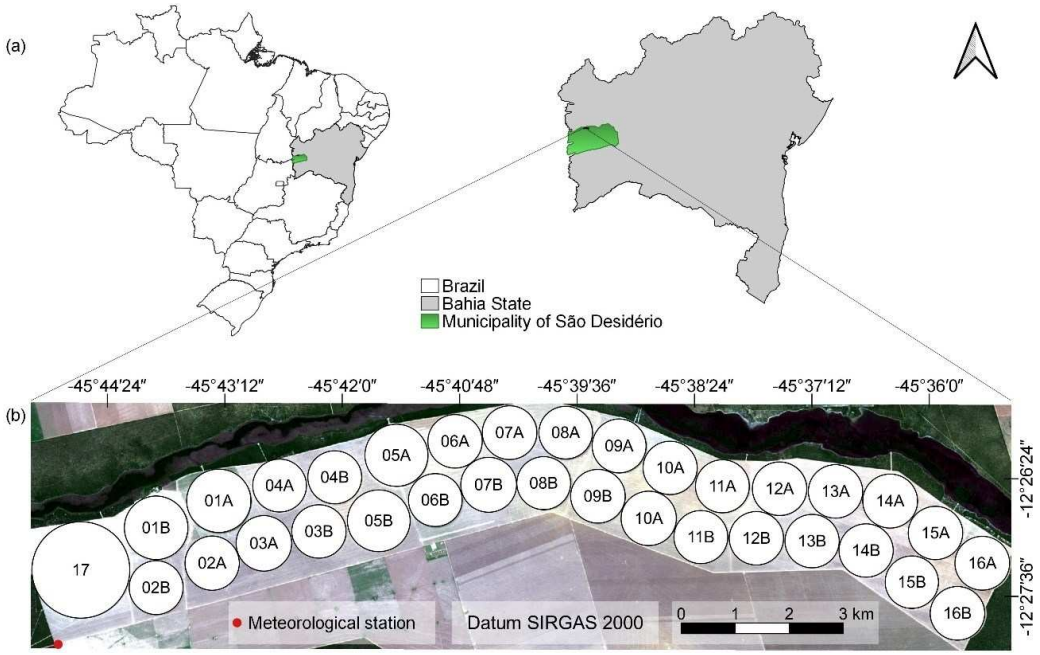

Figure 1. Location of study area (a), nomenclature and distribution of the center pivots in the fields (b), and meteorological station position.

According to Köppen's climatic classification (Alvares et al., 2013), the climate of region is Aw, tropical climate, with rainy season in summer and dry winter, with an annual normal precipitation in the region of 1003.4 mm (INMET (Instituto Nacional de Meteorologia), 2018), concentrated in the rainy season (October to April). The predominant soil type in the region of the fields is Yellow

Latosol (Santos et al., 2011). The farm has 17 center pivots (CP), 16 of them towable, indicated by the letters A and B in Figure 1b, being able to irrigate an area of 1598 hectares. Due to phytosanitary issues, the same CP is not cultivated in two consecutive seasons with the same crop. Major crops grown in these fields are corn (studied crop), soybean and cotton.

2.2. Field data

The study uses data of four corn growing seasons (2013, 2014, 2015 and 2016) collected by the company IRRIGER - Irrigation management and engineering (http://www.irriger.com.br/en-US/). This company was founded in 2005 and is market leader in Brazil in its area of expertise. Since its foundation, it has already monitored more than 690 farms, which corresponds to more than 2.5 million hectares. Currently, it monitors more than 4,123 center pivots and lateral move machines, center pivots being the great majority. One important point about the company refers to the field data. Since its foundation, it provides its field data for universities and research institutions to carry out several studies in the field of irrigation, mainly involving the crops of corn, bean, soybean, arabica coffee, cotton, sugarcane, wheat and potato (IRRIGER (Irrigation management and engineering), 2018).

2.2.1. Meteorological data

Meteorological data such as air temperature (Tm, °C), wind speed at 2 m height (U2, m s^{-1}), radiation (Ra, MJ m^2 dia^{-1}), relative humidity (RH, %) and rainfall (P, mm), were obtained from the automated meteorological station (Davis, Vantage Pro Plus, Hayward - CA), located near the CP (Figure 1b). These data were used to determine the daily reference evapotranspiration (ETo) using the Penman-Monteith equation (Allen et al., 1998) and then corn actual evapotranspiration (ET). Besides that, they were also used to determine the temperature stress coefficient.

2.2.2. Corn crop data

Collected data referring to corn crop growth were the sowing date (SD), harvest date (HD), duration of the cycle (DC), planting density (PD), grain yield (GY), and cultivated hybrid name (CH) for each center pivot (CP) field in the four harvests (Tables 1 and 2). Harvests are performed using harvesting machines from John Deere, 9670 STS model, and yield is measured by weighing the truck containing the harvested grains.

Table 1. Sowing date (SD), harvest date (HD), duration of the cycle (DC), planting density (PD), grain yield (GY) and cultivated hybrid name (CH) for each center pivot (CP) analyzed in the growing seasons of 2013 and 2014

CP	SD	HD	DC days	PD* pl ha^{-1}	GY Mg ha^{-1}	CH	CP	SD	HD	DC days	PD* pl ha^{-1}	GY Mg ha^{-1}	CH
2013							2014						
01A	04/23	09/05	135	68,000	9.87	H5	01B	05/23	10/10	140	72,000	10.68	H8
02A	04/29	09/05	129	68,000	5.38	H4	02B	05/26	10/10	137	72,000	11.74	H9
03A	04/27	09/05	131	68,000	4.98	H4	03B	05/27	10/21	147	72,000	11.24	H9
04A	04/25	09/05	133	68,000	9.89	H5	04B	05/31	10/21	143	72,000	11.12	H9
05A	04/26	09/05	132	68,000	5.33	H4	05B	05/29	10/21	145	68,000	11.55	H3
06B	05/10	09/16	129	68,000	6.04	H4	06A	06/03	10/26	145	68,000	10.06	H3
07B	05/10	09/16	129	68,000	6.94	H4	07A	06/04	10/26	144	68,000	10.72	H3
08B	05/09	09/16	130	68,000	6.84	H4	08A	06/05	10/26	143	68,000	10.09	H3
09B	05/08	09/16	131	68,000	7.64	H4	09A	06/07	10/26	141	70,000	11.21	H7
10B	05/05	09/16	134	68,000	6.95	H4	10A	06/06	10/26	142	70,000	11.50	H7
11B	05/03	09/16	136	68,000	6.34	H4	11A	06/09	10/26	139	70,000	10.88	H7
12B	05/01	09/16	138	68,000	7.16	H4	12A	06/10	10/22	134	70,000	10.83	H6

*The row spacing adopted at the farm is 0.5 m. *Hybrids names:* Dekalb DKB 390 Pro (H1), Dow AgroSciences 2B810 (H2), Pioneer 30F35 (H3), Pioneer 30F53 (H4), Pioneer 3431 (H5), Pioneer P2830 (H6), Pioneer P3646 (H7), Maximus Viptera 3 (H8), Status Viptera 3 (H9) and Supremo Viptera (H10).

Table 2. Sowing date (SD), harvest date (HD), duration of the cycle (DC), planting density (PD), grain yield (GY) and cultivated hybrid name (CH) for each center pivot (CP) analyzed in the growing seasons of 2015 and 2016

CP	SD	HD	DC days	PD* pl ha^{-1}	GY Mg ha^{-1}	CH	CP	SD	HD	DC days	PD* pl ha^{-1}	GY Mg ha^{-1}	CH
2015							2016						
01A	05/20	10/17	150	68,000	10.55	H1	03B	05/06	09/25	142	70,000	12.61	H2
04A	05/21	10/17	149	70,000	11.05	H7	04B	05/05	10/04	152	72,000	12.70	H9
05A	04/25	09/16	144	72,000	12.18	H9	05B	05/04	10/04	153	72,000	13.30	H9
06B	05/28	10/19	144	72,000	11.16	H9	06A	05/02	09/18	139	74,000	11.65	H6
07B	05/27	10/18	144	72,000	12.14	H9	07A	04/29	09/14	138	74,000	11.80	H6
08B	05/26	10/17	144	72,000	12.42	H9	08A	04/27	09/09	135	74,000	11.58	H7
09B	05/25	10/16	144	72,000	12.99	H9	09A	04/25	09/25	153	72,000	12.38	H3
10B	05/24	10/15	144	72,000	12.49	H9	10A	04/22	09/25	156	68,000	12.10	H3
11B	05/23	10/14	144	72,000	12.79	H9	11A	04/20	09/08	141	72,000	12.94	H10
12A	05/09	10/04	148	72,000	11.85	H9	12B	04/04	08/31	149	72,000	12.05	H9
13A	05/13	10/05	145	72,000	13.02	H9	13B	04/06	08/31	147	72,000	12.80	H9
14A	05/14	10/08	147	72,000	12.41	H9	14B	04/12	09/05	146	72,000	12.45	H9
15A	05/15	10/08	146	72,000	12.49	H9	15B	04/14	09/25	144	72,000	13.50	H9
16A	05/16	10/08	145	72,000	12.26	H9	16B	04/18	09/24	159	72,000	13.00	H9

*The row spacing adopted at the farm is 0.5 m. *Hybrids names:* Dekalb DKB 390 Pro (H1), Dow AgroSciences 2B810 (H2), Pioneer 30F35 (H3), Pioneer 30F53 (H4), Pioneer 3431 (H5), Pioneer P2830 (H6), Pioneer P3646 (H7), Maximus Viptera 3 (H8), Status Viptera 3 (H9) and Supremo Viptera (H10).

2.2.3. Actual corn evapotranspiration (ET) and applied irrigation data

The CP evaluated in this study are supervised and managed by IRRIGER Company. This company performs the calculation of actual crop evapotranspiration (ET) using the method called modified FAO method (MFAO) (Mantovani and Costa, 1998), based on method proposed by Doorenbos and Pruitt (1977). Doorenbos and Pruitt's method is simple and widely used for potential evapotranspiration estimation and practical irrigation water management. To increase the performance of Doorenbos and Pruitt (1977) method and make it more realistic, but without the complexity of FAO-56 dual-Kc approach (Allen et al., 1998), Mantovani and Costa (1998) added the water stress coefficient (K_S) and localized water application coefficient (K_L) (Equation 1).

$$ET = ETo \times K_c \times K_S \times K_L \qquad (1)$$

where ET is the actual crop evapotranspiration (mm d^{-1}), ETo is the reference evapotranspiration according to Allen et al. (1998) (mm d^{-1}), Kc is the crop coefficient, K_S is the water stress coefficient (Bernardo, 1989) and K_L is the localized water application coefficient (Keller and Bliesner, 1990); for the CP, K_L value is 1 (100% of cultivated area receives irrigation water).

MFAO method has been applied and validated by many researchers in Brazil for different crops and irrigation systems (Figueiredo et al., 2006; Mantovani et al., 2013; Medeiros et al., 2003; Souza et al., 2005b; Vieira et al., 2014). In terms of practical application, this method is used for ET estimation in irrigated plantations in Brazil, Paraguay, Argentina, Chile, Bolivia, Peru, Nicaragua, Venezuela, Mexico, United States, Nigeria, Sudan, Turkey, Ukraine, Russia and Laos (IRRIGER (Irrigation management and engineering), 2018).

2.3. Satellite Images - Landsat 8 OLI and Landsat 7 ETM+ data

Cloud-free satellite images of Enhanced Thematic Mapper Plus (ETM+) sensor (Landsat 7) and Operational Land Imager (OLI) sensor (Landsat 8), WRS-

2 path 220, row 069 for the corn season (usually April-October) for each year (2013, 2014, 2015 and 2016) were downloaded from the archives of USGS Earth Explorer website (https://espa.cr.usgs.gov/). Surface reflectance (SRe, top of atmosphere reflectance (TOA) corrected for atmospheric effect) products generated by the USGS on-demand processing system EROS Science Processing Architecture (ESPA) were used.

Landsat 7 Surface Reflectance data are generated from the Landsat Ecosystem Disturbance Adaptive Processing System (LEDAPS) Algorithm, described in Masek et al. (2006) and Schmidt et al. (2013). The corrections are based on the Second Simulation of a Satellite Signal in the Solar Spectrum (6S) (Kotchenova and Vermote, 2007; Vermote et al., 1997). Landsat 8 Surface Reflectance data are generated from the Landsat Surface Reflectance Code (LaSRC). LaSRC makes use of the coastal aerosol band to perform aerosol inversion tests, uses auxiliary climate data from MODIS and uses a unique radiative transfer model. Details about LaSRC and Landsat 8 Surface Reflectance data products can be found in the Landsat 8 Surface Reflectance Product Guide (USGS, 2018a).

The Landsat 7 and 8 acquisitions are precision terrain corrected (termed Level 1T) with processing that includes radiometric correction, systematic geometric correction, precision correction using ground control, and the use of a digital elevation model to correct parallax error due to local topographic relief (Lee et al., 2004; Storey et al., 2014). Access to and full descriptions of the products can be found online through the Landsat data Users Handbooks – USGS. The gaps of the Landsat 7 images (Chen et al., 2011), which in some periods of the corn growing season reached only the CP 01A, 01B, 02B, were converted to No Data values and had no influence on the statistical analysis.

We acquired 57 cloud-free images of the study area including both OLI and ETM+ sensors for the crop seasons of 2013, 2014, 2015 and 2016. The number of images used for AGB estimation varied by CP and by season, according to different sowing dates and presence of clouds on the area of interest (center pivot). However, two criteria were adopted: (i) using at least four images per central pivot, and (ii) among the four images, there must be an image with

date close to the beginning, middle and end of the crop cycle, in order to adequately describe it. The date with image available can be seen in Figure 2.

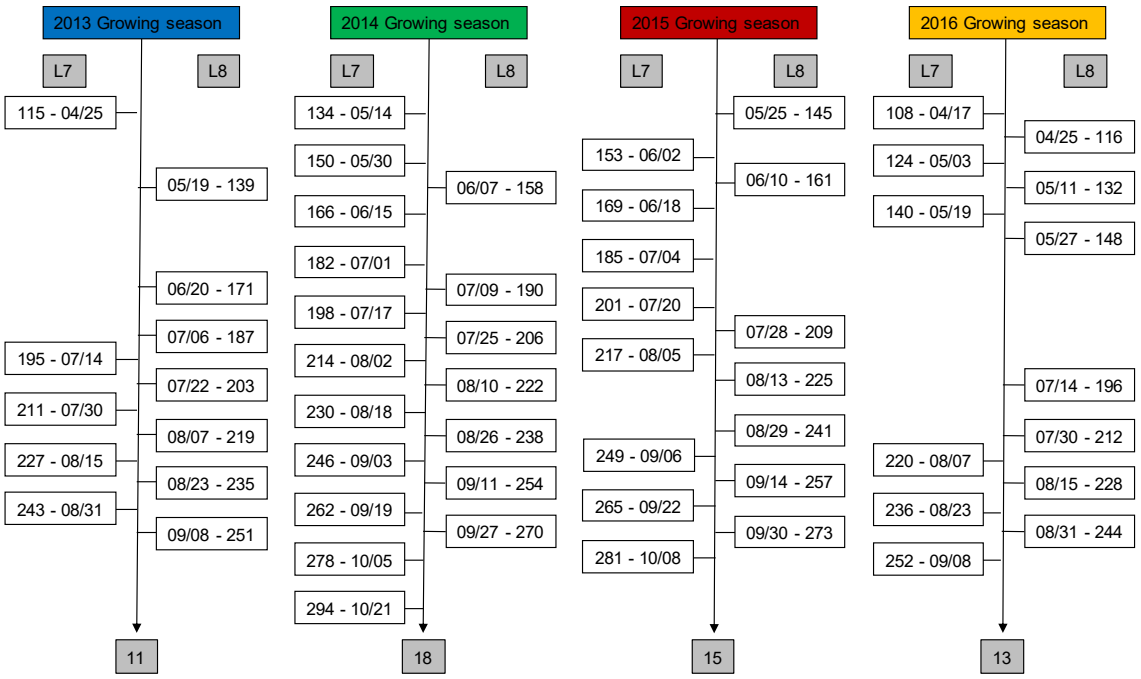

Figure 2. Day of year (DOY) with the respective date of cloud-free images for Landsat 7 (L7) and 8 (L8) for the study area during the growing seasons of 2014, 2015 and 2016, with the respective number of total images.

2.4. Biomass model general description

The model used in the present study was developed by Campos et al. (2018) using data of 11 consecutive corn growing seasons in Nebraska, USA. The formulation of the model was based on the methodology for AGB determination presented in the FAO-66 manual (Steduto et al., 2012) and on the work of Campos et al. (2017), about Kcb based on reflectance data. The main idea of the model is the real determination of AGB and crop yield, using a new concept of water productivity (WP) and RS data. A sequential description up to the final model equation is shown below.

The yield response to water approach adopted in the FAO Irrigation and Drainage Paper No. 33 (Doorenbos and Kassam, 1979) linked the reduction in the yield to a proportional reduction in evapotranspiration (transpiration and soil evaporation). The approach has drawbacks as a result of the aggregation of variables, that is, final yield is a function of the evapotranspiration rather than transpiration only. Thus, FAO 66 (Steduto et al., 2012), maintaining the original concept of a direct link between crop water use and crop yield, brings the estimation of AGB production directly from actual crop transpiration through a WP parameter (Equation 2). This approach is adopted in AquaCrop Model (Raes et al., 2018).

$$AGB = WP \times \sum Tr \qquad (2)$$

where AGB is the aboveground dry biomass produced cumulatively (kg m^{-2}), Tr is the crop transpiration (mm or m^3 per unit surface) and WP is the water productivity parameter (kg of biomass m^{-2} mm^{-1}, or kg of biomass m^{-3} of water transpired).

WP (Equation 2) is a non-conservative parameter, meaning that it generally varies with cultivar and is location-specific, which limits its application without a previous calibration. On the other hand, WP, when normalized for evaporative demand (designated as WP*), behaves conservatively (Steduto et al., 2007), that is, it remains virtually constant over a range of environments, which allows its application to diverse locations and seasons (Steduto et al., 2012). The normalization of WP involves two environmental factors (Equation 3): evaporative demand of the atmosphere as represented by ETo, and air carbon dioxide concentration ([CO_2]) for the reference year 2000 (Pasquale Steduto et al., 2009; Vanuytrecht et al., 2014).

$$WP^* = \left[\frac{AGB}{\sum \frac{T_r}{ETo}} \right]_{[CO_2]} \qquad (3)$$

Campos et al. (2018) has left behind the most common definition of normalized water productivity (WP*) and adopted a more innovative concept for it, called normalized water use efficiency for biomass production (WUE_B*, in g m^{-2}), although they are mathematically equal (Equation 4).

$$WUE_B^* = \frac{AGB}{\sum_{i=1}^{n} \frac{T_{adj}}{ETo}} \qquad (4)$$

where AGB is the aboveground dry biomass on a ground area basis (g m^{-2}), T_{adj} is the accumulated value of the ratio between adjusted transpiration (mm), considering the eventual presence of water stress, and ETo is the reference evapotranspiration (mm).

Notice that the WUE_B* approach considers the normalization of T_{adj} by ETo which is conceptually equivalent to the Kcb (Campos et al., 2018), according to Equation 5. The WUE_B*, like WP*, is a conservative parameter (i.e., non-location-specific but crop-specific parameter) and is almost constant for a given crop regardless of environmental stresses and locations (Steduto et al., 2012).

$$WUE_B^* = \frac{AGB}{\sum_{i=1}^{n} \frac{T_{adj}}{ETo}} = \frac{AGB}{\sum_{i=1}^{n} Kcb_{adj}} \qquad (5)$$

Being a conservative parameter, the WUE_B* is slightly affected by crop management, but may be reduced by nutrient deficiencies, particularly nitrogen (Steduto et al., 2012). The Kcb is affected by water stress, so this effect can be computed using the water stress coefficient (K_{SW}). Besides that, the authors consider also the temperature (cold) as a stress in the production of biomass, which is represented by a temperature stress coefficient (K_{ST}). By adding these effects in Equation 5 and rearranging it (Equation 6), it is possible to determine the real AGB. All the terms and units have been previously described.

$$AGB = WUE_B^* \times (\sum K_{cb} \times K_{ST} \times K_{SW}) \qquad (6)$$

Yield (grain) is estimated as the product of the simulated AGB multiplied by HI (Equation 7). The HI represents the ratio of weight of grains/plant to the aboveground dry biomass (Caviglia et al., 2014).

$$Yield = AGB \times HI \qquad (7)$$

2.5. Model parameters description

2.5.1. Normalized water use efficiency for biomass production (WUE_B^*)

Campos et al. (2018) called Normalized water use efficiency for biomass production (WUE_B^*) what the researchers commonly refer to as normalized crop water productivity or water productivity normalized for ETo and CO_2 (WP*) (Raes et al., 2017, 2009; Razzaghi et al., 2017; Steduto et al., 2007; Vanuytrecht et al., 2014). The WP* is considered constant for a given climate and crop, and it was set between 13 and 18 g m^{-2} for C3 crops and between 28 and 33 g m^{-2} for C4 crops (Raes et al., 2009). Recently, these values have been updated: variation of 30 - 35 g m^{-2} for C4 crops and 15 - 20 g m^{-2} for C3 crops (Raes et al., 2017). The WUE_B^* for corn in this study was considered as 33.4 g m^{-2}, value found by Campos et al. (2018) and in accordance with the recommended in the FAO 66 approach (i.e., 33.7 g m^{-2}) (Steduto et al., 2012).

2.5.2. Basal crop coefficient (Kcb)

As indicated previously, the Kcb is a fundamental parameter of the model and it is estimated from Soil-adjusted vegetation index - SAVI (Huete, 1988) (Equation 8). Previous studies have demonstrated the ability of vegetation indices to describe the temporal evolution of crop coefficients (Bausch, 1993; Bausch and Neale, 1987; Choudhury et al., 1994). A recent study conducted by Campos et al. (2017) showed the ability of the SAVI index to describe the temporal evolution of Kcb for corn over the growth season (Equation 9).

$$SAVI = \frac{(NIR - R)}{(NIR + R + L)} \times (1 + L) \qquad (8)$$

$$K_{cb} = 2 \times SAVI - 0.17 \qquad (9)$$

where NIR is the reflectance value of the near infrared band, R is reflectance of the red band, and L is the soil brightness correction factor (0.5 was used considering that the corn areas have an intermediate vegetation cover).

From Kcb values calculated using Equation 9, it is possible to determine AGB (Equation 6) over a period during the growing season using a numerical integration methodology. Thus, the precise definition of the interval for Kcb accumulation is a key point of this approach. The determination of this interval is variable, especially according to the climatic conditions, but the most common way of determination is based on Growing Degree Day – GDD (Angel et al., 2017; Meade et al., 2013) or Days after sowing (DAS). Campos et al. (2018), instead of working with GDD or DAS, found the interval for AGB accumulation based on SAVI values. These values are 0.20 and 0.40 for the start and end, respectively, considering a planting density of 84,500 plants per hectare. The lower limit of 0.2 is a reasonable limit, defined to avoid the accumulation of biomass out of the growing period (Campos and Gonçalves*, Personal Communication*) and 0.4 represents the period of physiological maturity.

Pre-tests based on the above-mentioned SAVI values (0.2 and 0.4) for biomass accumulation show very high estimates for Brazilian conditions (dry biomass above 35 Mg ha^{-1}). Was investigated the possible causes of these overestimates based on corn crop development and on photoassimilates distribution along the cycle. Was verified in a lot of studies that, during the grain filling period, there is a considerable remobilization of the dry matter accumulated in the vegetative parts of corn plant (i.e., stalk, leaf sheaths and leaf), mainly in the stalk, to the grains, assisting their filling together with the continuity of the

photosynthetic process to meet the reproductive phase (Allison and Watson, 1966; Rajcan and Tollenaar, 1999; Sangoi et al., 2002, 2001).

Based on this, to avoid this overestimate (due to the translocation of photoassimilates during reproductive period), was defined a new period based on GDD that did not extend until the physiological maturity. Thus, the best interval found was with start of Kcb accumulation at V_2 stage, when the plant has two fully emerged leaves and then is able to start the photosynthetic process (Fancelli and Dourado Neto, 2000). For the final period, worked with Kcb accumulated until the end of the R_5 stage called “Dent”. It’s important to point out that in this stage, the grains already have accumulated most of their maximum dry weight that would be reached until physiological maturity. (Hanway, 1966). The GDD values corresponding to the initial and final periods of Kcb accumulation were 250 and 1500 respectively, based on the study of Martins et al. (2017).

2.5.3. Water stress coefficient (K_{SW})

Water stress coefficient shows how crop transpiration is affected by water stress or irrigation water deficit. The model of Campos et al. (2018) uses the approach proposed in the FAO-56 manual (Allen et al., 1998) to determine K_{SW} (Equation 10).

$$K_{SW} = \frac{TAW - D_{r,i}}{TAW \times (1 - p)} \qquad (10)$$

where K_{SW} is a dimensionless transpiration reduction factor dependent on available soil water (0 – 1), Dr is root zone depletion (mm), TAW is total available soil water in the root zone (mm) and, p is the fraction of TAW that a crop can extract from the root zone without suffering water stress (dimensionless).

In Brazil, however, especially in the irrigated commercial farms which adopted any type of irrigation management, it is very hard to use the FAO dual-Kc approach presented in Allen et al. (1998), and consequently the K_{SW}, because of its greater complexity for application. In Brazil it is more common to use a

simpler methodology, such as that proposed by Bernardo (1989), according to Equation 11. This methodology was used to obtain the water stress coefficient (Ks) in areas of this study to the detriment of FAO K_{SW}.

$$K_S = \frac{\ln (1 + CSWS)}{\ln (1 + SWS)} \qquad (11)$$

where SWS is the total soil water storage (mm), and CSWS is the current soil water storage (mm) at a certain time.

Bernardo's methodology has been widely used in several scientific studies (Freitas et al., 2017; Santos et al., 2018; G. H. Silva et al., 2018; Vicente et al., 2017), and in several irrigated farms in Brazil by the IRRIGER company.

2.5.4. Temperature stress coefficient (K_{ST})

Plant growth and development rate is dependent upon the temperature surrounding the plant, and each species has a specific temperature range represented by a minimum or base (T_b), maximum or lethal (T_1), and optimum (T_o) (Campos et al., 2018; Hat and Prueger, 2015). Both temperatures (T_b and T_1) represent, respectively, the temperature above and below which the development is null or negligible, and the optimum temperature, as the name itself suggests, is the best temperature for plant growth and development. The temperature stress coefficient (K_{ST}) was used according to Raes et al. (2009). These authors propose a logistic relationship between K_{ST} and the relative water stress level (S_{relT}). Numerically, S_{relT} is a linear function of the daily mean air temperature (Tm), estimated from the maximum and minimum daily values, and the extremes for the canopy development T_b and T_o (Equation 12).

$$S_{relT} = \frac{T_o - T_m}{T_o - T_b} \qquad (12)$$

If mean temperature (Tm) > optimum temperature (T_o), K_{ST} is equal to 1, and if $T_{mean} \leq T_o$, K_{ST} is obtained using Equation 13 (Raes et al., 2009).

$$K_{ST} = \frac{(S_n \times S_x)}{S_n + (S_x - S_n)^{\exp(-r(1 - S_{relT}))}} \qquad (13)$$

where T_b and T_o for corn are 10 °C and 30 °C (Steduto et al., 2012). Where S_x and S_n are the upper and lower limits of K_{ST} and were assumed to be equal to 1.0 and 0.001, respectively, and r is the rate factor (15).

2.5.5. Harvest Index (HI)

Most of the studies on HI determination for corn show values for this index varying between 0.35 and 0.6, depending mainly on the hybrids, location and crop management. Examples can be seen in the works of (Bastiaanssen and Ali, 2003; O'Shaughnessy et al., 2017; Wang et al., 2018; ZHAI et al., 2017). With these values available in the literature, many researchers choose and apply them in their studies for corn yield determination.

A correct choice of the HI value is not easy, because of the factors cited above. Thus, to avoid a wrong choice of the HI value, and consequently a wrong yield determination, Campos et al. (2018) suggest a new way to determinate HI. These authors have created a methodology based on the hypotheses that the final yield is better correlated with the maximum biomass reached by the crop, in contrast to the relationship between yield and biomass at harvest. However, the disadvantage of this methodology in the meantime is the need for using grain yield to determine HI. Besides that, these authors highlight that the methodology needs to be validated with additional experiments and analyses.

Due to the above-cited disadvantages of Campos' methodology for HI determination, opted for using an empirical value of HI based on data reported in the literature. It has been reported in the scientific literature that HI values can range from 0.3 to 0.6, but the most common values remain between 0.4 and 0.5 (Bocianowski et al., 2019; Da Silva et al., 1999; Demétrio et al., 2008; Echarte and Andrade, 2003; Hütsch and Schubert, 2018, 2017; Koffi Djaman et al., 2013;

J. Li et al., 2015). Thus, chose to work with the value of 0.45, based on literature and informal field estimates reported by the agronomist of the farm.

In the growing season of 2013, there was a severe and sporadic attack of the bacterium *Erwinia chrysanthemi* pv. Zeae, causing a disease called Stalk rot of maize, leading to a sharp drop in yield. Stalk rot is a serious biotic constraint in all parts of the world, including America, Australia and Europe (Mir et al., 2018). Corn stalk rot may occur before the grain filling stage in vigorous young plants or close/after physiological maturation of the grains in senescent plants. In the first case, losses are due to the premature death of plants with negative effects on grain size and weight, as a consequence of the reduction in water and nutrient absorption. In the second case, the losses in the production are due to the tipping of the plants, which hinders the mechanical harvesting and exposes the ears to the action of rodents and the rotting by the contact with the soil (Casela et al., 2006). Normally, the yield losses in maize from the disease are about 10%, but this could be increase to 30-50% in adverse situation (Li et al., 2010).

The attack occurred in the fields of this study was the cited in the second case, that is, close/after to the physiological maturation (*Field supervisor, personal communication*). It occurred in all CP cultivated, mainly in the center pivots 02A, 03A, 05A, 06B, 07B, 08B, 09B, 10B, 11B and 12B, and a little less severe in 01A and 04A. Thus, for the less affected corn plants (01A and 04A) adopted the HI of 0.37 and for the others, 0.24. These HI values for 2013 were calculated based on relationship of the yield of this year with the yield of the 2014, 2015 and 2016 years and the HI for these three season (0.45), that's, using the rule of three. We choose working with this season in order have more variability in the data.

2.6. Model changes

Our main goal was to make a recent approach for assessing corn yield using RS data (SAVI) along with FAO 66 approach applicable with precision to an irrigated farm in the western region of Bahia, Brazil. Thus, it is necessary to consider the features of cultivation that are different from those of North American conditions. Therefore, some changes are expected to occur in the model. The

changes made in the model were mentioned above and are summarized in Table 3.

Table 3. Comparison between parameters of the original model (Campos et al., 2018) and the model adjusted to Brazilian conditions

Parameter	Original model	Adjusted model
WUE_B*, g m^{-2}	33.4 (Campos et al., 2018)	33.4 (Campos et al., 2018)
K_{ST}	Equation 12 and 13	Equation 12 and 13
K_{SW}	Equation 10	Equation 11
HI	Modelled	Empirical
$Kcb_{\ accumulated}$	SAVI values	GDD

2.7. Data statistical analysis

In order to assess the accuracy of the estimations, the statistical indicators Root Mean Square Error (RMSE), relative RMSE (RRMSE), Mean Bias Error (MBE), Mean Absolute Error (MAE) and Coefficient of Determination (r^2) were calculated according to Equations 14, 15, 16, 17 and 18.

$$RMSE = \sqrt{\frac{\sum_{i=1}^{n}(S_i - O_i)^2}{n}} \qquad (14)$$

$$RRMSE = \frac{RMSE}{\bar{O}} \times 100 \qquad (15)$$

$$MBE = \frac{\sum_{i=1}^{n}(S_i - O_i)}{n} \qquad (16)$$

$$MAE = \frac{\sum_{i=1}^{n}(|S_i - O_i|)}{n} \qquad (17)$$

$$r^2 = \left(\frac{\sum_{i=1}^{n}(|O_i - \bar{O}|)(|S_i - \bar{S}|)}{\sqrt{\sum_{i=1}^{n}(O_i - \bar{O})^2 \sum_{i=1}^{n}(S_i - \bar{S})^2}} \right)^2 \qquad (18)$$

where O_i is the observed value, S_i is the estimated value, $\overline{O}$ is the observed mean, $\overline{S}$ is the estimated mean, n is the total number of observations and i is the current observation.

2.8. Software programs

Microsoft Office Excel 2016 (Microsoft Corporation, Redmond, WA, USA) and Tool for Numerical Integration pixel by pixel ($TONI_{pbp}$) were applied for data processing and analysis. $TONI_{pbp}$ was developed by the GIS and Remote Sensing Group from the University of Castilla-La Mancha in the frame of the project FATIMA (http://fatima-h2020.eu). $TONI_{pbp}$ is a tool that allows you to obtain accumulated value maps temporarily on a daily scale of the input variable considered, usually images of NDVI or SAVI, and of derived variables such as transpiration, absorbed photosynthetically active radiation, among others. It operates pixel by pixel, and the time interval over which it performs the numerical integration can be a threshold value of the vegetation indices (VI) of the pixel for the start of the cycle and another for the end or also a date interval, thus characterizing the growth cycle of the crop. In the present study, $TONI_{pbp}$ was used to obtain accumulated value of the relation $Kcb \times K_{ST} \times K_S$ within a date interval defined based on GDD. QGIS 2.14.5 (OSGeo, Oregon, USA) was used to create the maps. In addition, to avoid a border effect, a 30 m buffer was applied in the vector layer of each CP.

3. RESULTS AND DISCUSSION

3.1. Meteorological conditions

Figure 3 presents the average monthly climatic conditions of daily mean air temperature (Tm), extraterrestrial radiation (Ra), relative humidity (RH), wind speed at 2 m height (U_2), grass reference evapotranspiration (ETo) and rainfall

recorded by the automated weather station, located near the CP (see Figure 1). The temperatures (Figure 3a) were very similar in the four seasons, approaching the historical average for the region (INMET (Instituto Nacional de Meteorologia), 2018), with exception for the January-May period in 2013, where the values of temperature were slightly lower than those of the other years. Another point to highlight is the big difference in the average wind speed values during the irrigation season of 2013 and 2016 (Figure 3c), 0.5 and 2.1 m s^{-1}, respectively.

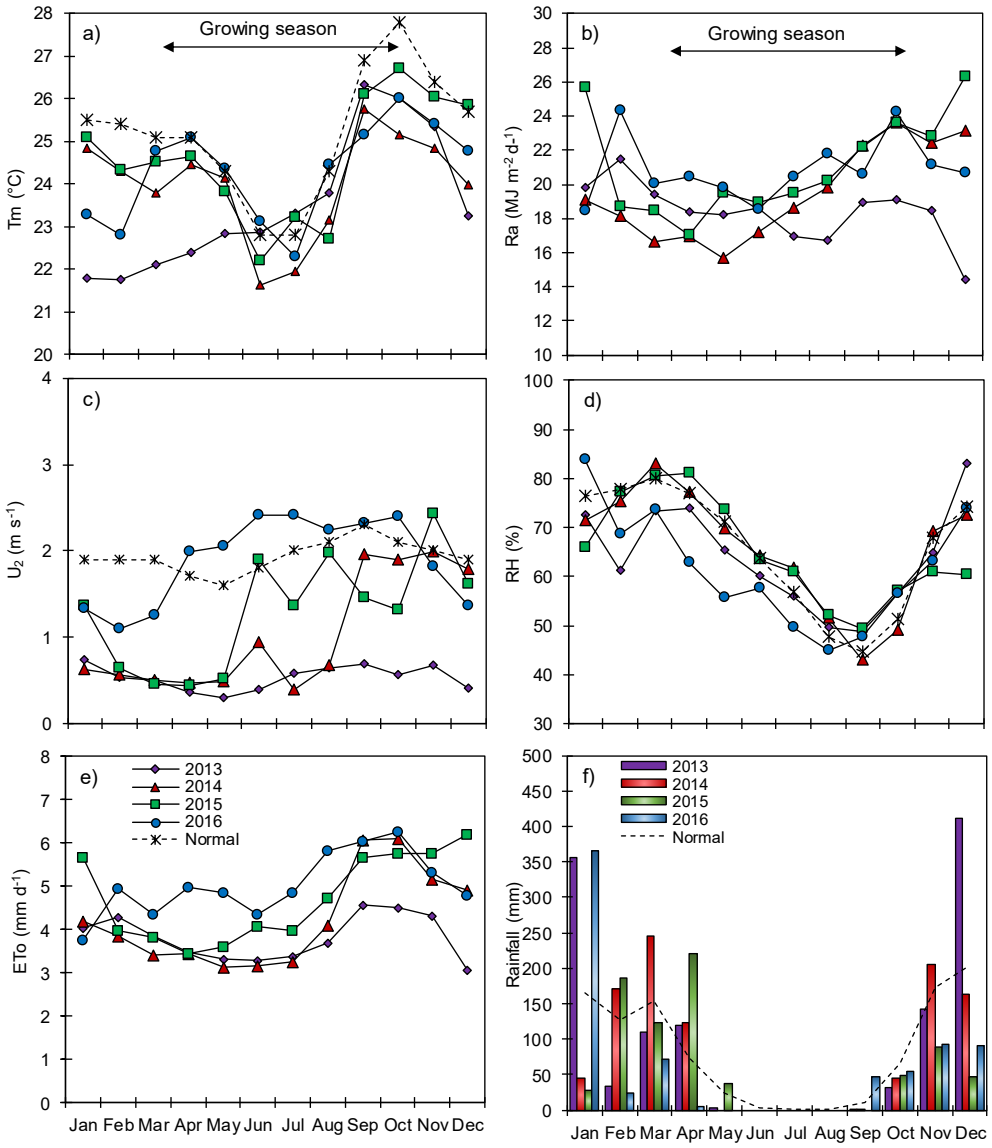

Figure 3. Comparison of monthly climatic conditions between the growing seasons of 2013, 2014, 2015 and 2016 using averages for: mean air temperature

(a); extraterrestrial radiation (b); wind speed at 2 m height (c), relative humidity (d); reference evapotranspiration (e) and, rainfall (f).

In relation to rainfall, during the corn season (April-September, normally), there are few rain events (Figure 3f). In June, July and August, for example, there were no rainfall events in any of the four seasons. For this reason, the gross irrigation depth applied during this period reaches ~850 mm and normally varies between 700 and 800 mm (Table 5). The ETo considerably increased after July (Figure 3e) and, for sowing in June (e.g., corn season of 2014, Table 1), the silking stage (9-10 weeks after sowing) may coincide with this increase of ETo. Thus, more attention should be given to the irrigation management for sowing in June.

3.2. Irrigation management data

The total irrigation applied in each CP varied little from year to year and from pivot to pivot due to the small variation of climatic conditions and its effect on ETo (Table 4). The year 2013 had the smallest irrigation depth applied (~400 mm) because of a sporadic and severe disease called Stalk rot in the corn fields of this season, causing irrigation management to be finished earlier and strongly impacting corn yield. The growing cycle of 2016 had the highest mean value of ET, with 648.7 mm (Table 4). This is a result of the high values of temperature, solar radiation, and mainly wind speed, and low relative humidity observed in this year in comparison with the others (Figure 3).

Table 4. Accumulated values of irrigation (Irr), actual corn evapotranspiration (ET), and reference evapotranspiration (ETo) during the growing season for each center pivot (CP) analyzed in the corn growing seasons of 2013, 2014, 2015 and 2016

CP	Irr	ET	ETo	CP	Irr	ET	ETo
-	mm	mm	mm	-	mm	mm	mm
2013				2014			
01A	519.3	300.9	333.1	01B	820.2	569.6	580.6
02A	383.2	283.8	310.9	02B	747.5	547.6	574.6

03A	393.6	290.9	320.5	03B	747.2	544.8	571.6
04A	485.6	296.7	329.9	04B	790.8	555.4	580.8
05A	426.7	301.6	324.6	05B	807.4	556.9	578.9
06B	369.9	244.9	271.3	06A	821.6	599.3	624.4
07B	357.7	246.7	274.0	07A	826.7	594.8	622.7
08B	353.9	251.0	276.9	08A	832.6	595.1	620.1
09B	343.0	252.6	280.2	09A	796.5	594.8	614.0
10B	368.7	264.8	293.9	10A	810.8	591.9	610.8
11B	422.6	271.9	286.5	11A	784.6	580.0	598.2
12B	392.3	273.3	305.2	12A	760.3	504.8	589.3
2015				2016			
01A	745.0	571.2	611.3	03B	703.6	610.7	737.5
04A	737.9	594.8	619.7	04B	780.1	703.4	786.6
05A	587.4	519.2	535.2	05B	847.4	706.7	766.6
06B	768.8	634.9	685.6	06A	688.2	609.7	729.8
07B	766.0	631.0	684.2	07A	707.4	656.8	758.8
08B	771.4	629.3	682.2	08A	733.9	713.0	798.9
09B	747.2	626.2	679.1	09A	756.7	719.8	804.4
10B	772.4	623.5	676.1	10A	766.0	683.6	755.9
11B	772.5	622.8	673.5	11A	676.3	546.0	654.5
12A	710.4	570.5	606.8	12B	686.0	598.4	654.7
13A	708.6	565.6	595.6	13B	698.0	592.7	646.5
14A	750.7	563.7	592.5	14B	754.7	645.5	739.7
15A	698.7	561.1	586.8	15B	714.2	637.1	740.5
16A	737.0	557.4	581.0	16B	756.8	658.9	747.2

In respect to the comparison between ET and ETo, the amounts accumulated were similar, but accumulated ETo was greater than ET, which means that the average crop coefficient, especially, is less than one during the corn cycle, as previously demonstrated in the scientific literature (Djaman and Irmak, 2013; Piccinni et al., 2009; Segovia-Cardozo et al., 2019).

3.3. Water stress coefficient (K_S) and temperature stress coefficient (K_{ST})

Figure 4 shows the daily K_S values for selected CP, determined by the model of Bernardo (1989) for irrigation seasons of 2013 to 2016. In general terms, during all growing seasons, the K_S values were close to 1, except on the first and second days, when sowing is normally being performed, and in the late season, when irrigation intervals are longer because corn is almost reaching physiological

maturity (Figure 4). Bernardo's methodology causes a decrease in K_S value from the first millimeter extracted from the soil (see Equation 11), differently from the FAO-56 approach, which considers a fraction of total soil water available in the root zone that the crop can extract without suffering water stress. Based on that, it is possible to affirm that cultivated fields do not have any problems with water stress, a claim that can be supported by the high yield obtained in the fields (Tables 1 and 2).

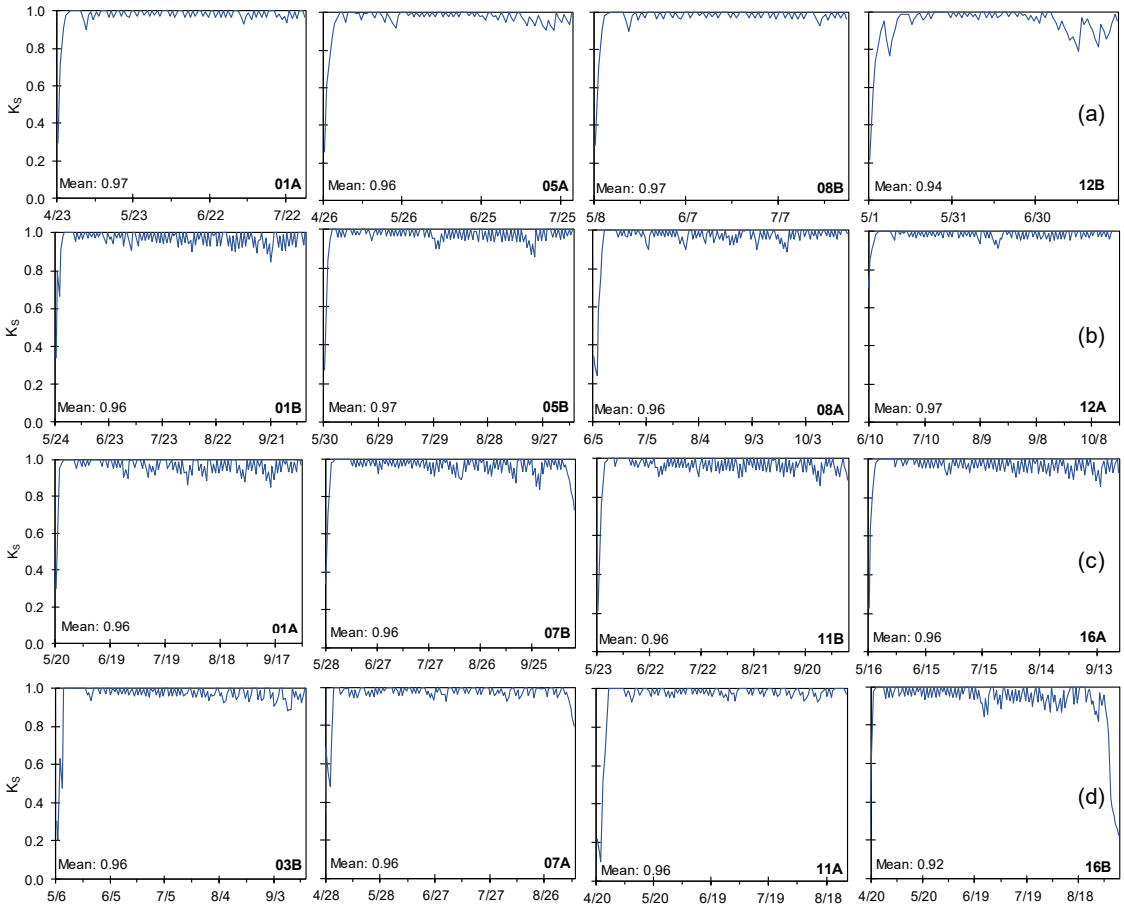

Figure 4. Temporal evolution of the water stress coefficient (K_S) obtained in selected center pivots of 2013 (a), 2014 (b), 2015 (c) and 2016 (d).

During the growing season of 2013, the period of irrigation had a duration of ~100 days (Figure 4a), due to a phytosanitary problem with a severe attack of the bacterium *Erwinia chrysanthemi* pv. zeae in all fields in 2013. In the other

years (Figures 4b, c and d), the period extended to around 125 days, that is, irrigation ended when corn reached physiological maturity. However, regardless of irrigation management duration, Ks values were very similar for the four seasons analyzed.

Figure 5 brings the temperature (cold) stress coefficient (K_{ST}) for the corn growing seasons of 2013, 2014, 2015 and 2016. The lowest values of K_{ST} are seen during the initial days of the winter in Brazil, which starts in June 20 or 21, with the lowest value occurred in 2015. The average values of K_{ST} were 0.96 for 2013 and 2014 and 0.97 for 2015 and 2016, meaning that the cold temperature has a low impact on biomass production under Brazilian conditions. These results are expected because Brazil is a country of tropical climate, and although corn is cultivated during autumn/winter season, the air temperatures of the region during this period are compatible with those required by corn along its development, that is, between 25 and 30 °C (Fancelli and Dourado Neto, 2000).

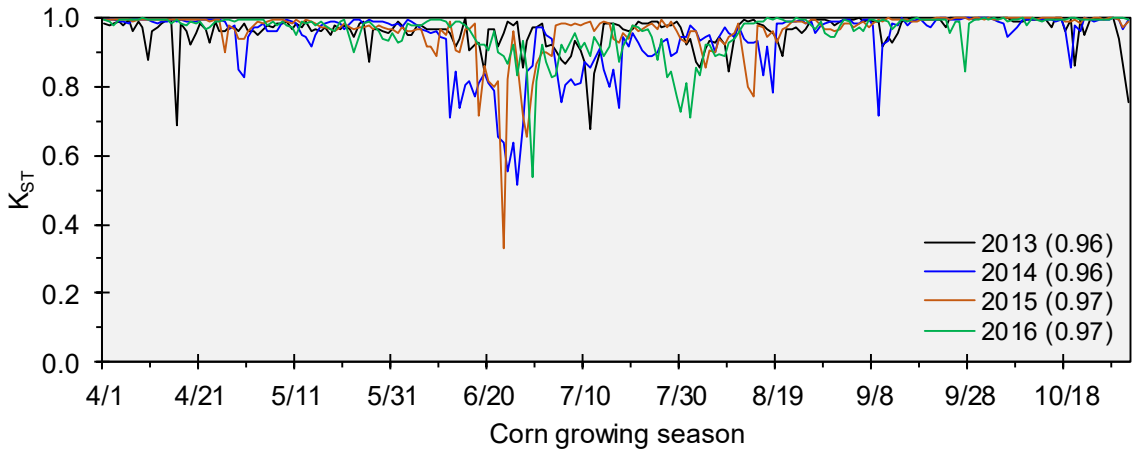

Figure 5. Temporal evolution of the temperature stress coefficient (K_{ST}) and average values (between parentheses) during the corn growing seasons of 2013, 2014, 2015, and 2016).

3.4. Corn crop development

Understanding patterns of vegetation based on VI is essential for crop management, helping for instance in the decision-making with respect to nitrogen

status (Feng et al., 2015; Huang et al., 2015; F. Li et al., 2014), weed identification (Peña et al., 2013), crop water stress (Holzman et al., 2014; Moran et al., 1994; Veysi et al., 2017), among others. Figure 6 shows the patterns of temporal evolution of the SAVI in each CP over the growing seasons of 2013, 2014, 2015 and 2016. In the four seasons analyzed it is possible to see a very similar behavior, with a fast increase at the start of the growing cycle, a stability during the mid-season and a reduction at the end. The lowest SAVI values are observed in the first and six images (e.g., June 07 and Oct 21, Figure 6b), because of the great amount of exposed soil and plant senescence, respectively, in these periods.

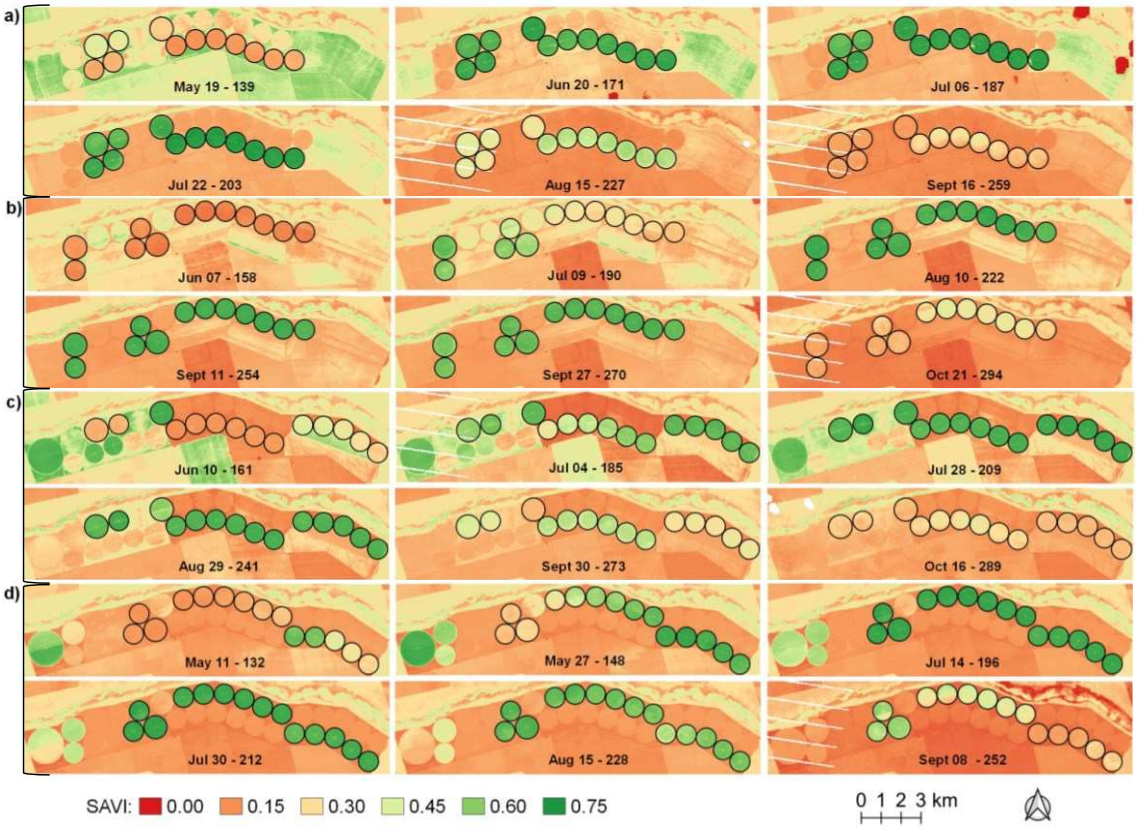

Figure 6. Maps of the temporal evolution of the SAVI derived from Landsat 7 and Landsat 8 images for the center pivots cultivated (dark edge) in the growing seasons of 2013 (a), 2014 (b), 2015 (c) and 2016 (d). Six imagens which best described the growing seasons were selected.

On the other hand, from the second to the fourth image high values of SAVI are verified, because leaf area index increases (Campos et al., 2017; Gitelson et al., 2003). The highest SAVI values are observed between 70 and 80 DAS, when the plants are in silking stage. This stage is one of the most critical stages in determining yield potential (Claassen and Shaw, 1970) and is one of the stages which most require water (Abirdew et al., 2018; Kamali and Nazari, 2018; Kranz et al., 2008); thus, special attention should be given to it.

The attack of the bacterium *Erwinia chrysanthemi* pv. zeae in all fields of 2013 (already mentioned above), had its effect reflected in the image of Aug 15 – 227 (Figure 6a), with relatively low values for the period, because of the death of parts of infected plants and also because plants toppled down (Bertolin et al., 2017). Besides that, irrigations were suspended in the fields, on July 29 (~100 days after sowing), affecting plant vigor because of the accumulated water deficit .

SAVI values along the four seasons ranged from 0.11 to 0.72, with an average value around 0.5. Although the maximum value reached 0.72 a few times, most of the maximum values were between 0.68 and 0.7 (Figure 7), which are the most common in corn fields (Bausch, 1993; Campos et al., 2017). In general terms, vegetation conditions were slightly variable between fields over the four growing seasons, with very close amplitude and average SAVI values (Figure 7). This is a consequence of the high technological level adopted on the farm, which mainly involves hybrid of high performance and a correct irrigation management. As the interested it's the AGB estimation, which depends heavily on the values of SAVI, the visualization of these values and confirmation that they are representing corn development very well at the four seasons analyzed is very important, and this will ensure that can obtain estimates accurately.

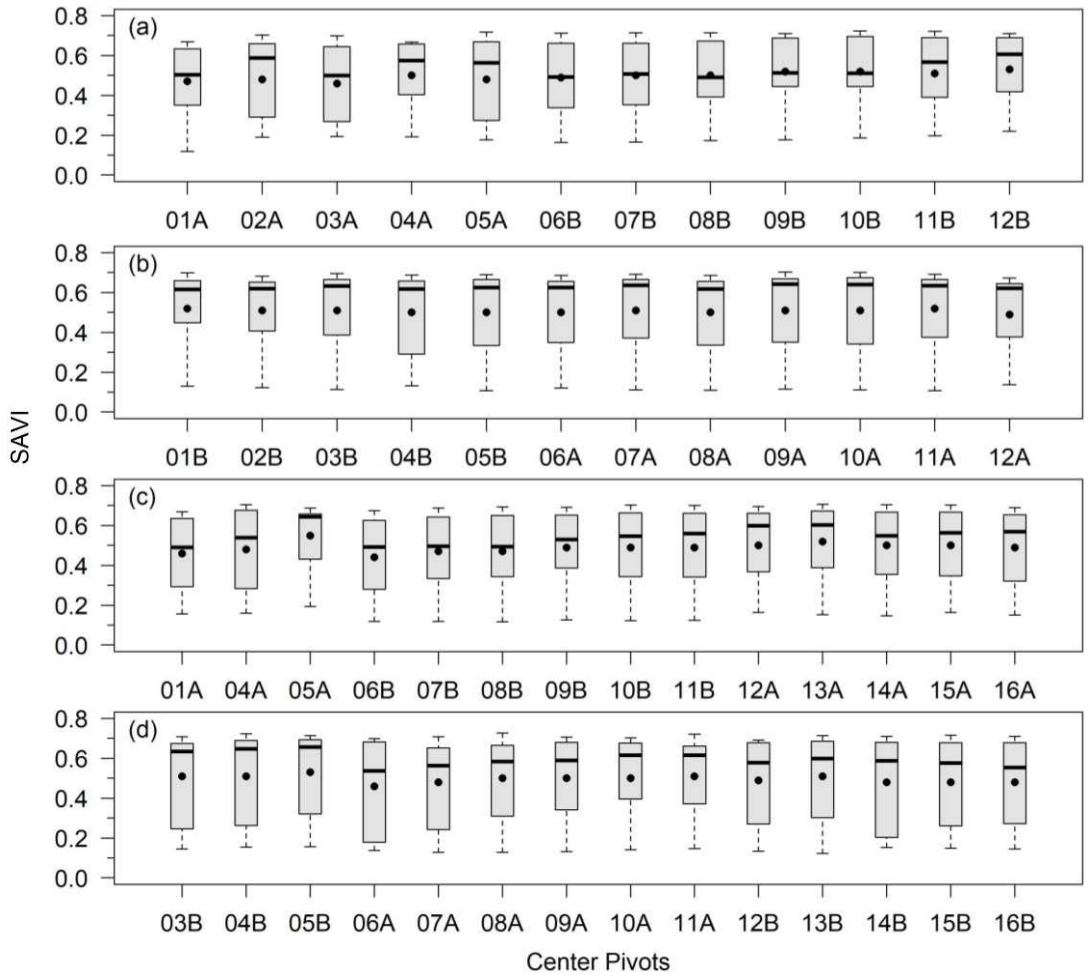

Figure 7. Boxplot of SAVI for the growing seasons of 2013 (a), 2014 (b) 2015 (c) and 2016 (d).

In complementation to Figure 6 and 7, was generated the curves of SAVI values with selected CP (Figure 8). The main objective of this figure is to show clearly the evolution of SAVI according to the four major crop development phases. In the growing season of 2015 (Figure 8c) it is possible to see a very good curve of SAVI over the season, with increases (early season) and decreases (late season), and without considerable gaps due to the presence of clouds. These results corroborate the importance of using satellites with high temporal resolution (e.g., Sentinel 2) or coupled use of 2 or more satellites, as done in the present study with the Landsat 7 and 8 to study crops with fast development, such as corn, soybean and bean, for instance.

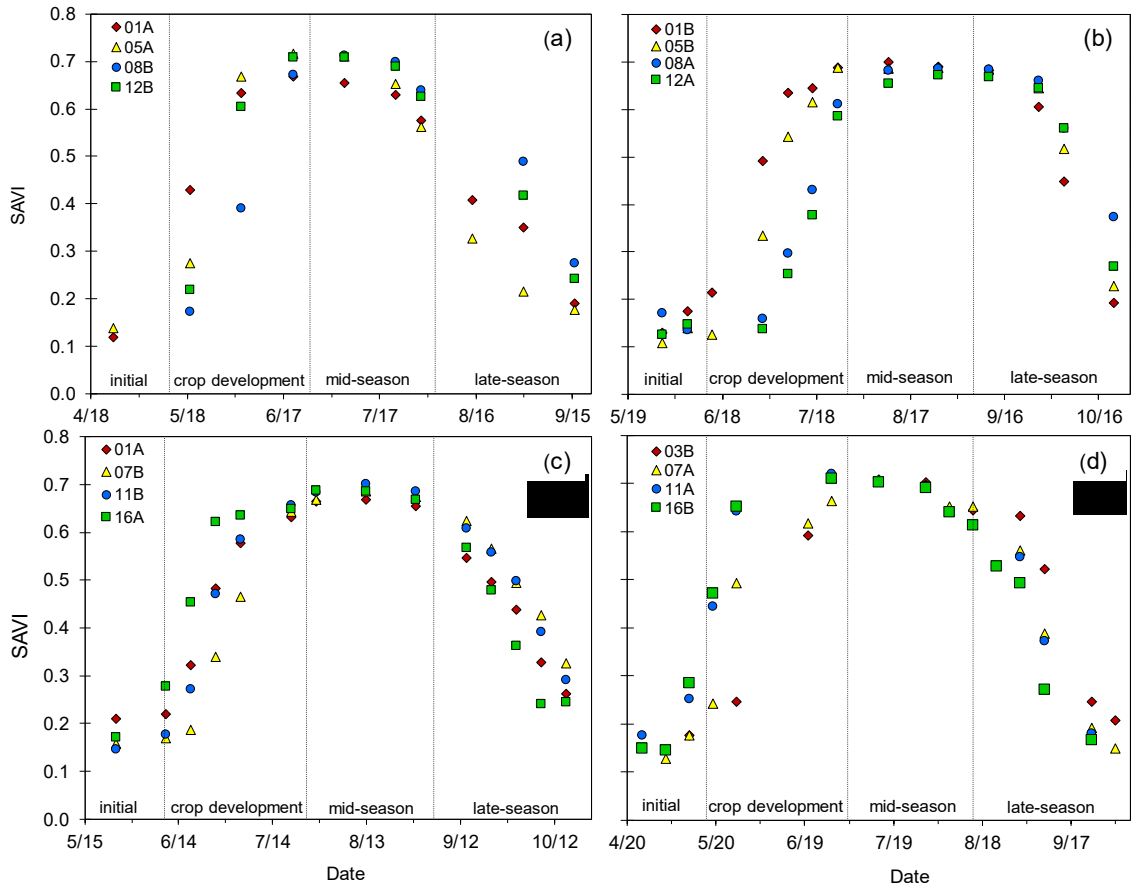

Figure 8. Temporal evolution of SAVI for selected fields in the corn seasons of 2013 (a), 2014 (b), 2015 (c) and 2016 (d).

3.5. Basal crop coefficient adjusted (Kcb_{adj})

The basal crop coefficient is defined as the ratio of crop evapotranspiration over the reference evapotranspiration when the soil surface is dry, but transpiration is occurring at a potential rate (i.e., water is not limiting transpiration). However, when water is limited in the soil there is a reduction in Kcb values, which is done by means of their multiplication by a water stress coefficient (Allen et al., 1998). Campos et al. (2018) demonstrated the clear relationship between AGB production and the accumulated values of Kcb derived from satellite data and, subsequently, the compatibility of the Kcb data derived from satellite images with the transpiration coefficient described in the FAO-66 manual (Allen et al., 1998).

In addition, they also considered a temperature (cold) stress on Kcb instead of only water stress (Allen et al., 1998), that is, Kcb adjusted to water deficit and cold temperature stress (Campos et al., 2018). Figure 9 shows the map of Kcb adjusted for temperature and water stress conditions (Kcb_{adj}) of each irrigated corn field in four consecutive growing seasons (2013 to 2016). Kcb_{adj} ranged from 69 to 94, with average values of 79.3, 75.2, 81.6 and 87.9 for 2013, 2014, 2015 and 2016, respectively (Figure 9). The results obtained in this work were similar to those of Campos et al. (2018), obtained under the conditions of Nebraska (USA).

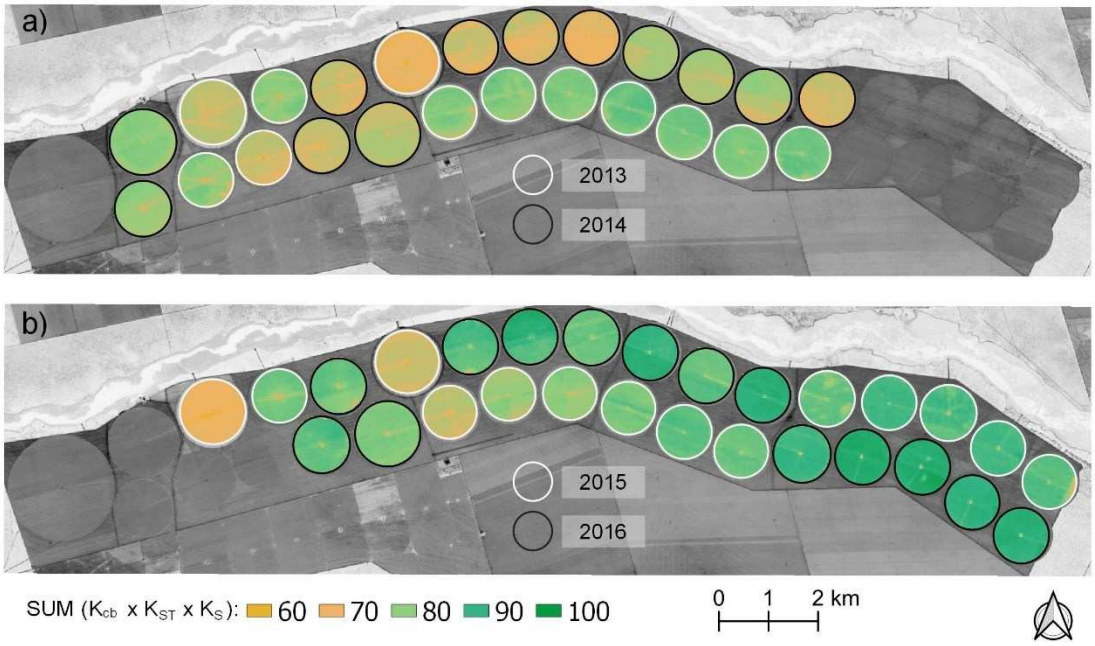

Figure 9. Map of accumulated basal crop coefficient adjusted for temperature and water stress conditions ($\sum Kcb \times K_{ST} \times K_S$) of each irrigated corn field in four consecutive growing seasons (2013 to 2016). The white circles correspond to center pivots of 2013 and 2015 and the black circles to center pivots of 2014 and 2016.

Although the 2013 growing season had problems with a disease (Stalk rot of maize), the Kcb_{adj} was slightly higher than in 2014 (Figure 9a), due to the symptoms of attack became more evident after the period of Kcb accumulation

(end of the R4 stage), since the attack occurred close to physiological maturation of the grains (~120 DAS). The 2016 growing season had the highest values among the four growing seasons (Figure 9b), which is directly related to a higher yield. In general terms, the Kcb_{adj} values showed a little variation within the same season, and most of this small difference can be attributed to the cultivation of different corn hybrids (see Tables 1 and 2).

3.6. Aboveground dry biomass (AGB) and grain yield

The Kcb_{adj} times WUE_B* determines the AGB. The data referring to AGB is presented in Figure 10, which shows that AGB ranged between 18 and 34 Mg ha^{-1}. These results compare well with the findings of Campos et al. (2018), Kross et al. (2015) and Yang et al. (2017). Relatively low AGB is observed in 2013 and 2014 (Figure 10a) in comparison to 2015 and 2016 (Figure 10b), with the highest AGB occurring in 2016 (Figure 10b). In general terms, the fields had an evolution of production over the season, which can be seen better in the yield results presented in the sequence. It is important to point out that AGB can undergo considerable variations as a function of the WUE_B* (normally referred to as WP*) adopted, because this value, even if normalized, is variable between 30 and 35 g m^{-2} (Raes et al., 2017).

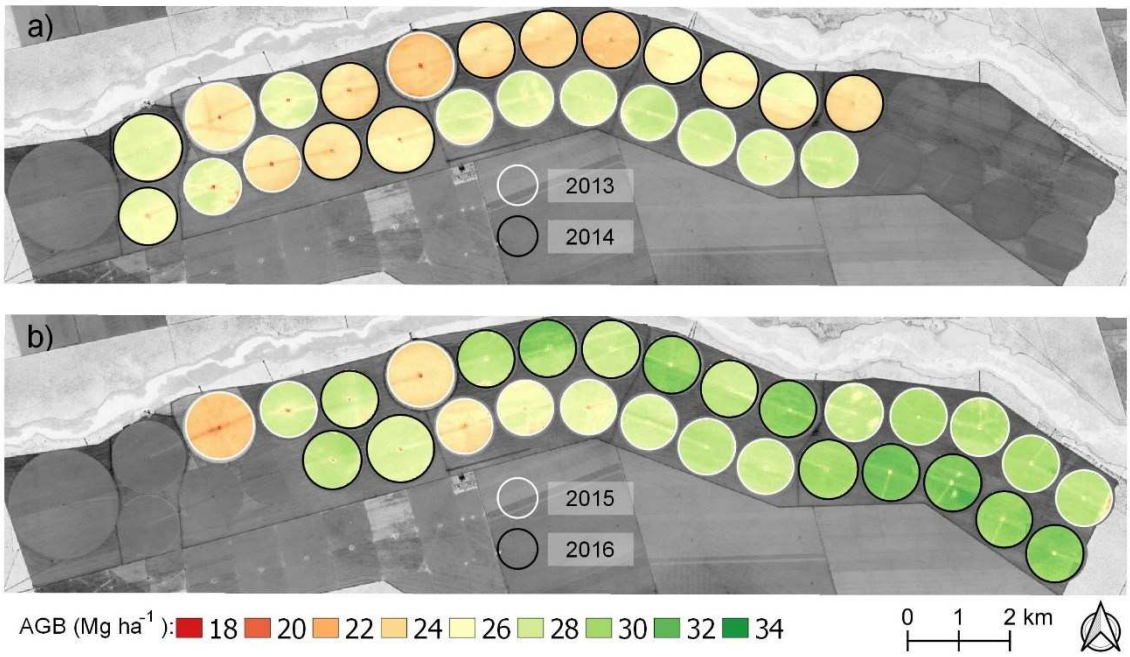

Figure 10. Map of accumulated aboveground dry biomass (AGB) of each irrigated corn field in four consecutive growing seasons (2013 to 2016). The white circles correspond to center pivots of 2013 and 2015 and the black circles to center pivots of 2014 and 2016.

Figure 11 shows the measured versus estimated yields of corn grains for the growing seasons of 2013, 2014, 2015 and 2016. In 2013 the lowest yield of the four seasons was verified, with some values near 5 Mg ha^{-1} (Figure 11a), which is considered as very low given the technological level adopted at the farm. These results are consequence of an attack of the bacterium *Erwinia chrysanthemi* pv. zeae. Two CP fields were less attacked than the others (01A and 04A); thus, using two different harvest indices (HI) was considered as more realistic. One value for group more attacked and one for the less attacked, which were obviously less than the other years, considered as normal.

Regarding the estimation performance of 2013, good agreement was observed with r^2 = 0.87. Based on RRMSE (8.3%), which is expressed as a percentage, where lower values indicate less residual variance, good agreement is also observed (Figure 11a). The statistical parameters were also good with RMSE equal to 0.573 Mg ha^{-1} and MAE equal to 0.489 Mg ha^{-1}, with slight underestimation (MBE = -0.032 Mg ha^{-1}).

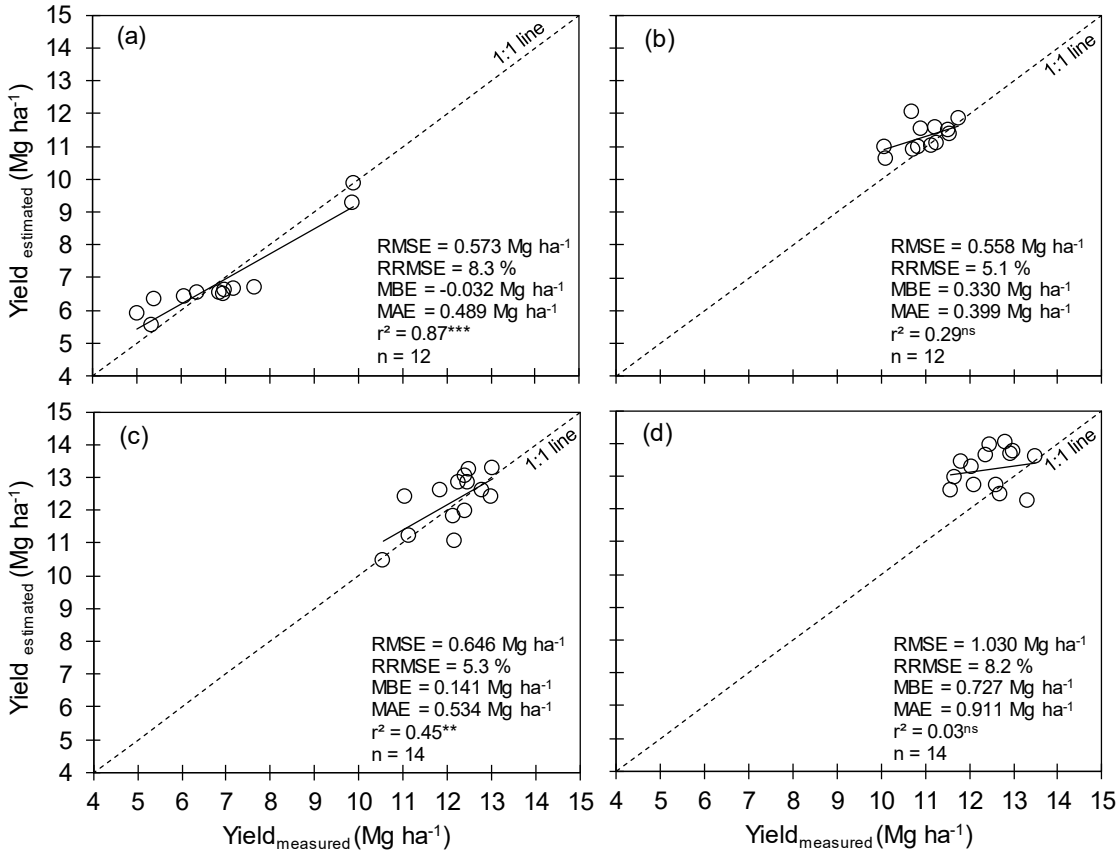

Figure 11. Measured versus estimated yields of corn grains for the growing seasons of 2013, 2014, 2015 and 2016 with the respective statistical parameters, with no separation of hybrids. ^{ns} indicates not significant, * indicates significance of regression at p-value < 0.05, ** indicates significance of regression at p-value < 0.01 and *** indicates significance of regression at p-value < 0.001.

In the 2014 harvest, the regression was not statistically significant, which means that does not relationship between the predictor variable and the response variable (Figure 11b). And, if compared to 2013 there was a large decrease in r² (Figure11a). On the other hand, RMSE and MAE showed small differences in the year 2013. RRMSE was 5.1%, while MBE indicated overestimation of the data (0.330 Mg ha^{-1}). Regarding the 2015 growing season, RMSE (NRMSE) between measured and simulated values was 0.646 Mg ha^{-1} (5.3 %) and the r² had a good improvement (0.45) compared to the previous year (Figure 11c). The MBE was 0.141 Mg ha^{-1}, a relatively low overestimate considering the average yield, while MAE was 0.534 Mg ha^{-1}.

As well as in 2014, the regression for 2016 growing season was not statistically significant, presenting the worst results of the four seasons analyzed, with r^2 = 0.03 and RMSE greater than one (1.030 Mg ha^{-1}) (Figure 11d). The RRMSE was similar to that of 2013 (8.3%). The MBE and MAE confirm that the values estimated for 2016 were poor, with overestimate reaching 0.727 Mg ha^{-1} and MAE equal to 0.911 Mg ha^{-1}. In the 2016 growing season, six different corn hybrids were sown, the season with the highest number of hybrids, which may have contributed to these poor results, due to the use of a single HI (HI = 0.45) for six hybrids.

Figure 12 brings the absolute difference in percentage between estimated and measured values of yield, for the growing seasons of 2013, 2014, 2015 and 2016. The higher difference was observed in 2013 (pivot 03A), with a value of 18.8% followed by 17.9% in the CP 02A also in 2013 (Figure 12a). Growing seasons of 2014 had only one value greater than 10% (Figure 12b), as well as in 2015 (Figure 12c), while 2016 was the year with the greatest amount of values higher than 10% (Figure 12d). Additionally, in some cases the differences are less than 1%, and the majority remained between -10 and 10%.

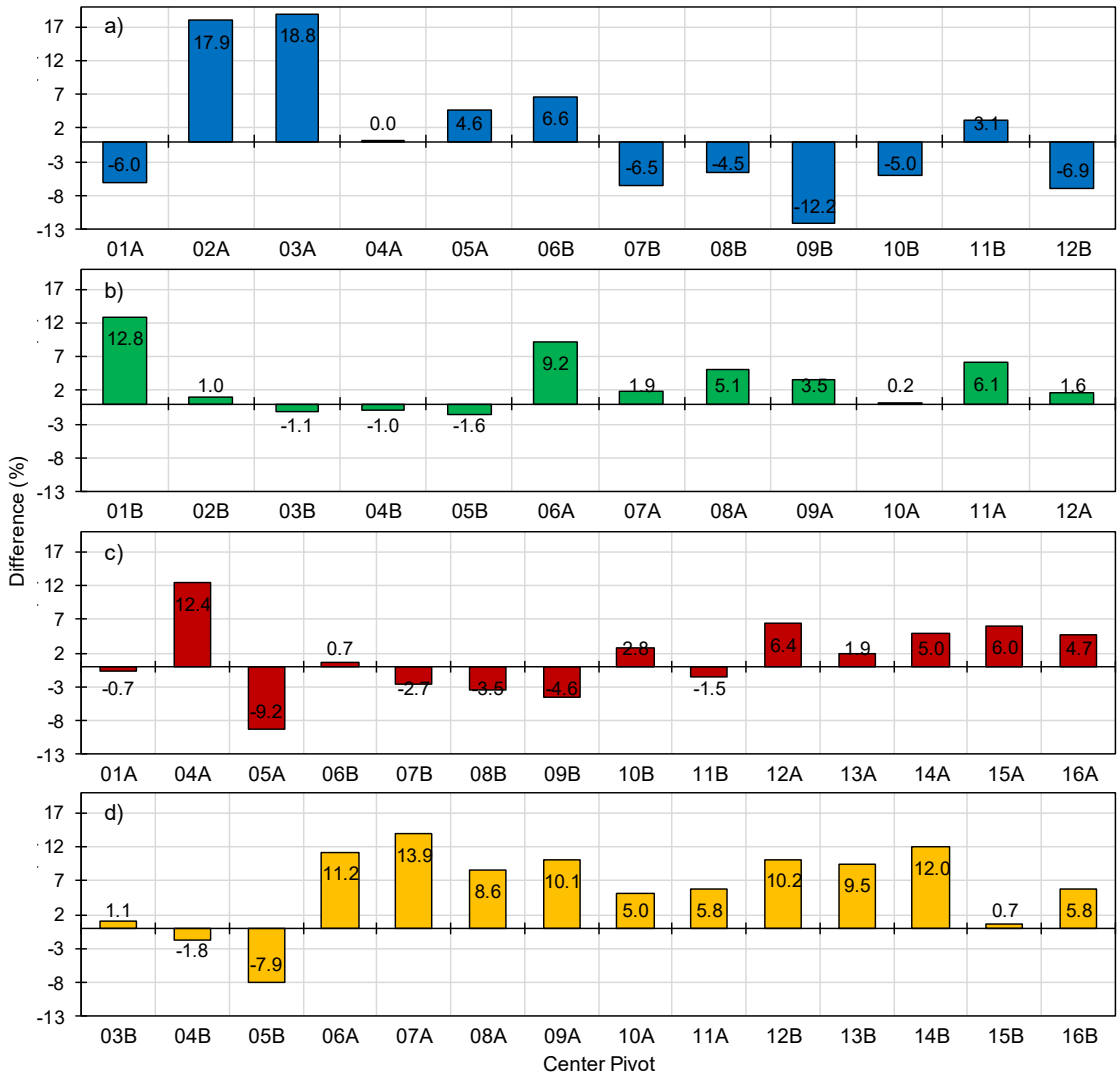

Figure 12. Percentage difference between estimated and measured values of yield for each center pivot analyzed in the growing seasons of 2013 (a), 2014 (b), 2015 (c) and 2016 (d).

Overall, there were no good results of estimated yield in Figure 11, although of difference presented in Figure 12 can be considered as low. Probably, as consequence of the use of a single HI value for different hybrids and, consequently, their joint analysis. For this reason, was performed a new analysis considering the two groups (Figure 12): (i) Pioneer hybrids and (ii) Status Viptera 3 hybrid, using data growing seasons of 2013, 2014, 2015 and 2016. Regarding Pioneer hybrids, which had three different materials planted in the above mentioned harvests (i.e., Pioneer 30F35, Pioneer P2830 and Pioneer P3646),

the grouping based on similarity of these material available in the Pioneer website (Pioneer, 2017) and according to field supervisor, which directly observing corns hybrids phenology within fields.

These two groups of hybrids, represented 92.3% of the cultivated area at the farm during the four seasons, as shown in Table 1 and 2. Thus, was used a HI of 0.43 for Pioneer hybrids considering their low relative yield, while a value of 0.45 was maintained for Status Viptera 3. It is also important to mention about the possible effect of planting density (PD) on final yield, since different PD values are used in the fields. However, this aspect was not considered here because the difference is small (means of 70,286 and 72,000 for Pioneer and Status Viptera 3 hybrid, respectively).

Significant correlation between observed and predicted yields was observed when considering the hybrids separately (Figure 13). In Figure 13a it is possible to see a good agreement for Pioneer hybrids, with estimates close to the 1:1 line and the estimated values explained 71% of the variation of the measured data. RMSE reached 0.536 Mg ha^{-1}, a relatively low value considering the average yield of these hybrids (11.24 Mg ha^{-1} for the 2014, 2015 and 2016 harvests) and a low value of RRMSE (4.8%). With MBE = 0.175 Mg ha^{-1}, the overestimates can be considered as subtle. In addition, MAE was equal to 0.477 Mg ha^{-1}.

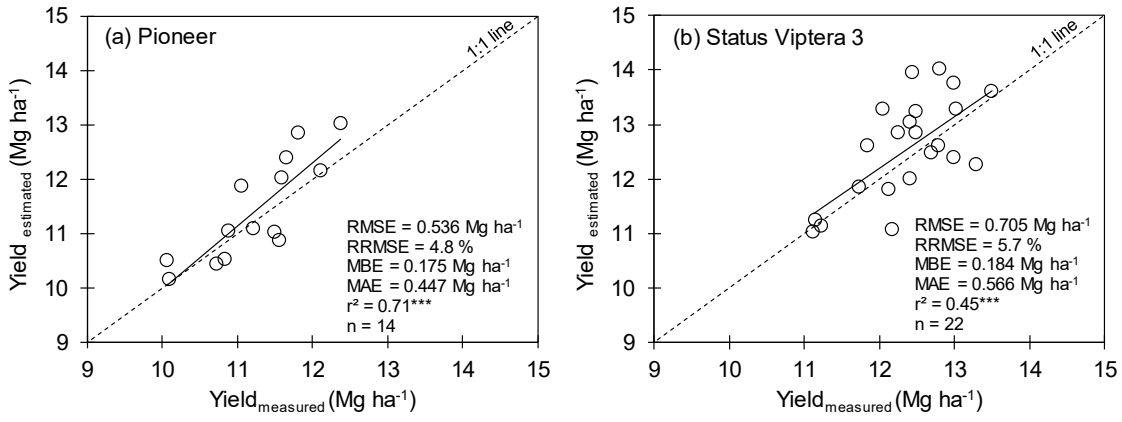

Figure 13. Measured versus estimated yields of corn grains for the growing seasons of 2013, 2014, 2015 and 2016 with the respective statistical parameters,

with grouping of hybrids. *** indicates significance of regression at p-value < 0.001.

Regarding the Status Viptera 3 hybrid, developed by Syngenta company, a reasonable value for r^2 was obtained (0.45). RMSE (0.705 Mg ha^{-1}) was a little greater than that for Pioneer hybrids, as also occurred for RRMSE (5.7%) (Figure 13b). The MBE obtained was equal to 0.184 Mg ha^{-1}, which represents an overestimation of the data. RMSE values obtained for both hybrids are similar to the results found in Holzman and Rivas (2016), Sakamoto et al. (2013). In comparison to the results of Sibley et al. (2014), RMSE values in the present study are very good, since these authors found RMSE above 2 Mg ha^{-1} for the tested approach and considered it as promising.

Figure 14 brings the absolute difference in percentage between estimated and measured values of yield, considering the two groups of hybrids. The higher difference for the Pioneer hybrids was 8.8%, while the smaller values were 0.4 and 0.5%, for the 08A and 10A CP fields (Figure 14a). The majority of the values remained between -5 and 5%. In respect to Status Viptera 3, as was maintained the HI equal to 0.45 for it, the differences are the same of the Figure 12, but here, they were grouped in a single local (Figure 14b). Of a total of 22 CP fields, 13 of them (59%), presented values ranged between -5 and 5%, with 90.9% them, between -10 and 10%.

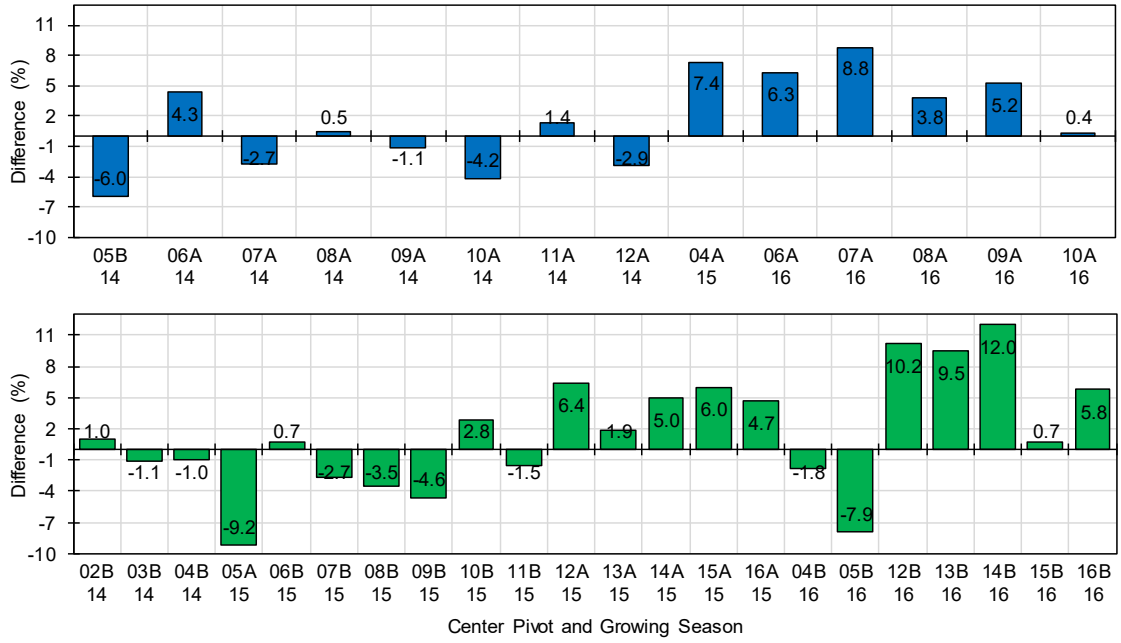

Figure 14. Percentage difference between estimated and measured values of yield, considering the two groups: (a) Pioneer hybrids and (b) Status Viptera 3, using a HI of 0.43 for Pioneer hybrids, while a value of 0.45 was maintained for Status Viptera 3.

Overall, considered the predicted data after the new analysis (i.e., considering two groups of hybrids) as very good, given the complexity of working with field data on farm level. Firstly, was used an extensive data set of 52 CP fields of four growing seasons, which are not subject the same controls of an experiment involving small plots, where manual harvest can be carried out with high precision. In these 52 fields, harvest is performed using harvesting machines, which may lead to considerable losses. Previous study of Loureiro et al. (2012) have demonstrated that losses in corn during mechanized harvesting may reach 8.2%.

Besides that, the fields are fully harvested, (i.e., including their boundaries), which were excluded from our analysis, to avoid border effect. Another point is related to the precision of weighing the truck with harvested grains. After being harvested corn grains are loaded on a truck for weighing and storage. During this process, errors may occur, for instance, assigning the

production weight of one central pivot to another. Thus, these facts explain part of the difference in the yield estimates. Although the problems cited above occur, considered the present work as very useful, especially because of its application to the real condition of production fields. According to Sibley et al. (2014), for RS to be useful for analyzing crop yield gaps, methods should be accurate at the field scale without need for local ground calibration.

3.7. Yield zone map

Within precision agriculture, the management zone delineation using RS data is reliable and feasible (Song et al., 2009). The predicted yield maps of the four growing seasons are presented in Figure 15. These maps were created using two HI for 2013 corn harvest (0.24 and 0.37), 0.43 for the Pioneer hybrids and 0.45 for Status Viptera 3 and other hybrids (see Table 1 and 2), as previously discussed. These maps showed a considerable variation of yield, considering all fields as represented by the eleven classes, and low variation considering individual fields, normally two or three classes by CP (Figure 15). It was not possible to observe a pattern of yield class distributed across the fields, although the boundaries are commonly regions of low yield. Also, it is important to highlight that part of yield variability is a consequence of soil natural differences (e.g., soil patches). Additionally, there is a notable trend of yield increase over the years, mainly due to technological advancements, such as fertilization, irrigation management and weed control.

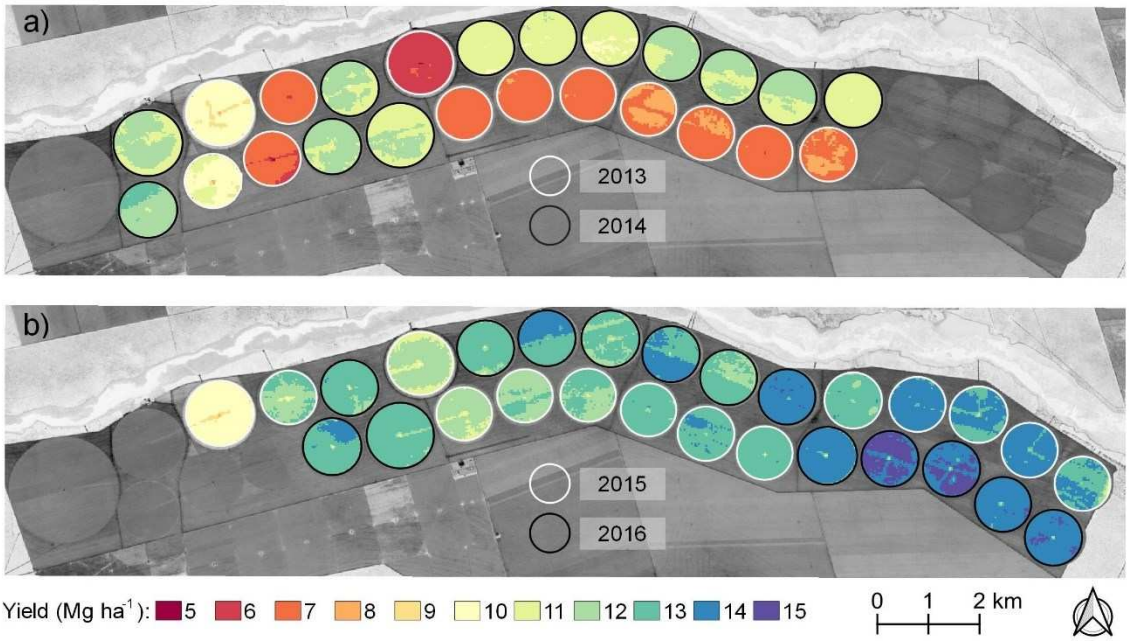

Figure 15. Predicted yield zone map of each irrigated corn field in four consecutive growing seasons (2013 to 2016). The white circles correspond to center pivots of 2013 and 2015 and the black circles to center pivots of 2014 and 2016.

These yield zone maps can be very useful during harvest, because they can be implemented in the harvesting machine and thus, harvest can be carried out by yield zones. Different yields sometimes need different settings of the machines, so one can avoid harvesting the entire area considering yield as uniform and, consequently, decreasing the losses during this step. Yield maps also are a valuable archive of field performance and the changes that management might have had on the fields (Franzen, 2018). In addition, yield maps are a reference for the next planting, helping decisions about soil fertility correction, compaction soil analysis, among others.

Figure 16 shows the percentage of area referring to each yield interval, an important information to help in decision-makes. In 2013 (Figure 16a), more than 60% of the areas had 5 ≤ yields < 7.0 Mg ha^{-1}. Although these values are compatible with the Brazilian average corn yield (CONAB, 2018), they are very low considering irrigated plantations, which normally produce more than 10 Mg ha^{-1}. These low values are consequence of a disease and reinforce that

agriculture is a high-risk activity, that is, the producers may have their production reduced by several factors (e.g., disease, pest, drought, excess of rainfall, among others).

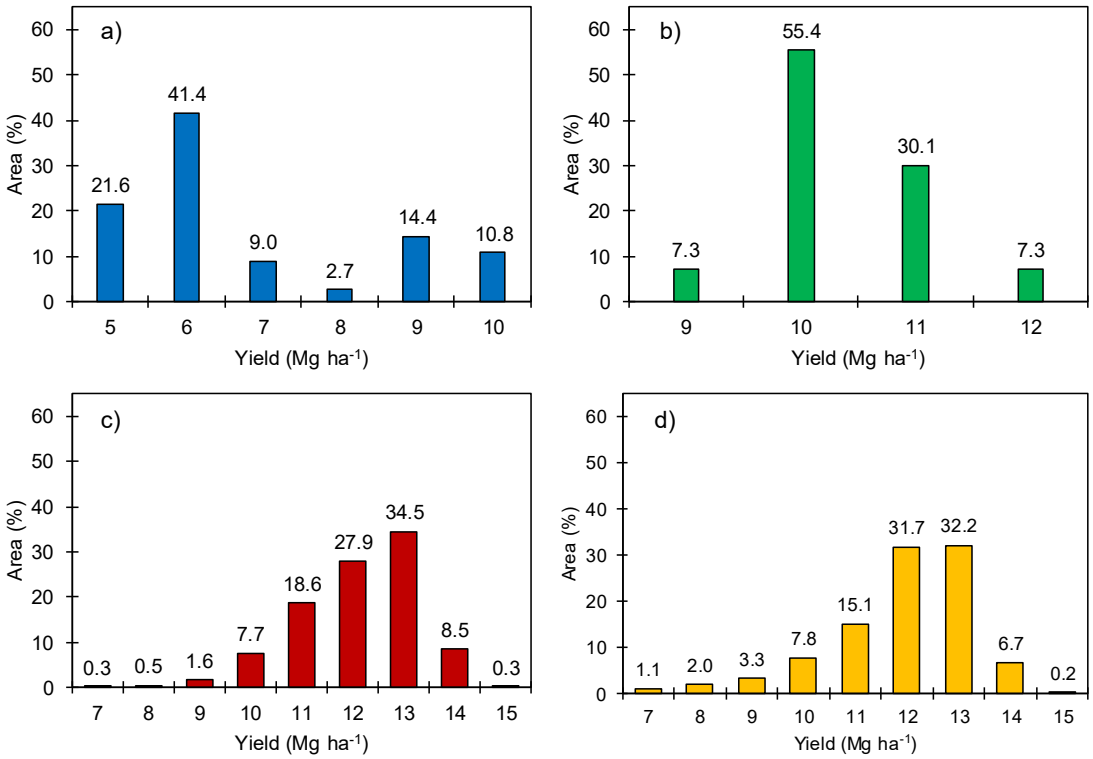

Figure 16. Percentage area of the center pivots according to corn yield average values for the growing seasons of 2013 (a), 2014 (b), 2015 (c) and 2016 (d).

With respect to 2014, 2015 and 2016, normal production years, the yields were in most cases greater than 10 Mg ha^{-1} (Figures 16b, c and d). In 2014, only 7.3% produced less than 10 Mg ha^{-1} (Figure 16b) and in 2015 almost 63% of the area had yields in the range from 12 to 13 Mg ha^{-1} (Figure 16c). In 2016, there were more yield classes, with variation from 7 to 15 Mg ha^{-1}, but with similarities to the years 2014 and 2015, with yield mostly around 12 Mg ha^{-1}. The predominance of corn fields with yield around 12 Mg ha^{-1} for these years allows them to be as of high production, since the Brazilian average is 5.058 Mg ha^{-1}, considering the 2017/18 harvest data and involving irrigated and rainfed fields (CONAB, 2018). In addition, the yield zone analysis highlights the potential of

using precision agriculture in the enhancement of the productivity through managing the low yield locations for more profitability (Al-Gaadi et al., 2016).

4. CONCLUSIONS AND REMARKS

Remote sensing-based model for forecasting corn yield at farm scale based on basal crop coefficient adjusted to water and cold temperatures stress (Kcb_{adj}) and in the water use efficiency for biomass production (WUE^*_B) parameter, were evaluated using surface reflectance images of the Landsat 7 and 8 satellites in four growing seasons involving 52 center pivots. This study evaluated an extensive data set of yield estimates belonging to a commercial farm which employs a high technological level in its production processes, combined with precise knowledge on CP boundaries, to perform a rigorous testing of remote sensing estimates of corn yields. The results obtained from this research showed that Campos et al. (2018) model with some adjustment (i.e., different method for water stress coefficient calculation and interval for Kcb accumulation based on GDD) can be a useful tool for analyzing crop yield in corn plantations established in Brazilian farms.

Agreement between observed and predicted yields was highest when similar hybrids were grouped, especially for Pioneer hybrids, with the majority of the differences, between predicted yield values and measured, remained between -5 and 5%. However, considered that the prediction could be better if some practices were different. The first of them would be the corn harvesting process that would not cause losses (e.g., manual harvest in small plots). Another point is the utilization of a HI specific for each hybrid, considering planting density, crop management, among other factors. It would also be important not to include field boundary in the harvest because, during the zonal statistical analysis, the vector layer of each CP had 30 m of boundary eliminated, according to the spatial resolution of Landsat. Additionally, a probable source of error is the truck weighing process, for instance, assigning the weight of the production of one central pivot to another. This would explain part of the difference in the yield estimates.

Finally, the obtained results are promising and show that pre-harvest corn yield forecasting is operationally feasible because it is easy to acquire satellite images for free and implement the model. Pre-harvest forecasting based on RS data can help in food security, decision-making and export strategies. Yield zone maps can help farmers in their decision-making, identifying problems in areas with low yields and, therefore, adjust their management practices.

Future research should consider some of the sources of error cited above, for instance, considering individual HI and decreasing the losses during harvest , and also testing the model in other regions with different hybrids and managements. In summary, our study demonstrated that the Campos et al. (2018) model with some adjustment for application under Brazilian conditions is able to successfully estimate most of the yield in irrigated corn fields in the western region of Bahia state, Brazil.

5. REFERENCES

Abirdew, S., Mamo, G., Mengesha, M., 2018. Determination of crop water requirements for maize in abshege Woreda, Gurage Zone, Ethiopia. Journal of Earth Science & Climatic Change 09, 2017–2019.

AIBA - Associação de Agricultores e Irrigantes da Bahia, 2017. Anuário da região oeste da Bahia: safra 2016/2017. Barreiras: Bahia, Brazil.

AIBA - Associação de Agricultores e Irrigantes da Bahia, 2016. Anuário agropecuário oeste da Bahia: safra 2015/2016. Barreiras: Bahia, Brazil.

Al-Gaadi, K.A., Hassaballa, A.A., Tola, E., Kayad, A.G., Madugundu, R., Alblewi, B., Assiri, F., 2016. Prediction of potato crop yield using precision agriculture techniques. PLoS ONE 11, 1–16.

Allen, R.G., Pereira, L.S., Raes, D., Smith, M., 1998. Crop evapotranspiration: Guidelines for computing crop water requirements, FAO Irrigation and Drainage Paper No. 56. FAO, Rome, Italy.

Allison, J.C.S., Watson, D.J., 1966. The production and distribution of dry matter in maize after flowering. Annals of Botany 30, 365–381.

Alvares, C.A., Stape, J.L., Sentelhas, P.C., Gonçalves, J.L. De M., Sparovek, G., 2013. Köppen's climate classification map for Brazil. Meteorologische Zeitschrift 22, 711–728.

Angel, J.R., Widhalm, M., Todey, D., Massey, R., Biehl, L., 2017. The U2U corn growing degree day tool: Tracking corn growth across the US Corn Belt. Climate Risk Management 15, 73–81.

Bastiaanssen, W.G.M., Ali, S., 2003. A new crop yield forecasting model based on satellite measurements applied across the Indus Basin, Pakistan. Agriculture, Ecosystems & Environment 94, 321–340.

Battude, M., Al Bitar, A., Morin, D., Cros, J., Huc, M., Marais Sicre, C., Le Dantec, V., Demarez, V., 2016. Estimating maize biomass and yield over large areas using high spatial and temporal resolution Sentinel-2 like remote sensing data. Remote Sensing of Environment 184, 668–681.

Bausch, W.C., 1993. Soil background effects on reflectance-based crop coefficients for corn. Remote Sensing of Environment 46, 213–222.

Bausch, W.C., Neale, C.M.U., 1987. Crop Coefficients Derived from Reflected Canopy Radiation: A Concept. Transactions of the ASAE 30, 703–709.

Bernardo, S., 1989. Manual de Irrigação, 5th ed. UFV, Viçosa.

Bertolin, N. de O., Filgueiras, R., Venancio, L.P., Mantovani, E.C., 2017. Predição da produtividade de milho irrigado com auxílio de imagens de satélite. Revista Brasileira de Agricultura Irrigada 11, 1627–1638.

Bocianowski, J., Nowosad, K., Szulc, P., 2019. Soil tillage methods by years interaction for harvest index of maize (*Zea mays* L.) using additive main effects and multiplicative interaction model. Acta Agriculturae Scandinavica, Section B — Soil & Plant Science 69, 75–81.

Campos, I., Neale, C.M.U., Arkebauer, T.J., Suyker, A.E., Gonçalves, I.Z., 2018. Water productivity and crop yield: A simplified remote sensing driven operational approach. Agricultural and Forest Meteorology 249, 501–511.

Campos, I., Neale, C.M.U., Suyker, A.E., Arkebauer, T.J., Gonçalves, I.Z., 2017. Reflectance-based crop coefficients REDUX: For operational evapotranspiration estimates in the age of high producing hybrid varieties. Agricultural Water Management 187, 140–153.

Casela, C.R., Ferreira, A.S.., de Almeida Pinto, N.F.J., 2006. Doenças na cultura do milho, Circular técnica No. 83. Embrapa, Sete Lagoas, MG.

Caviglia, O.P., Melchiori, R.J.M., Sadras, V.O., 2014. Nitrogen utilization efficiency in maize as affected by hybrid and N rate in late-sown crops. Field Crops Research 168, 27–37.

Chen, J., Zhu, X., Vogelmann, J.E., Gao, F., Jin, S., 2011. A simple and effective method for filling gaps in Landsat ETM+ SLC-off images. Remote Sensing of Environment 115, 1053–1064.

Choudhury, B.J., Ahmed, N.U., Idso, S.B., Reginato, R.J., Daughtry, C.S.., 1994. Relations between evaporation coefficients and vegetation indices studied by model simulations. Remote Sensing Environment 50, 1–17.

Claassen, M., Shaw, R.H., 1970. Water Deficit Effects on Corn. Grain Components. Agronomy Journal 62, 649–652.

CONAB - Companhia Nacional de Abastecimento, 2018. Acompanhamento da safra brasileira de grãos: v.5 - safra 2017/18 - n. 7 - sétimo levantamento, abril 2018. http://www.conab.gov.br (accessed 8.20.18).

Da Silva, P.R.F., Argenta, G., Rezera, F., 1999. Resposta de híbridos de milho irrigado à densidade de plantas em três épocas de semeadura. Pesquisa Agropecuaria Brasileira 34, 585–592.

Demétrio, C.S., Fornasieri Filho, D., Cazetta, J.O., Cazetta, D.A., 2008. Desempenho de híbridos de milho submetidos a diferentes espaçamentos e densidades populacionais. Pesquisa Agropecuaria Brasileira 43, 1691–1697.

Djaman, K., Irmak, S., 2013. Actual crop evapotranspiration and alfalfa- and grass-reference crop coefficients of maize under full and limited irrigation and rainfed conditions. Journal of Irrigation and Drainage Engineering 139, 433–446.

Doorenbos, J., Kassam, A.H., 1979. Yield response to water. FAO Irrigation and Drainage Paper No. 33, Rome, Italy.

Doorenbos, J., Pruitt, W.O., 1977. Guidelines for predicting crop water requirements. FAO Irrigation and Drainage Paper No. 24, Rome, Italy.

Echarte, L., Andrade, F.H., 2003. Harvest index stability of Argentinean maize hybrids released between 1965 and 1993. Field Crops Research 82, 1–12.

Fancelli, A.L., Dourado Neto, D., 2000. Produção de milho. Agropecuária, Guaíba, RS.

Feng, W., Guo, B. Bin, Zhang, H.Y., He, L., Zhang, Y.S., Wang, Y.H., Zhu, Y.J., Guo, T.C., 2015. Remote estimation of above ground nitrogen uptake during vegetative growth in winter wheat using hyperspectral red-edge ratio data. Field Crops Research 180, 197–206.

Figueiredo, F.P. De, Mantovani, E.C., Soares, A.A., Costa, L.C., Ramos, M.M., Oliveira, F.G., 2006. Produtividade e qualidade da banana prata anã, influenciada por lâminas de água, cultivada no Norte de Minas Gerais. Revista Brasileira de Engenharia Agrícola e Ambiental 10, 798–803.

Frampton, W.J., Dash, J., Watmough, G., Milton, E.J., 2013. Evaluating the capabilities of Sentinel-2 for quantitative estimation of biophysical variables in vegetation. ISPRS Journal of Photogrammetry and Remote Sensing 82, 83–92.

Franzen, D.W., 2018. Yield mapping and use of yield map data, North Dakota state university extension. Fargo, North Dakota.

Freitas, E.M., Giovanelli, L.B., Delazari, F.T., Dos Santos, M.L., Pereira, S.B., Da Silva, D.J.H., 2017. Arugula production as a function of irrigation depths and potassium fertilization. Revista Brasileira de Engenharia Agricola e Ambiental 21, 197–202.

Gitelson, A.A., Viña, A., Arkebauer, T.J., Rundquist, D.C., Keydan, G., Leavitt, B., 2003. Remote estimation of leaf area index and green leaf biomass in maize canopies. Geophysical Research Letters 30, 1248.

Hanway, J.J., 1966. How a corn plant develops, Iowa State University of Science and Technology, Cooperative Extension Service. Ames, Iowa.

Hat, J.L., Prueger, J.H., 2015. Temperature extremes : Effect on plant growth and development. Weather and Climate Extremes 10, 4–10.

Holzman, M.E., Rivas, R.E., 2016. Early Maize Yield Forecasting from Remotely Sensed Temperature/Vegetation Index Measurements. IEEE Journal of Selected Topics in Applied Earth Observations and Remote Sensing 9, 507–519.

Holzman, M.E.E., Rivas, R., Piccolo, M.C.C., 2014. Estimating soil moisture and the relationship with crop yield using surface temperature and vegetation index. International Journal of Applied Earth Observation and Geoinformation 28, 181–192.

Huang, J., Ma, H., Liu, J., Zhu, D., Zhang, X., 2013. Regional winter wheat yield estimation by assimilating MODIS ET and LAI products into SWAP model. 2013 2nd International Conference on Agro-Geoinformatics: Information for Sustainable Agriculture, Agro-Geoinformatics 2013 454–459.

Huang, S., Miao, Y., Zhao, G., Yuan, F., Ma, X., Tan, C., Yu, W., Gnyp, M.L., Lenz-Wiedemann, V.I.S., Rascher, U., Bareth, G., 2015. Satellite remote sensing-based in-season diagnosis of rice nitrogen status in Northeast China. Remote Sensing 7, 10646–10667.

Huete, A.R., 1988. A soil-adjusted vegetation index (SAVI). Remote Sensing of Environment 25, 295–309.

Hütsch, B.W., Schubert, S., 2018. Maize harvest index and water use efficiency can be improved by inhibition of gibberellin biosynthesis. Journal of Agronomy and Crop Science 204, 209–218.

Hütsch, B.W., Schubert, S., 2017. Harvest Index of Maize (*Zea mays* L.): Are There Possibilities for Improvement?, in: Sparks, D.L. (Ed.), Advances in Agronomy. Press, Academic, Cambridge, MA, United States, pp. 37–82.

INMET - Instituto Nacional de Meteorologia, 2018. Brazilian climatological normals 1981-2010. Brasília, Brazil. http://www.inmet.gov.br/portal/ (accessed 12.17.18).

IRRIGER - Irrigation management and engineering, 2018. IRRIGER quem somos http://www.irriger.com.br/en-US/ (accessed 7.27.18).

Jin, X., Kumar, L., Li, Z., Feng, H., Xu, X., Yang, G., Wang, J., 2018. A review of data assimilation of remote sensing and crop models. European Journal of Agronomy 92, 141–152.

Kamali, M.I., Nazari, R., 2018. Determination of maize water requirement using remote sensing data and SEBAL algorithm. Agricultural Water Management 209, 197–205.

Koffi Djaman, Suat Irmak, William R. Rathje, Derrel L. Martin, Dean E. Eisenhauer, 2013. Maize Evapotranspiration, Yield Production Functions,

Biomass, Grain Yield, Harvest Index, and Yield Response Factors under Full and Limited Irrigation. Transactions of the ASABE 56, 373–393.

Kotchenova, S.Y., Vermote, E.F., 2007. Validation of a vector version of the 6S radiative transfer code for atmospheric correction of satellite data Part II Homogeneous Lambertian and anisotropic surfaces. Applied Optics 46, 4455–4464.

Kranz, W.., Irmak, S., van Donk, S.J., Yonts, C.D., Martin, D.L., 2008. Irrigation management for corn, NebGuide-G1850.

Kross, A., McNairn, H., Lapen, D., Sunohara, M., Champagne, C., 2015. Assessment of RapidEye vegetation indices for estimation of leaf area index and biomass in corn and soybean crops. International Journal of Applied Earth Observation and Geoinformation 34, 235–248.

Lee, D.S., Storey, J.C., Choate, M.J., Hayes, R.W., 2004. Four years of Landsat-7 on-orbit geometric calibration and performance. IEEE Transactions on Geoscience and Remote Sensing 42, 2786–2795.

Li, F., Miao, Y., Feng, G., Yuan, F., Yue, S., Gao, X., Liu, Y., Liu, B., Ustin, S.L., Chen, X., 2014. Improving estimation of summer maize nitrogen status with red edge-based spectral vegetation indices. Field Crops Research 157, 111–123.

Li, J., Xie, R.Z., Wang, K.R., Ming, B., Guo, Y.Q., Zhang, G.Q., Li, S.K., 2015. Variations in maize dry matter, harvest index, and grain yield with plant density. Agronomy Journal 107, 829–834.

Li, W.J., He, P., Jin, J.Y., 2010. Effect of potassium on ultrastructure of maize stalk pith and young root and their relation to stalk rot resistance. Agricultural Sciences in China 9, 1467–1474.

Lin, H., Chen, J., Pei, Z., Zhang, S., Hu, X., 2009. Monitoring sugarcane growth using ENVISAT ASAR data. IEEE Transactions on Geoscience and Remote Sensing 47, 2572–2580.

Loureiro, D.R., Fernandes, H.C., Teixeira, M.M., Leite, D.M., Fernandes, L.S., 2012. Perdas germinativas na colheita mecanizada do milho cultivado em espaçamentos reduzido e convencional. Semina: Cieências Agrárias 33, 1351–1358.

Mantovani, E., Delazari, F., Dias, L., Assis, I., Viera, G., Landim, F., 2013. Yield and water use efficiency for two sweet potato cultivars depending on irrigation depths. Horticultura Brasileira 31, 602–606.

Mantovani, E.C., Costa, L.C., 1998. Manual do SISDA 2.0, in: Workshop Internacional sobre Manejo Integrado das Culturas e Recursos Hídricos. SRH/UFV, Brasília, DF, p. 153.

Martins, K. V., Dourado-Neto, D., Reichardt, K., Favarin, J.L., Sartori, F.F., Felisberto, G., Mello, S.C., 2017. Maize dry matter production and macronutrient extraction model as a new approach for fertilizer rate estimation. Anais da Academia Brasileira de Ciencias 89, 705–716.

Masek, J.G., Vermote, E.F., Saleous, N.E., Wolfe, R., Hall, F.G., Huemmrich, K.F., Gao, F., Kutler, J., Lim, T., 2006. A landsat surface reflectance dataset. IEEE Geoscience and Remote Sensing Letters 3, 68–72.

Meade, K.A., Cooper, M., Beavis, W.D., 2013. Modeling biomass accumulation in maize kernels. Field Crops Research 151, 92–100.

Medeiros, S. de S., Soares, A.A., Ramos, M.M., Mantovani, E.C., Souza, J.A.A. de, 2003. Avaliação do manejo de irrigação no perímetro irrigado de Pirapora, MG. Revista Brasileira de Engenharia Agrícola e Ambiental 7, 80–84.

Mir, Z.R., Singh, P.K., Zaidi, P.H., Vinayan, M.T., Sharma, S.S., Krishna, M.K., Vemula, A.K., Rathore, A., Nair, S.K., 2018. Genetic analysis of resistance to post flowering stalk rot in tropical germplasm of maize (*Zea mays* L.). Crop Protection 106, 42–49.

Mokhtari, A., Noory, H., Vazifedoust, M., 2018. Improving crop yield estimation by assimilating LAI and inputting satellite-based surface incoming solar radiation into SWAP model. Agricultural and Forest Meteorology 250–251, 159–170.

Moran, M.S., Clarke, T.R., Inoue, Y., Vidal, A., 1994. Estimating crop water deficit using the relation between surface-air temperature and spectral vegetation index. Remote Sensing of Environment 49, 246–263.

O'Shaughnessy, S.A., Andrade, M.A., Evett, S.R., 2017. Using an integrated crop water stress index for irrigation scheduling of two corn hybrids in a semi-arid region. Irrigation Science 35, 451–467.

Peña, J.M., Torres-Sánchez, J., de Castro, A.I., Kelly, M., López-Granados, F., 2013. Weed mapping in early-season maize fields using object-based analysis of Unmanned Aerial Vehicle (UAV) images. PLoS ONE 8, 1–11.

Piccinni, G., Ko, J., Marek, T., Howell, T., 2009. Determination of growth-stage-specific crop coefficients (Kc) of maize and sorghum. Agricultural Water Management 96, 1698–1704.

Pioneer, D., 2017. DuPont Pioneer/Milho/Central de Produtos. http://www.pioneersementes.com.br/milho/central-de-produtos (accessed 12.13.18).

Przybylska, A., Kornobis, F., Obrępalska-Stęplowska, A., 2018. Analysis of defense gene expression changes in susceptible and tolerant cultivars of

maize (*Zea mays*) upon Meloidogyne arenaria infection. Physiological and Molecular Plant Pathology 103, 78–83.

Raes, D., Steduto, P., Hsiao, T.C., Fereres, E., 2018. Chapter 1: FAO crop-water productivity model to simulate yield response to water, in: AquaCrop Version 6.0 – 6.1: Reference Manual. FAO, Rome, Italy, p. 25.

Raes, D., Steduto, P., Hsiao, T.C., Fereres, E., 2017. Chapter 3: Calculation procedures, in: AquaCrop Version 6.0: Reference Manual. FAO, Rome, Italy, p. 151.

Raes, D., Steduto, P., Hsiao, T.C., Fereres, E., 2009. Chapter 2: Users guide, in: AquaCrop: Reference Manual. FAO, Rome, Italy, p. 89.

Rajcan, I., Tollenaar, M., 1999. Source:sink ratio and leaf senescence in maize: Field Crops Research 60, 255–265.

Ranum, P., Peña-Rosas, J.P., Garcia-Casal, M.N., 2014. Global maize production, utilization, and consumption. Annals of the New York Academy of Sciences 1312, 105–112.

Razzaghi, F., Zhou, Z., Andersen, M.N., Plauborg, F., 2017. Simulation of potato yield in temperate condition by the AquaCrop model. Agricultural Water Management 191, 113–123.

Richter, G.M., Agostini, F., Barker, A., Costomiris, D., Qi, A., 2016. Assessing on-farm productivity of Miscanthus crops by combining soil mapping, yield modelling and remote sensing. Biomass and Bioenergy 85, 252–261.

Sakamoto, T., Gitelson, A.A., Arkebauer, T.J., 2013. MODIS-based corn grain yield estimation model incorporating crop phenology information. Remote Sensing of Environment 131, 215–231.

Sangoi, L., Lech, V.A., Rampazzo, C., Gracietti, L.C., 2002. Acúmulo de matéria seca em híbridos de milho sob diferentes relações entre fonte e dreno. Pesquisa Agropecuaria Brasileira 37, 259–267.

Sangoi, L., Almeida, M.L. De, Lech, V.A., Gracietti, L.C., Rampazzo, C., 2001. Desempenho de híbridos de milho com ciclos contrastantes em função da desfolha e da população de plantas. Scientia Agricola 58, 271–276.

Santos, H.G. dos, Carvalho-Júnior, W. de, Dart, R. de O., Áglio, M.L.D., Sousa, J.S. de., Pares, J.G., Fontana, A., Martins, A.L. da S., Oliveira, A.P. de O., 2011. O novo mapa de solos do Brasil: Legenda atualizada, Embrapa. Rio de Janeiro.

Santos, O.F., Cunha, F.F., Taira, T.L., Souza, E.J., Leal, A.J.F., 2018. Increase in pea productivity associated with irrigation management. Horticultura Brasileira 36, 178–183.

Schmidt, G., Jenkerson, C., Masek, J., Vermote, E., Gao, F., 2013. Landsat Ecosystem Disturbance Adaptive Processing System (LEDAPS) Algorithm Description, Open-file Report 2013-1057. Reston, Virginia.

Segovia-Cardozo, D.A., Rodríguez-Sinobas, L., Zubelzu, S., 2019. Water use efficiency of corn among the irrigation districts across the Duero river basin (Spain): Estimation of local crop coefficients by satellite images. Agricultural Water Management 212, 241–251.

Sibley, A.M., Grassini, P., Thomas, N.E., Cassman, K.G., Lobell, D.B., 2014. Testing remote sensing approaches for assessing yield variability among maize fields. Agronomy Journal 106, 24–32.

Silva, G.H., Ferreira, M.G., Pereira, S.B., Delazari, F.T., Silva, D.J.H., 2018. Response of bell pepper crop subjected to irrigation depths calculated by different methodologies. Revista Brasileira de Engenharia Agrícola e Ambiental 22, 45–50.

Song, X., Wang, J., Huang, W., Liu, L., Yan, G., Pu, R., 2009. The delineation of agricultural management zones with high resolution remotely sensed data. Precision Agriculture 10, 471–487.

Souza, J. de, Ramos, M., Soares, A., 2005. Efeitos da fertirrigação com água residuária de origem urbana sobre a produtividade do cafeeiro. Revista Brasileira de Engenharia Agrícola e Ambiental 128–132.

Statista – The portal for statistics, 2018. Worldwide production of grain in 2017/18, by type (in million metric tons). https://www.statista.com/ (accessed 7.27.18).

Steduto, P., Hsiao, T.C., Fereres, E., 2007. On the conservative behavior of biomass water productivity. Irrigation Science 25, 189–207.

Steduto, P., Hsiao, T.C., Fereres, E., Raes, D., 2012. Crop yield response to water, FAO Irrigation and Drainage Paper 66. FAO, Rome.

Steduto, P., Hsiao, T.C., Raes, D., Fereres, E., 2009. Aquacrop-the FAO crop model to simulate yield response to water: I. concepts and underlying principles. Agronomy Journal 101, 426–437.

Storey, J., Choate, M., Lee, K., 2014. Landsat 8 operational land imager on-orbit geometric calibration and performance. Remote Sensing 6, 11127–11152.

USGS - United States Geological Survey, 2018. Landsat8 Surface Reflectance code (LaSRC) Version 4.3 PRODUCT: Product Guide. https://landsat.usgs.gov/sites/default/files/documents/lasrc_product_guide.pdf (accessed 2.15.18).

Vanuytrecht, E., Raes, D., Steduto, P., Hsiao, T.C., Fereres, E., Heng, L.K., Garcia Vila, M., Mejias Moreno, P., 2014. AquaCrop: FAO's crop water productivity and yield response model. Environmental Modelling and Software 62, 351–360.

Veloso, A., Mermoz, S., Bouvet, A., Le Toan, T., Planells, M., Dejoux, J.F., Ceschia, E., 2017. Understanding the temporal behavior of crops using Sentinel-1 and Sentinel-2-like data for agricultural applications. Remote Sensing of Environment 199, 415–426.

Vermote, E.F., Tanré, D., Deuzé, J.L., Herman, M., Morcrette, J.J., 1997. Second simulation of the satellite signal in the solar spectrum, 6S: An overview. IEEE Transactions on Geoscience and Remote Sensing 35, 675–686.

Veysi, S., Naseri, A.A., Hamzeh, S., Bartholomeus, H., 2017. A satellite based crop water stress index for irrigation scheduling in sugarcane fields. Agricultural Water Management 189, 70–86.

Vicente, M.R., Mantovani, E.C., Fernandes, A.L.T., Neves, J.C.L., Figueredo, E.M., Delazari, F.T., 2017. Spacial distribution of fertigated coffee root system. Ciencia e Agrotecnologia 41, 72–80.

Vieira, G.H.S., Mantovani, E.C., Sediyama, G.C., Delazari, F.T., 2014. Produtividade e rendimento industrial da cana-de-açúcar em função de lâminas de irrigação. Bioscience Journal 30, 55–64.

Wang, J., Li, X., Lu, L., Fang, F., 2013. Parameter sensitivity analysis of crop growth models based on the extended Fourier Amplitude Sensitivity Test method. Environmental Modelling and Software 48, 171–182.

Wang, L., Li, X.G., Guan, Z.-H.H., Jia, B., Turner, N.C., Li, F.-M.M., 2018. The effects of plastic-film mulch on the grain yield and root biomass of maize vary with cultivar in a cold semiarid environment. Field Crops Research 216, 89–99.

Xie, Y., Wang, P., Bai, X., Khan, J., Zhang, S., Li, L., Wang, L., 2017. Assimilation of the leaf area index and vegetation temperature condition index for winter wheat yield estimation using Landsat imagery and the CERES-Wheat model. Agricultural and Forest Meteorology 246, 194–206.

Yang, H., Grassini, P., Cassman, K.G., Aiken, R.M., Coyne, P.I., 2017. Field Crops Research Improvements to the Hybrid-Maize model for simulating maize yields in harsh rainfed environments. Field Crops Research 204, 180–190.

Zhai, L., Xie, R., Li, S., Fan, P., 2017. Relationship between population competitive intensity and yield in maize cultivars. Journal of Integrative Agriculture 16, 1312–1321.

CHAPTER 3

Assessing vegetation spectral indices' performance for corn biomass production estimation based on photosynthetically active vegetation sub-pixel fraction

ABSTRACT

Biomass production (Bio) estimation prior to harvest is very important for several processes of decision-making, as that parameter, in turn, can be estimated from vegetation spectral indices (VI), because many of them showed a close relationship with absorbed photosynthetically active radiation (APAR), which is proportional to Bio. The goal of this study was to investigate the performance of nine vegetation indices for Bio estimation in irrigated corn fields by means of their comparison with the photosynthetically active vegetation sub-pixel fraction estimated from Spectral Mixture Analysis. A specific goal, from the findings of the first study, was find the best interval of VI accumulation (days) for corn grain yield estimation, using the three best classified indices in the general goal. For the first objective, field data of center pivots cultivated with corn during the irrigated season of 2015 were used along with OLI images, while for the second objective data of corn grown in the 2018 season and Sentinel 2 images were used. EVI was the VI which had the best results in the comparison, with Pearson's correlation coefficient, RMSE and Willmott's index of agreement equal to 0.99, 6.5%, and 0.948, respectively. Among the analyzed indices EVI, SAVI and OSAVI were considered the first, second and third best, respectively, for corn Bio estimation, based on their comparison with photosynthetically active vegetation sub-pixel fraction. The intervals that extended up to 120 days after sowing were the best.

Keywords: Corn biomass, spectral vegetation indices, spectral unmixing, irrigation.

1. INTRODUCTION

Vegetation spectral indices (VI) can be defined as the arithmetic combination of two or more bands related to the spectral characteristics of vegetation (Matsushita et al., 2007). Applications of remote sensing data in agriculture typically involve the use of these VI to indicate vegetation vigor and amount, because they are normally proportional to the value of biophysical parameters (Ji and Peters, 2007), such as biomass production (Bio) of the corn crop (Kross et al., 2015). Bio estimation using VI is possible because many of them provide a stable and near-linear estimate of absorbed photosynthetically active radiation - APAR (Goward and Huemmrich, 1992; Myneni and Williams, 1994; Tan et al., 2013), which is proportional to total biomass (Daughtry et al., 1992; Gallo et al., 1982; Kalaitzidis et al., 2010; Liu et al., 2010, 2004; Monteith, 1972).

Among the existing VI for APAR estimation, the most recommended ones based on their formulation (i.e., physical meaning of spectral index), and also the best known, according to Qin et al. (2018) are: Simple Ratio – SR (Jordan, 1969), Normalized Difference Vegetation Index – NDVI (Rouse et al., 1973), green NDVI – gNDVI (Gitelson et al., 1996) and Enhanced Vegetation Index – EVI (Huete et al., 2002). Additionally, VI related to leaf area index (LAI) and chlorophyll content (Chl) can also be considered in studies involving crop biomass estimation, because these parameters are also an important factor influencing the APAR (Qin et al., 2018).

Regarding Chl for example, it can be considered a coarse surrogate for the ability of vegetation to photosynthesize (i.e., higher chlorophyll content = greater photosynthesis ability = higher APAR), and the same applies to leaf area (i.e., higher LAI = increased light uptake = greater photosynthesis = higher APAR). Thus, the green chlorophyll index - CI_{green} (Gitelson et al., 2005), developed for remotely estimating chlorophyll in maize and soybean canopies (Gitelson et al., 2005) and soil-adjusted vegetation index – SAVI (Huete, 1988), more indicated for LAI estimation (Hatfield and Prueger, 2010), can be considered for APAR and Bio estimation.

In this context, several VI can be listed for the estimation of APAR, LAI and Chl, and consequently Bio, where each one has its own merits and limitations (Ji and Peters, 2007). An ideal VI should be highly sensitive to biophysical parameters while being relatively insensitive to noise caused by canopy background and atmospheric effects (Huemmrich, 1996; Ji and Peters, 2007). Thus, it is always very important to evaluate these VI aiming to know better the influence of these merits and limitations, when the VI are used to assess a certain biophysical parameter, Bio in the present study, taking into account its close relationship with LAI, Chl and specially with APAR.

These vegetation indices can be evaluated using the fraction of photosynthetically active radiation (fPV). Since the fPV is the class of vegetation of a plant responsible for photosynthesis, mainly by means of leaf area (Li and Guo, 2015), thus, VI well-related to it are also strongly related to Bio. Besides that, the fPV when compared to VI is less subject to variations in factors, such as scene lighting conditions and atmospheric variations (Shimabukuro et al., 1998); thus, it can be used as reference for evaluation of these VI. Lastly, these evaluations could offer more precise insight into the relationship between the VI and Bio, identifying the best ones.

The fPV can be estimated using Spectral Mixture Analysis - SMA (Adams et al., 1986), which is a well-established and effective technique to address this mixture problem (Somers et al., 2011). The SMA model is based on the assumption that the spectra of materials in an instrumental instantaneous field of view (IFOV) combine linearly with proportions given by their relative abundances (Adams et al., 1995, 1986; Roberts et al., 1998; Shimabukuro and Smith, 1991). SMA is a method widely employed (Shimabukuro and Ponzoni, 2017), especially in areas with low spectral variability and low variation in the number and the type of endmember classes contained from pixel to pixel (Sun et al., 2017), such as irrigated corn fields.

These kinds of fields normally contain: (i) photosynthetic vegetation (healthy corn plants), (ii) soil and (iii) shade. Besides fPV, the application of SMA model generates also the shade fraction (fSh), which may be an interesting additional information because shade can lead to either reduction or total loss of information in an image, and this can potentially lead to corruption of biophysical

parameters derived from pixels values, such as vegetation indices (Zhang and Huang, 2015).

In this context, considering the close relation between Bio and APAR, LAI and Chl, and that these three biophysical parameters can be estimated from vegetation indices, the general goal of the present study was to investigate the performance of nine vegetation indices for Bio estimation in irrigated corn fields by means of their comparison with the photosynthetically active vegetation sub-pixel fraction estimated from Spectral Mixture Analysis, defining the three best ones. Considering that corn Bio is directly related to grain yield by means of a harvest index, the second objective was to answer the following question: what is the best interval of VI accumulation (days) for corn grain yield estimation, using the three best classified indices in the general goal?

2. MATERIAL AND METHODS

2.1. Study areas and ground data

The study areas belong to two commercial farms, located in the western region of Bahia state, Brazil. The primary study area (A1) was a center pivot field (13°13'50.32"S, 43°42'35.83"W and 458 m above mean sea level), located in the municipality of Serra do Ramalho (Figure 1b). The field has approximately 90 ha of cropped area with soil classified as Yellow Latosol (Santos et al., 2011).

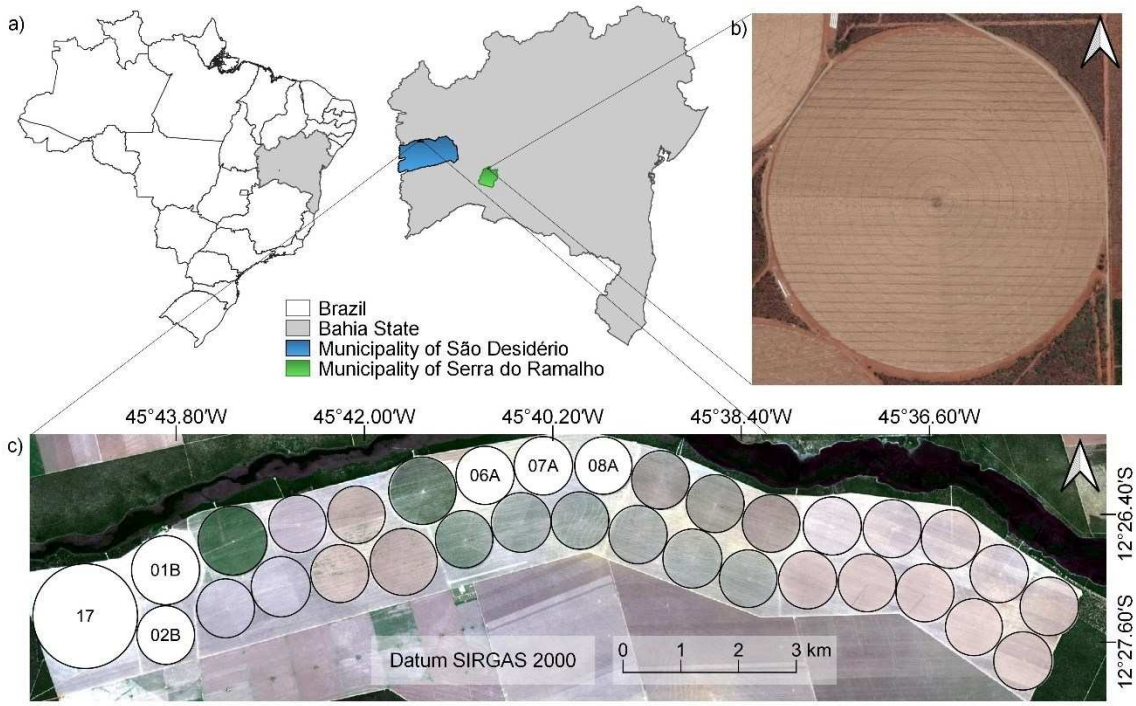

Figure 1. Location of study areas in the Brazilian territory (a), first (b) and second (c) fields of study.

The second field (A2) involved six center pivots in the municipality of São Desidério and is inserted in the rectangle bounded by the following coordinate pairs: lower-left 12°28'08"S; 45°45'12"W and upper-right 12°25'40"S; 45°34'55"W, reference system of geographic coordinates, Datum SIRGAS-2000, with an average altitude of 750 m above sea level (Figure 1c). As in the first area of study, the predominant soil type in A2 is Yellow Latosol (Santos et al., 2011). These two farms have a flat relief and, according to Köppen's climatic classification (Alvares et al., 2013), the climate of the region is Aw, tropical climate, with rainy season in the summer and dry winter.

A1 was used in the first part of the study, which involved the investigation of the performance of nine vegetation indices for Bio estimation based on their relationship with the fraction of photosynthetically active radiation (fPV) images derived from the Spectral Mixture Analysis (SMA). Regarding A2, it was used in the second study, about corn grain yield estimation based on cumulative vegetation indices over different periods of the growing season. This study was conducted using field data of the corn crop (*Zea mays* L.) collected by the

company IRRIGER - Irrigation management and engineering (http://www.irriger.com.br/en-US/). The following data were used: sowing and harvest dates, duration of the cycle, hybrid name and grain yield for each one of the center pivots cultivated (Table 1).

Table 1. Sowing date (SD), harvest date (HD), duration of the cycle (DC) and cultivated hybrid name for each center pivot (CP) analyzed

CP	SD	HD	DC	Hybrid	Area	Yield
-	-	-	days	-	ha	Mg ha^{-1}
			A1			
11	05/05/2015	09/22/2015	140	DBK 390 Pro 2	90	7.03
			A2			
01B	04/12/2018	09/18/2018	159	Status Viptera 3	115	10.81
02B	04/13/2018	09/18/2018	158	Status Viptera 3	80	11.37
06A	04/16/2018	09/08/2018	145	DuPont Pioneer 30F35	80	10.23
07A	04/17/2018	09/09/2018	145	DuPont Pioneer 30F35	80	10.34
08A	04/18/2018	09/10/2018	145	DuPont Pioneer 30F35	80	10.96
17	04/20/2018	09/20/2018	153	Supremo Viptera 3	260	12.01

Figure 2 provides the overall processes followed in this study and a detailed description is subsequently provided.

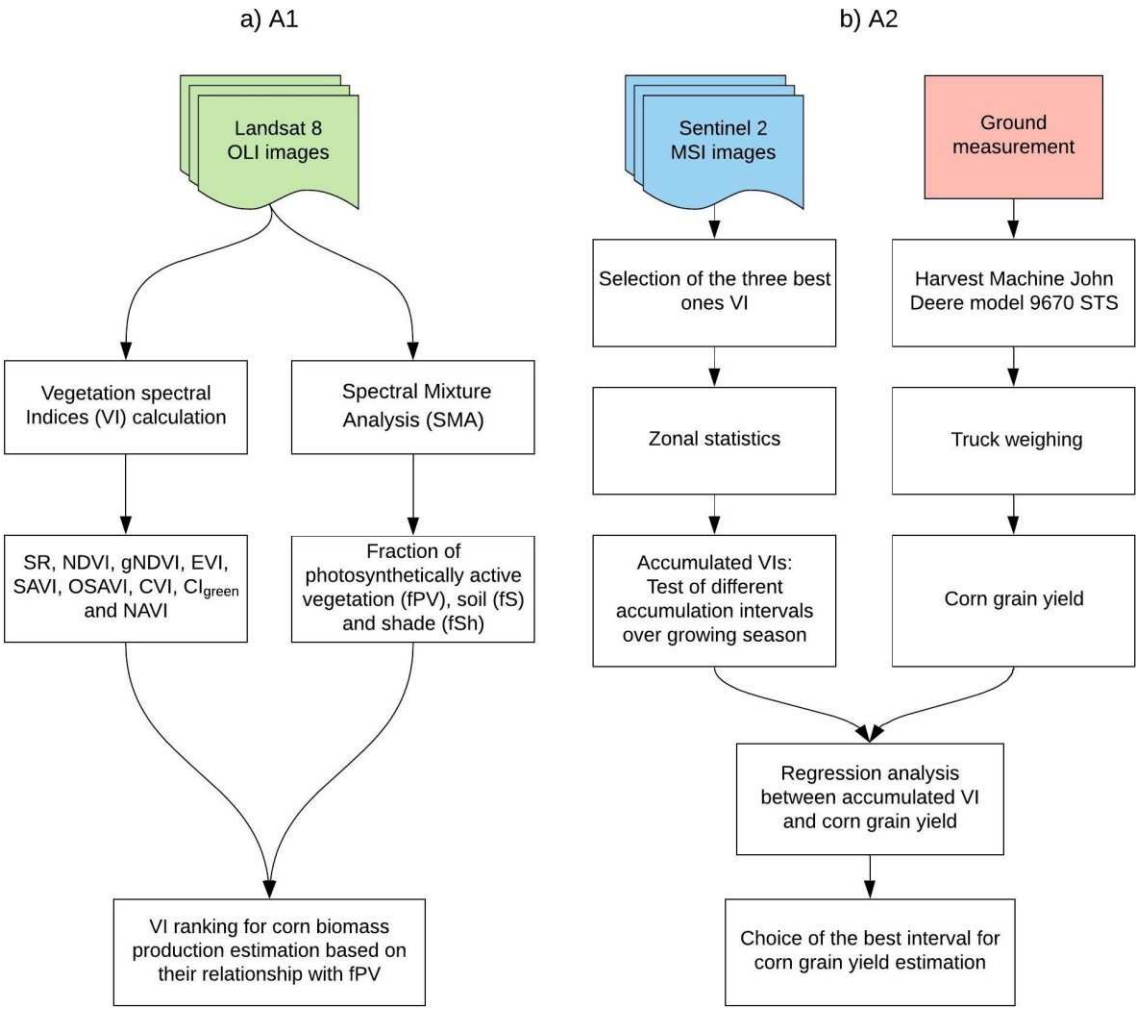

Figure 2. Step-by-step flowchart followed to assess the performance of nine VI used for corn biomass production estimation based on fraction of photosynthetically active radiation estimated from the Spectral Mixture Analysis (a), and for corn grain yield estimation from cumulative VI (b).

2.2. Satellite data and data pre-processing

The present study used images of the Operational Land Imager (OLI) sensor - Landsat 8 and images of the MultiSpectral Instrument (MSI) – sensor Sentinel 2A and B. Landsat OLI had spatial resolution of 30 m, temporal resolution of 16 days and spectral bands such as 1-Coastal blue (0.435-0.451 μm), 2-Blue (0.452-0.512 μm), 3-Green (0.533-0.590 μm), 4-Red (0.636-0.673 μm), 5-near infrared (0.851-0.879 μm), 6-shortwave infrared-1 (1.566-1.651 μm)

and 7-shortwave infrared-2 (2.107-2.294 μm) (Roy et al., 2014; USGS (United States Geological Survey), 2016).

Landsat 8 images are originally distributed as Level 1 terrain corrected (L1T) products, which means that images have systematic radiometric and geometric accuracy, orthorectification with a digital elevation model (DEM) and precision correction assisted by ground control chips (Peña and Brenning, 2015; Roy et al., 2014; USGS (United States Geological Survey), 2016). OLI sensor images (path: 219 and row: 069) were downloaded from the United States Geological Survey (USGS) EarthExplore (https://earthexplorer.usgs.gov/). Surface reflectance (SRe, top of atmosphere reflectance (TOA) corrected for atmospheric effect) images were utilized. SR images are generated by the USGS on-demand processing system EROS Science Processing Architecture (ESPA) (https://espa.cr.usgs.gov/).

Sentinel 2 is a mission comprising twin satellites named Sentinel-2A (launched on June 23, 2015) and Sentinel-2B (launched in mid-2016) in the same orbit, phased at 180° to each other, thus the revisit time is reduced from 10 days to 5 days. They acquire images in 13 bands positioned in the visible (VIS), red-edge, near infrared (NIR) and shortwave infrared (SWIR) spectral regions having spatial resolutions ranging from 10 to 60 m (ESA, 2015; Navarro et al., 2017). The present study used the bands of red, green, blue and NIR, which have 10 m spatial resolution. The spectral width of these bands (in μm) for 2A and 2B satellites, respectively, are: blue (0.458-0.523 and 0.443-0.541), green (0.543-0.578 and 0.536-0.582), red (0.650-0680 and 0.646-0.685) and NIR (0.785-0.900 and 0.767-0.900).

MSI sensor images were downloaded from the Copernicus Open Access Hub (https://scihub.copernicus.eu). The standard MSI data product is a radiometrically and geometrically corrected image referred to as Level-1C (L1C). The L1C product contains ortho-rectified scaled top-of-atmosphere (TOA) reflectance (Barsi et al., 2018). The surface reflectance images were obtained by means of Dark-Object Subtraction (DOS1) atmospheric correction method (Chavez, 1996, 1988) using the Semi-automatic Classification Plugin (SCP) in the QGIS (Congedo, 2018).

A total of seven cloud-free images covering the A1 (Figure 1b) and belonging to the OLI sensor were acquired during the irrigated corn growing season of 2015, resulting in 20-day temporal resolution of the series. In respect to MSI sensor, a total of 23 cloud-free images covering the A2 (Figure 1c) were downloaded, concerning to the corn harvest of 2018, resulting in 6.6-day temporal resolution of the series. The number of images of the MSI sensor used for corn grain yield estimation changed between the six center pivots, according to different sowing and harvest dates of the fields (see Table 1).

2.3. Vegetation indices

Table 2 shows the nine spectral vegetation indices related to the APAR, LAI and Chl, used in this work. For each one of the biophysical parameters (i.e., APAR, LAI and Chl), three VI which have close relationship with them were selected based on their physical meaning and previous studies. However, it should be pointed out that all these VI relate to other biophysical parameters of vegetation in general. These VI use a combination of visible and near-infrared bands.

Table 2. Vegetative indices evaluated in this study

Name	Equation	References
SR[1]	$SR = \frac{\rho_{NIR}}{\rho_{red}}$	(Jordan, 1969)
NDVI[1]	$NDVI = \frac{(\rho_{NIR} - \rho_{red})}{(\rho_{NIR} + \rho_{red})}$	(Rouse et al., 1973)
gNDVI[1]	$gNDVI = \frac{(\rho_{NIR} - \rho_{green})}{(\rho_{NIR} + \rho_{green})}$	(Gitelson et al., 1996)
EVI[2]	$EVI = 2.5\frac{(\rho_{NIR} - \rho_{red})}{(\rho_{NIR} + 6 \times \rho_{red} - 7.5 \times \rho_{blue} + 1)}$	(Huete et al., 2002)
SAVI[2]	$SAVI = \frac{(\rho_{NIR} - \rho_{red})}{(\rho_{NIR} + \rho_{red} + L)} \times (1+ L)$	(Huete, 1988)

OSAVI[2]	$OSAVI = \frac{(\rho_{NIR} - \rho_{red})}{(\rho_{NIR} + \rho_{red} + 0.16)}$	(Rondeaux et al., 1996)
CVI[3]	$CVI = \frac{\rho_{NIR}}{\rho_{green}} \times \frac{\rho_{red}}{\rho_{green}}$	(Vincini et al., 2008)
CI_{green}[3]	$CI_{green} = \frac{\rho_{NIR}}{\rho_{green}} - 1$	(Gitelson et al., 2005)
NAVI[3]	$NAVI = 1 - \frac{\rho_{red}}{\rho_{NIR}}$	(Carmona et al., 2015)

SR = simple ratio; NDVI = normalized difference vegetative index; gNDVI = green normalized difference vegetative index; EVI = enhanced vegetation index; SAVI = soil-adjusted vegetation index; OSAVI = optimized soil-adjusted vegetation index; CVI = chlorophyll vegetation index; CI_{green} = green chlorophyll index and NAVI = normalized area vegetation index. ρ_{NIR}, ρ_{red}, ρ_{green}, ρ_{blue} refer to the reflectance of near-infrared, red, green, and blue spectral bands and L is the soil brightness correction factor (0.5 was used). Number subscribed next to index name: [1] meaning that the VI is more indicated for APAR estimation, [2] meaning that the VI is more indicated for LAI estimation and [3] meaning that the VI is more indicated for Chl estimation.

2.4. Spectral Mixture Analysis (SMA)

From a mathematical point of view, any mixed pixel of corn plantation areas in no-till system can be denoted as a linear combination of spectral endmembers, such as: (i) photosynthetic vegetation (i.e., healthy corn plants), (ii) soil, and (iii) shade. Thus, the SMA model aims to separate each one of the components and its respective proportion in the interest area (Adams et al., 1995, 1986; Roberts et al., 1998; Shimabukuro and Smith, 1991). It is important to point out that, since the spectral behavior of non-photosynthetically active vegetation (fNPV) is very similar to that of a soil, especially dark soils (Adams et al., 1995; Xiao and Moody, 2005), it is modelled as a soil in the SMA application. The application of SMA model consists basically in the following five steps: (i) endmembers selection; (ii) developing a spectral library; (iii) establishment of constraints; (iv) mathematical resolution of the SMA model, and (v) evaluation of results. These steps will be detailed below.

SMA decomposition was accomplished by means of an open-source plug-in for the ENVI software named Visualization and Image Processing for Environmental Research (VIPER) Tools, version 1.5 (Roberts et al., 2007) available at https://sites.google.com/site/ucsbviperlab/viper-tools. VIPER Tools can be used on a wide variety of data types for a diversity of applications such as creation and management of endmember spectral libraries, creation of spectral libraries from region of interest (ROI) in the images, view of spectral library, statistical analysis of separability among spectral classes, among others (Roberts et al., 2007).

2.4.1. Endmembers selections and spectral library

Endmembers are spectral signatures of constituent materials in an image scene (Yin et al., 2019), and selecting endmembers involves identifying both the number and type of endmembers and their corresponding spectral signatures (Shrivastava et al., 2016). In this paper, the multispectral bands 1 to 7 of the OLI sensor were used as input to find the endmembers, after a layer stack creation with these bands. The endmembers (i.e., photosynthetic vegetation and soil) were obtained from the image of May 18, 2015, using the tool called region of interest (ROI), being used for SMA model application in all seven images.

Since the endmember is selected from the image data, it receives the name of image endmember (IE). An IE is obtained by locating a pixel in the scene with the maximum abundance of the physical endmember it will represent (Quintano et al., 2012). Image endmembers have the advantage of being collected at the same scale and under the same environmental conditions as the remotely sensed data and can, thus, be more easily associated with spectral components in the image scene (Plaza et al., 2004; Shimabukuro and Ponzoni, 2017). It is important to point out that VIPER Tools allows the shade component to be computed from the difference between the user-defined summation and the values of the other components, dispensing the user from the selection of endmembers of this component (Roberts et al., 2007).

The endmembers were selected from the image based on the distribution of the pixels in the red-infrared sample space (i.e., 2D scatter plot) and

considering the simplex theory (Bajjouk et al., 1998) where the purest pixels are at the vertices of the distribution. The NIR and red bands were better able to produce triangles with straight and distinct, as previously described by some authors in similar works (Baig et al., 2014; Kao et al., 2014). Once a spectral library is developed from IE, the VIPER tools allows the SMA model to be run. The endmember spectra used for spectral mixture analysis of the OLI images can be seen in Figure 3.

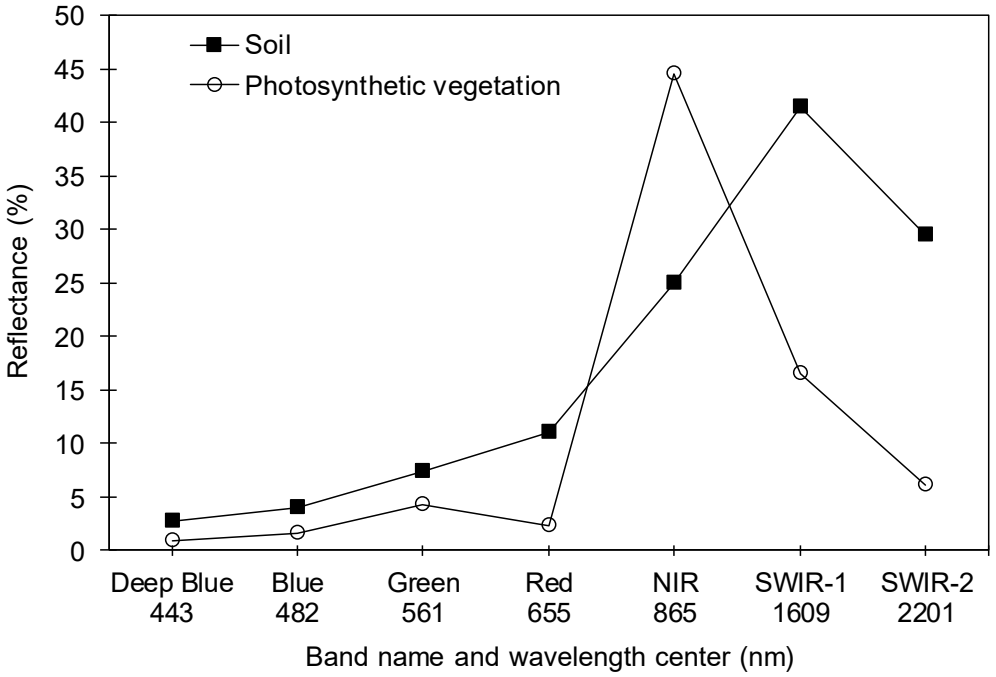

Figure 3. Endmember spectra used for spectral mixture analysis of the OLI images. NIR (near infrared) and SWIR (shortwave Infrared).

2.4.2. Establishment of constraints

The constraints in the VIPER tools are optional. The following constraint options are available: (i) minimum endmember fraction; (ii) maximum endmember fraction; (iii) maximum shade fraction, (iv) maximum RMSE and residual constraints. Was adopted the minimum allowable endmember fraction, maximum allowable endmember fraction, maximum allowable shade fraction and a

maximum allowable RMSE as follows: − 0.05, 1.05, and 0.8 and 0.025, respectively. These values used are the standard of Viper tools.

2.4.3. *Mathematical resolution of the model and evaluation of results*

There are several mathematical approaches that allow arriving at a spectral mixture analysis model solution, and estimating the components of the mixture, and the most common ones available in the image processing software are the Constrained Least Squares (CLS), Weighted Least Square (WLS), and Principal Component Analysis (PCA) (Shimabukuro and Ponzoni, 2017). VIPER tools works with these three mathematical models and for each pixel the residual spectrum is calculated as the image spectrum minus the model spectrum, where the model is the best fit model for that pixel as determined by minimum RMSE (Roberts et al., 2007).

The default outputs are an SMA image which contains endmember fraction(s), shade fraction, model number and model RMSE (Roberts et al., 2007). A valid and meaningful spectral unmixing requires that (i) the sum of all endmember fractions in a pixel should be equal to 1, and (ii) any endmember fraction should range from 0 to 1 (Yang et al., 2014).

2.5. Vegetation indices evaluation

In order to rank the three best VI to be used in the estimation of corn aboveground dry biomass considering their relationship with fraction of photosynthetically active vegetation (fPV), was analyzed the Pearson's correlation coefficient between these VI and fPV. Previous studies have been performed using linear correlation to verify the relationship between these variables of remote sensing (Jiménez-Muñoz et al., 2009; Rundquist, 2002). Thus, considered which of the VI had a better performance, higher positive correlation with fPV (reference), since this fraction when compared to VI is subject to less variations in factors, such as scene lighting conditions and atmospheric variations (Shimabukuro et al., 1998).

Regarding the fraction of shade (fSh), its influence on VI is not easy to be analyzed. Studies with this focus commonly involve the use of specific equipment, such as field imaging spectrometer system (Zhang and Huang, 2015) or push-broom scanning sensor (Zhou et al., 2017). Thus, fSh was considered as additional information, with the following criterion: the VI with better performance, in general terms, are those which have no correlation (close to 0) or higher negative correlation (close to -1) with fSh. This criterion was established based on the premises of Zhang and Huang (2015). These authors cite that shadows can lead to either a reduction or total loss of information in an image, and this can potentially lead to corruption of biophysical parameters derived from pixel values, such as vegetation indices.

In addition, the VI performance also was assessed by comparing them with fPV values by means of Root Mean Square Error (RMSE) and Willmott's index of agreement (d) (Willmott, 1982). To make possible the comparisons between the fPV and VI, they were normalized to the range from 0 to 1. These analyses used data of center pivot number 11 in the 2015 year, located in A1 (Figure 1b) and the information was extracted from 904 pixels regularly spaced inside the field (Figure 4).

Figure 4. Regular point grid spacing resulting in 904 pixels within the center pivot field after a -30 m buffer from the original vector layer (white line) to avoid a border effect. Source: Google Earth Pro 11/18/2018.

2.6. Corn grain yield estimation based on cumulative VI

From the Bio, corn grain yield can be assessed using a harvest index (HI) (Caviglia et al., 2014; Hütsch and Schubert, 2018; Koffi Djaman et al., 2013). Thus, the VI used to assess corn biomass is also useful for grain estimation, as seen in previous studies with corn (Bertolin et al., 2017; Fang et al., 2011; Tagarakis and Ketterings, 2017) and wheat (Sultana et al., 2014). The three VI classified as the best ones were used to conduct the second part of the study, which aimed to estimate corn grain yield based on VI accumulated in different intervals over the corn growth season. For this purpose, corn grain yield measured in the 2018 growing season and MSI sensor images were used. Harvests are performed using harvesting machines from John Deere, 9670 STS model, and yield is measured by weighing the truck containing the harvested grains. The used intervals, taking into account important phenological stages of the corn crop and defined based on days after sowing (DAS), are presented in Table 3.

Table 3. Interval number, initial (DASi) and final (DAS_f) days after sowing of accumulation and the respective description of interval

Interval	DAS_i	DAS_f	Interval description
1	0	77	From sowing to flowering/ pollination
2	0	120	From sowing to physiological maturity
3	7	77	From emergence to flowering/ pollination
4	7	120	From emergence to physiological maturity
5	14	77	From beginning of photosynthetic processes to flowering/ pollination
6	14	120	From beginning of photosynthetic processes to physiological maturity

These DAS values represent the average values, because these events can change according to climatic conditions, hybrid, crop management, among others.

The choice of the best interval, among the six analyzed, was based on r^2 value. No independent validation of the results was performed. Only was evaluated the best interval for corn grain yield estimation. It is important to point out that the lack of image near the sowing and harvest dates is disadvantageous for the creation of the curves of vegetation indices and, consequently, for the estimation of cumulative VI. Thus, worked with mean values for these dates. The values were obtained from center pivot fields that had ± four days of difference between sowing date and image date. For the harvest date, the criterion was the use of image coinciding with this date or until three days before.

3. RESULTS AND DISCUSSION

3.1. SMA model application

Figure 5 presents sub-pixel fractions of photosynthetic vegetation (fPV), soil (fS) and shade (fSh), resulting from SMA model application, along with an RGB image. The light areas in these images indicate the highest proportion of the components (fPV, fS and fSh) in the pixels. As a function of crop corn development, fPV and fS had an antagonistic behavior, and fSh had the lowest variation among the fractions. After 13 DAS, fPV represents only 4.5% of the image, while most of it is formed by fS (Figure 5).

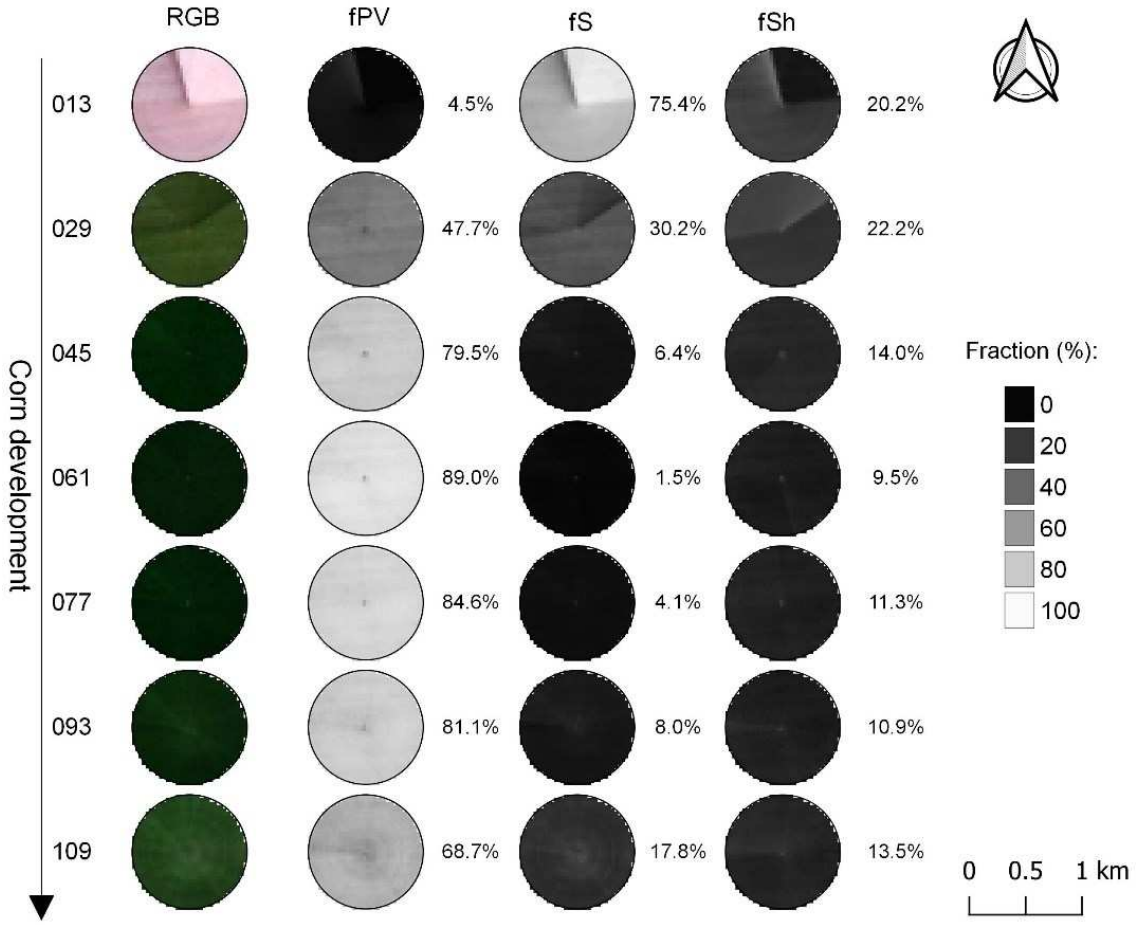

Figure 5. RGB432 Landsat 8 and photosynthetic vegetation (fPV), soil (fS) and shade (fSh) sub-pixel fractions as a function of the days after sowing (DAS).

With 61 DAS, the corn crop showed the highest values of fPV among the seven images and probably this value is close to the maximum values, since the maximum leaf area index (LAI) is observed between 60 and 70 DAS (Bergamaschi et al., 2006; Kross et al., 2015; Lizaso et al., 2005; Lukeba et al., 2013; Soleymani, 2018; Soufizadeh et al., 2018; Wolschick et al., 2003), which in terms of growing degree days (GDD) is around 700-800 (Campos et al., 2017). After 77 DAS, the fPV tends to decrease because the corn plant reached its maximum height (Lizaso et al., 2005; Lukeba et al., 2013), starting from this moment onwards the reproductive phases (Hanway, 1966). In respect to the fS, its proportion is automatically linked to the fPV; thus, as fPV increased there was a decrease in fS, and the opposite is also true (Figure 5).

The highest values of fSh were observed during the initial stage, 20.2% and 22.2% at 13 and 29 DAS, respectively (Figure 5). This behavior results from the shadow generated by the corn plant, projecting on the ground and, then, being measured by the imager sensor. As the crop develops, the fSh would tend to increase, but the sensor cannot measure it, as in the initial stage, since corn leaves are the top of the surface (i.e., the element to be captured). Due to these facts, fSh showed the lowest value at 61 DAS (9.5%), when LAI tends to be maximum, as discussed previously.

3.2. Corn development access by means of VI and fPV

Figure 6 shows the spatial and temporal distribution of fPV and VI over the corn growing season, after the normalization for 0 to 1 interval. The spatial and temporal distributions of corn growth of the nine vegetation indices are well matched with fPV. It can be seen from Figure 6 that, with 13 DAS, all VI had low values, indicating the start of corn growth, since corn emergence normally occurs in a period less than eight days under normal conditions of air temperature (20 to 30 °C) (Schneider and Gupta, 1985), and with 13 DAS, only two leaves are fully emerged normally (Hanway, 1966). With 29 DAS, corn plants have six leaves fully emerged (Hanway, 1966), which provides good soil cover, from 40 to 50%, taking into account the fPV (Figure 6). This soil cover can be seen reflected in a considerable increase of VI value compared to the 13 DAS.

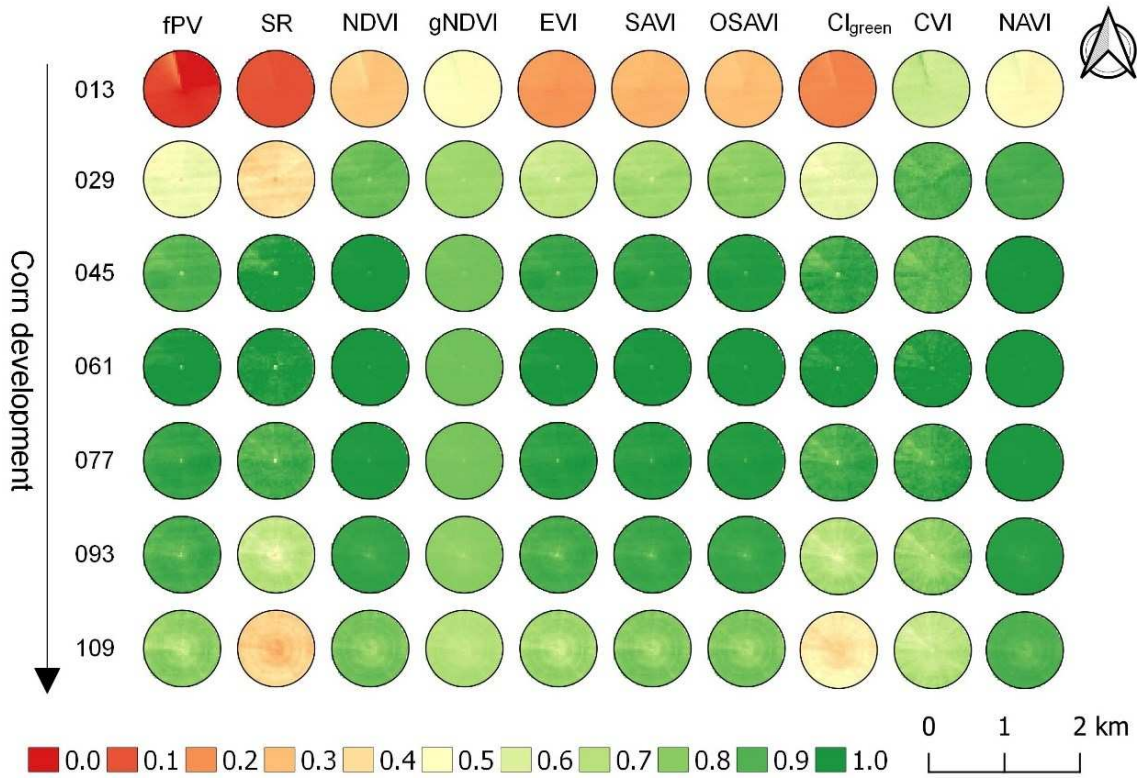

Figure 6. Spatial and temporal distribution of vegetation indices (VI) as a function of the days after sowing (DAS).

With 61 DAS, the maximum values were observed for the majority of the VI, as a reflex of the maximum leaf area index (LAI), also observed around this period (Bergamaschi et al., 2006; Kross et al., 2015; Lizaso et al., 2005; Lukeba et al., 2013; Soleymani, 2018; Soufizadeh et al., 2018; Wolschick et al., 2003). Despite high values in this period, the differences between 45 and 77 DAS are very subtle (Figure 6), due to the establishment of the plant stand, covering all soil, and few physical changes of the canopy. Thus, the occurrence of problems in the fields in this period, (e.g., pest attack), can be more easily detected than in other parts of the cycle.

From 77 DAS, VI values begin to decrease, which will continue until harvest time, when the values are similar to those of the beginning of the cycle, but slightly higher. These decreases are a consequence of the beginning of the reproductive phase, which normally starts at ±77 DAS (Hanway, 1966). From this period, since the plant reached maximum height, photoassimilates will be used

exclusively for pollination, fertilization, and dry matter accumulation in the grains, as shown by Bender et al. (2013). As a consequence, the plant loses vegetative vigor, reflecting in the VI values. Due to the sensitivity to corn crop changes, the VI are widely used for a limited number of studies involving this crop, such as in the determination of dry biomass (Campos et al., 2018; Kross et al., 2015), leaf area index (Kross et al., 2015), and plant nitrogen content (Maresma et al., 2016).

No abnormality was verified in the field (Figure 6), for example, variability in rings, which may indicate clogged nozzles or other water delivery problems. Although many events may influence corn life cycle, the spatial distribution of the VI demonstrate average field conditions within the fields.

In order to identify more easily the difference between fPV and VI, was created the Figure 7, which shows the temporal pattern of fPV and VI over the corn season, after their normalization for 0 to 1 interval. Both VI and fPV rapidly increased from 13 to 61 DAS, except for SR, NDVI NAVI, which reached the peak earlier, at 45 DAS (Figure 7). Regarding the early season, it is possible to verify that CVI, gNDVI and NAVI, mainly, do not have a good agreement with fPV, showing an overestimate. On the other hand, under or overestimates are not the main problem, the limitation occurs when the VI does not have a pattern of temporal variation similar to fPV, as verified for the CVI (Figure 7). This VI started the cycle with overestimates, stabilized during a period in which fPV increased (29 to 45 DAS) and, in the late season, underestimated fPV (Figure 7).

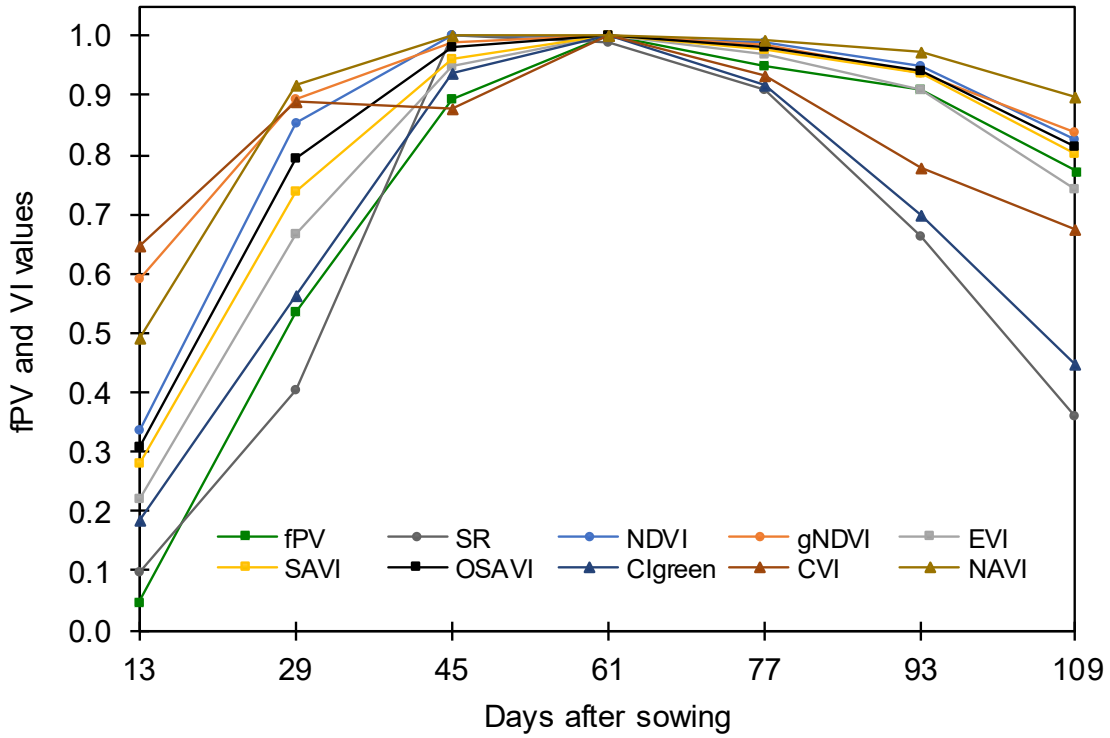

Figure 7. Temporal pattern of VI and fPV as a function of the days after sowing, after their normalization for 0 to 1 interval.

By analyzing the final portion of the season (i.e., from 77 DAS), it is possible to clearly observe a poor agreement for SR and CI_{green} with the fPV. On the other hand, EVI, SAVI, OSAVI and NDVI exhibited a more similar behavior to that of fPV, especially EVI, with great proximity between the temporal curves over the entire season (Figure 7).

3.3. Vegetation indices performance

A good to great Pearson correlation coefficient (r) is observed between the fPV and VI, with the highest values observed for EVI and SAVI (0.99), followed by OSAVI (0.98), NDVI (0.96), NAVI (0.95) and gNDVI (0.94) (Figure 8) On the other hand, low r value was verified for CVI (0.64), which was also was not significant. Lastly, SR and CI_{green} showed reasonable r values, 0.86 and 0.88, respectively (Figure 8). Guo et al. (2007) compared NDVI and EVI with the levels of vegetation cover and verified that the correlation of EVI was better than that of

NDVI especially at the higher levels of vegetation cover. Shafian et al. (2018) working with sorghum, verified that among NDVI, EVI, gNDVI, and MTVI2, the first mentioned showed the highest correlation with fraction of photosynthetically active vegetation. However, it is important to point out that the difference between crops (i.e., corn and sorghum) can lead to these results.

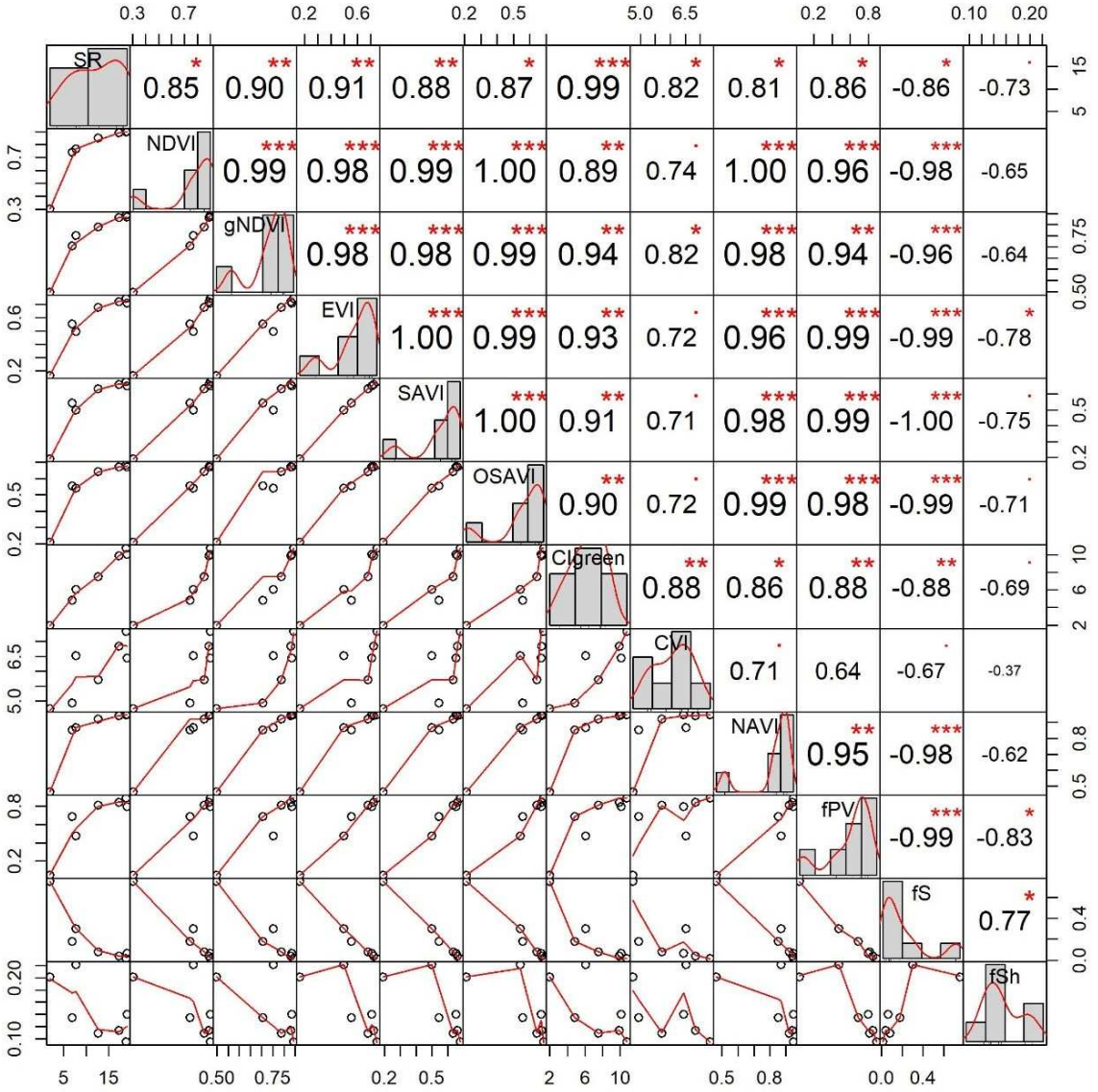

Figure 8. Correlation matrix between vegetation indices (SR, NDVI, gNDVI, EVI, SAVI, OSAVI, CI_{green}, CVI and NAVI) and photosynthetic vegetation, soil and shade sub-pixel fractions. * indicates significance of regression at p-value < 0.05, ** indicates significance of regression at p-value < 0.01 and *** indicates significance of regression at p-value < 0.001.

The high linear correlation between fPV and some VI verified for the majority of VI occurs due to the fact that both fPV and VI highlight the amount of green vegetation in the pixels (Shimabukuro et al., 1998), and a greater or lesser correlation is linked to some factors, such as sensitivity of the VI to the biophysical parameters analyzed and also to the noise caused by canopy background and atmospheric effects.

In respect to noise problems, for instance, EVI, if compared to NDVI, has reduced air and soil influence in the spectral canopy response (Huete et al., 2002). The same occurs with SAVI, since it was created to overcome the NDVI limitations related to soil background brightness (Huete, 1988). Thus, the higher r values for SAVI and EVI, compared to NDVI, may be reflex of these advantages cited above. However, it is important to point out that, despite these positive points for SAVI and EVI, the NDVI is the most widely used vegetation indices for retrieval of vegetation canopy biophysical properties (Adole et al., 2016; Jiang et al., 2006; Matsushita et al., 2007).

All VI correlated negatively with the fraction of shade (fSh), according to Figure 8, and EVI had the highest negative value of Pearson correlation coefficient, with r equal to -0.78, and CVI had the lowest value (r = -0.37); however, the last was not significant. According to the premise of Zhang and Huang (2015), that shadows can lead to either a reduction or total loss of information in an image and then, can potentially lead to corruption of biophysical parameters derived from pixel values, such as vegetation indices, the best indices, in general terms, are those which have no correlation (close to 0) or higher negative correlation (close to -1) with fSh. However, to verify the real shadow effects on VI, a more complex study is necessary, for instance, comparing the shaded and sunlit leaves, as can be seen in the work of Zhou et al. (2017) with rice. These authors investigated the spectral properties of sunlit and shaded components in rice canopies with near-ground imaging spectroscopy data.

Table 4 shows Root Mean Square Error (RMSE) and Willmott's index of agreement (d) values, resulting from the comparison between VI and fPV. Considering the quantitative accuracy assessment based on RMSE, it is possible to observe that EVI shows the best agreement with fPV, with average RMSE

values of 6.5%. With RMSE of 9.8%, SAVI was the second best VI with respect to this statistical parameter, closely followed by CI_{green} and OSAVI, with 11.5 and 11.8, respectively. NDVI had an intermediate RMSE (13%), showing the fifth highest value (Table 4). The highest RMSE values were observed for RS (23.6%) and CVI (21.1%).

Table 4. Root Mean Square Error (RMSE) and Willmott's index of agreement (d) with average value (μ) referring to the comparison of the vegetation indices with fraction of photosynthetically active vegetation (fPV) as a function of the days after sowing, after their normalization for 0 to 1 interval

DAS	SR	NDVI	gNDVI	EVI	SAVI	OSAVI	CI_{green}	CVI	NAVI
Root Mean Square Error – RMSE (%)									
13	4.7	28.1	53.7	17.1	23.2	25.7	12.9	50.7	43.6
29	21.1	31.8	36.9	13.4	20.8	26.6	1.7	24.8	39.1
45	10.7	11.8	12.3	6.8	8.4	10.8	2.8	11.0	13.0
61	21.6	2.4	3.5	1.7	2.3	2.8	2.8	11.0	3.3
77	22.9	5.4	6.6	3.1	4.4	5.6	5.6	12.0	7.1
93	37.4	5.2	5.5	1.5	4.4	5.4	22.2	21.1	8.7
109	47.1	6.6	8.9	2.0	4.8	6.2	32.2	16.9	14.8
μ	23.6	13.0	18.2	6.5	9.8	11.9	11.5	21.1	18.5
Willmott's index of agreement – d									
13	0.984	0.594	0.250	0.808	0.685	0.637	0.884	0.278	0.352
29	0.801	0.521	0.433	0.879	0.739	0.621	0.998	0.654	0.400
45	0.934	0.902	0.893	0.966	0.949	0.917	0.995	0.929	0.881
61	0.785	0.996	0.991	0.998	0.996	0.994	0.994	0.930	0.992
77	0.771	0.978	0.968	0.993	0.985	0.977	0.979	0.917	0.963
93	0.588	0.980	0.977	0.998	0.986	0.978	0.780	0.795	0.944
109	0.502	0.968	0.941	0.997	0.983	0.971	0.654	0.854	0.849
μ	0.766	0.848	0.779	0.948	0.903	0.871	0.898	0.765	0.769

RS and CI_{green} showed higher RMSE values in the late season, differently from the other VI (Table 4). Near-infrared reflectance (750-1350 nm) is determined by the inner structural features of leaves, the structural organization of the spongy mesophyll, and the ratio of cells to air spaces within this tissue (Gates et al., 1965; Knipling, 1970; Pinto et al., 2017). Reflectance in the visible region (400-700 nm), however, is determined mostly by photosynthetic pigments (Gates et al., 1965). Therefore, with leaf senescence, there is a disorganization

in the structural features, reducing reflectance in the near-infrared region, and an increase in the red region, due to the decrease of absorption by the photosynthetic pigments (Gates et al., 1965; Knipling, 1970), leading to an abrupt reduction in SR value (see Eq. 5) in the late season. For normalized vegetation indices, these decreases tend to be subtler.

Regarding CI_{green}, the analysis is similar, but with the difference that it uses the green instead of red band for division. Thus, with plant senescence, the reflectance in the green wavelength, which is relatively high when the plant has a high vigor, decreases. This decrease in a first moment may lead to an increase in CI_{green} value; however, the near infrared reflectance decreases in a much greater proportion, which culminates with quick VI diminution.

Among the seven VI with highest RMSE during the early season (Table 4), gNDVI, CVI and NAVI were those which obtained the highest RMSE values. Differently, SR, EVI and CI_{green} had the lowest values. NDVI, SAVI and OSAVI showed intermediate average RMSE values (Table 4). Comparing the most traditional VI, that is, NDVI, SAVI and EVI, the first-named had higher RMSE values for all seven images.

An important detail involving the NDVI is that, with 61 DAS, RMSE values for SAVI and NDVI were very close, 2.3 and 2.4, respectively. However, with 77 days after sowing, when corn reaches maximum height (Lizaso et al., 2005; Lukeba et al., 2013), and consequently a dense biomass, the distance between them increased, with 4.4 and 5.4 for SAVI and NDVI, respectively. These values suggest a saturation of NDVI at high biomass values and as a consequence, they become distant from the fPV. Previous studies have demonstrated problems with NDVI saturation in corn plantations (Chen et al., 2006; Hatfield and Prueger, 2010; K. Wang et al., 2013; Wang et al., 2016). Summarizing the RMSE analysis, considering the average values, EVI followed by SAVI, CIgreen and OSVAI, are the best VI.

The results of Willmott's index of agreement (d) are presented in Table 4. CVI had the worst result (d = 0.765), which in turn was very close to those of SR, NAVI and gNDVI (Table 4). NDVI and OSAVI had intermediate values considering all nine indices, with 0.848 and 0.871, respectively. Lastly, the best results were observed for EVI (d = 0.948), SAVI (d = 0.903) and CI_{green} (d =

0.903). The difference between these three VI was the equilibrium in the "d" values over the season, which have always remained high, differently from the others, which had a greater amplitude. For instance, for the EVI, the lowest “d” value was 0.808 at 13 DAS, with the majority of the values above 0.94. (Table 4). Considering all VI examined, the best RMSE values are verified from 45 to 93 DAS, when the soil cover by plants is very intense.

The three best VI were ranked to be used in corn dry biomass estimation considering their relationship with fraction of photosynthetically active vegetation (fPV). EVI and SAVI, respectively, had the best results for the statistical parameters analyzed (i.e., Pearson Correlation Coefficient, Root Mean Square Error and Willmott’s index of agreement), besides the good agreement of the visual analysis. CI_{green} showed slightly higher results for RMSE and Willmott’s index of agreement in comparison to OSAVI, but the last had a much higher Pearson Correlation Coefficient (0.98 versus 0.88). Furthermore, according to Figure 7, OSAVI showed a more similar behavior to that of fPV than CI_{green}, during the entire corn season. Thus, OSAVI was considered as the third best VI.

The final rank containing the three best VI from Bio estimation taking into account the close relationship between Bio-APAR and APAR-VI, from best to worst was: EVI, SAVI and OSAVI. Still, it is important to highlight that this work does not replace works that aim to directly find the best vegetation indices for assessing vegetation biophysical parameters. The results presented here need to be seen as a complementary information, which will help choosing the vegetation indices with highest potential for the purpose, in the present case, for biomass estimation.

3.4. Corn grain yield estimation based on cumulative VI

To conduct this second study, EVI, SAVI and OSAVI were selected, since these indices showed the best performance in the first goal. Table 5 shows the mean values for EVI, SAVI, and OSAVI relative to the sowing and harvest dates in the study area 2 (Figure 1c) during the season of 2018. For EVI and SAVI, the values of SD remained around 0.09, while for OSAVI they remained around

0.1135. For HD, VI values were higher than those for SD, with a greater difference between SAVI and EVI regarding the sowing date.

Table 5. Mean values with standard deviation for EVI, SAVI, and OSAVI for sowing date (SD) and harvest date (HD) in the study area 2 in the season of 2018

Vegetation indices	SD	HD
EVI	0.0926 ± 0.0048	0.1394 ± 0.0101
SAVI	0.0992 ± 0.0075	0.1588 ± 0.0106
OSAVI	0.1135 ± 0.0085	0.1819 ± 0.0126

Figure 9 shows the relationship between EVI accumulated and grain yield measured. Among the six intervals of accumulation, the intervals which extend until 120 DAS had the best results, with highest r^2 value verified in the interval of 7-120 DAS (Figure 9d), followed by 14-120 (Figure 9f). On the other hand, when the interval was limited between 0 and 77 DAS (Figure 9a), r^2 reached the lowest value (0.756), which was very close to that of 7-77, $r^2 = 0.757$ (Figure 9c).

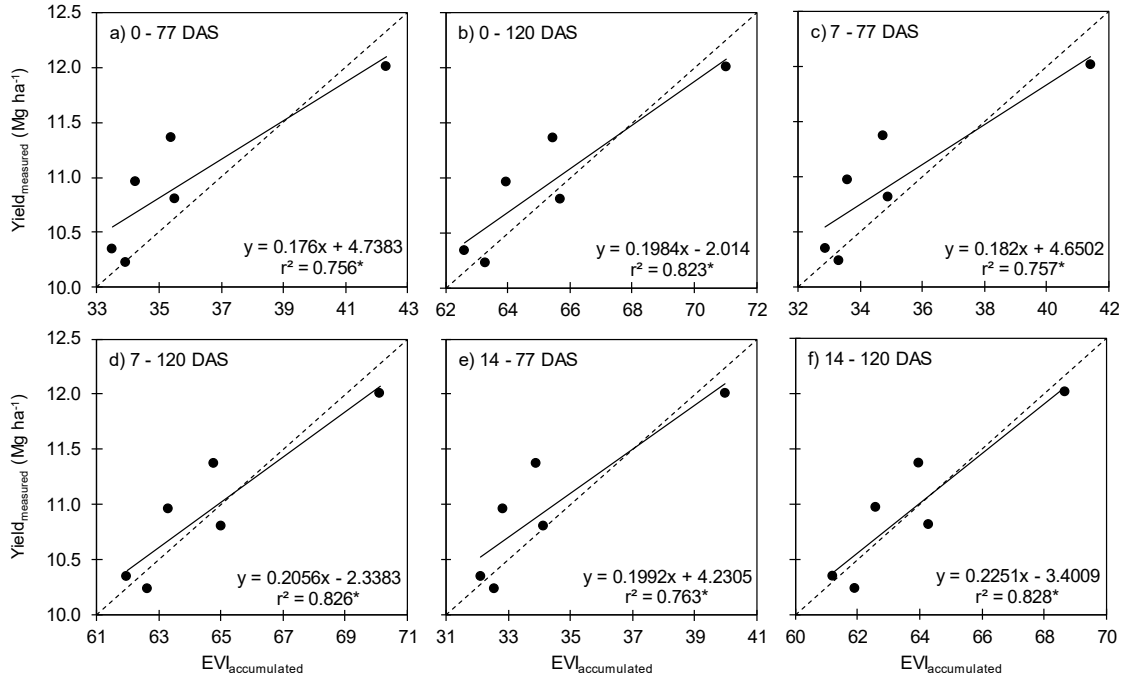

Figure 9. Relationships between EVI accumulated and corn grain yield. * indicates significance at p-value < 0.05. The dotted lines represent the 1:1 line and the solid black lines represent the linear regressions.

The relationships between SAVI accumulated in different intervals over the season and grain yield measured are presented in Figure 10. The results are similar to those verified for EVI, with highest r² value occurring in the interval of 14-120 DAS (Figure 10f). This interval had a slightly higher r² compared to the 7-120 interval (Figure 10d). Only 77 days of accumulation (0-77 DAS) lead to the worst results of estimation, with a r² equal to 0.756 (Figure 10a).

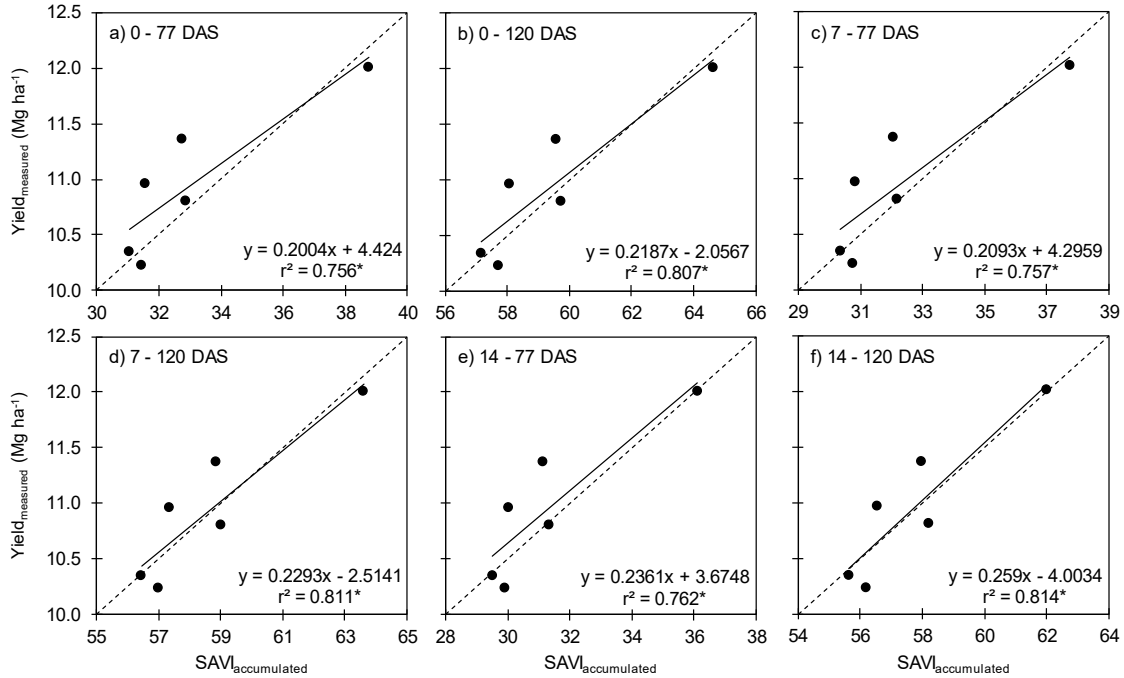

Figure 10. Relationships between SAVI accumulated and corn grain yield. * indicates significance at p-value < 0.05. The dotted lines represent the 1:1 line and the solid black lines represent the linear regressions.

Figure 11 shows the relationship between six different intervals of OSAVI and grain yield measured. As observed for EVI and SAVI, when accumulated between 14 until 120 DAS, OSAVI showed the best performance for yield estimation, with a r² of 0.79 (Figure 11f). However, the difference from the 7-120 DAS interval is very small. The worst interval again was 0-77 DAS (Figure 10a), which was also found previously with EVI and SAVI.

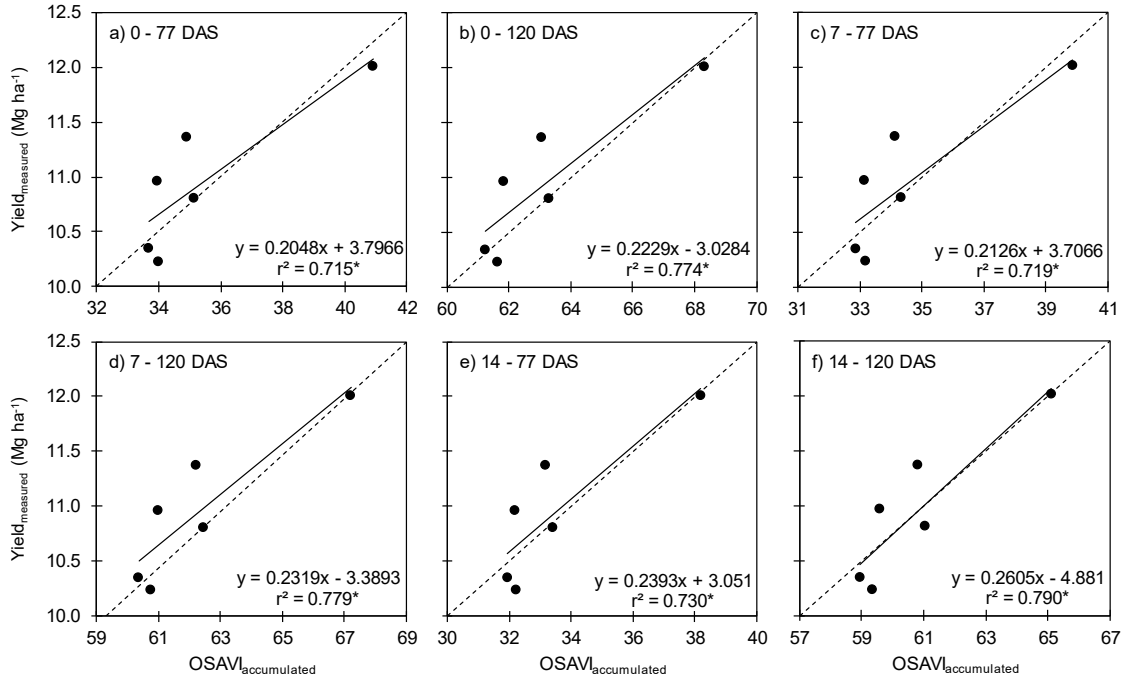

Figure 11. Relationships between OSAVI accumulated and corn grain yield. * indicates significance at p-value < 0.05. The dotted lines represent the 1:1 line and the solid black lines represent the linear regressions.

For the three vegetation indices (EVI, SAVI and OSAVI) examined, the interval of 14-120 DAS was the best for grain yield estimation, showing the highest r² values. However, the differences from the 7-120 DAS interval were very subtle, especially for EVI and SAVI. These results can be explained based on the physiological behavior of corn plants. With 14 DAS, corn plants normally have two leaves fully emerged (Hanway, 1966) and then, they are able to start the photosynthetic process (Fancelli and Dourado Neto, 2000). Thus, defining the start of VI accumulation at 14 days after sowing prevents biomass accumulation before the start of the photosynthetic process (i.e., starting with 0 DAS) and, consequently an overestimate of yield. The study of Gava et al. (2010) showed that dry biomass accumulation in corn plants has a sigmoidal pattern and begins around 10 days after emergence.

Regarding 120 DAS, when corn plants reach this point, they are very close to physiological maturity and the grain requires no more moisture or nutrient input from the plant (Angel et al., 2017). Thus, extending the accumulation further is

not justified. An accumulation until 77 DAS is important because it would have very early results of yield, facilitating the planning of harvest, storage, etc. Besides that, although the r^2 is higher for intervals with 120 DAS, there is a great risk of not being able to get cloudless images in this period, and the risk is lower in 14-77 DAS, with a small loss of r^2. On the other hand, with only 77 DAS, all the reproductive phases are left out, considering that the vegetative stages are normally finished at this time (Hanway, 1966). Thus, many factors that may occur in these stages and affect grain production would not be considered, such as water stress, pest and diseases, lack of nutrients, for example.

Lastly, this last study, despite being very interesting, needs to be more robust by using larger data sets. With the use of these small data pairs, outliers become much more dangerous, for example, they can get proportionally large and significantly alter the model.

4. CONCLUSIONS AND REMARKS

Nine vegetation indices (SR, NDVI, gNDVI, EVI, SAVI, OSAVI, CIgreen, CVI and NAVI), calculated for a commercial corn field irrigated by center pivot were evaluated by means of their relationship with fraction of photosynthetically active vegetation estimated from the spectral mixture analysis (SMA). Additional information to infer on vegetation indices performance is very useful, because many times, these remote sensing variables are used without a previous knowledge about their efficiency on aboveground dry biomass or yield estimation, being chosen based on their popularity, for instance.

Among the nine VI analyzed, EVI was considered the best one for corn aboveground dry biomass estimation, based on its comparison with fraction of photosynthetically active vegetation resulting in Pearson correlation coefficient, RMSE and Willmott's index of agreement equal to 0.99, 6.5%, and 0.948, respectively. The final ranking of the three indices, from to worst was: EVI, SAVI and OSAVI.

Corn yield estimation from VI accumulated is a very interesting application of remote sensing data, because it involves practicality (i.e., for VI obtaining) and

efficiency (i.e., VI in well-represented grain yield). Six intervals of accumulation were tested over the season using the three best ranked vegetation indices in the primary objective. The intervals that extended up to 120 days after sowing were the best. Additionally, it is important to point out that the number of samples used was low (n = 6) and for more robustness of results it is important to use higher “n” and an independent validation. This can be done more easily in future studies, from these findings.

5. REFERENCES

Adams, J., Sabol, D.E., Kapos, V., Almeida Filho, R., Roberts, D.A., Smith, M.O., Gillespie, A.R., 1995. Classification of multispectral images based on fractions of endmembers: Application to land-cover change in the Brazilian Amazon. Remote Sensing Environment 52, 137–154.

Adams, J.B., Smith, M.O., Johnson, P.E., 1986. Spectral mixture modeling: A new analysis of rock and soil types at the Viking Lander 1 Site. Journal of Geophysical Research 91, 8098–8112.

Adole, T., Dash, J., Atkinson, P.M., 2016. A systematic review of vegetation phenology in Africa. Ecological Informatics 34, 117–128.

Alvares, C.A., Stape, J.L., Sentelhas, P.C., Gonçalves, J.L. De M., Sparovek, G., 2013. Köppen's climate classification map for Brazil. Meteorologische Zeitschrift 22, 711–728.

Angel, J.R., Widhalm, M., Todey, D., Massey, R., Biehl, L., 2017. The U2U Corn Growing Degree Day tool: Tracking corn growth across the US Corn Belt. Climate Risk Management 15, 73–81.

Baig, M.H.A., Zhang, L., Shuai, T., Tong, Q., 2014. Derivation of a tasselled cap transformation based on Landsat 8 at-satellite reflectance. Remote Sensing Letters 5, 423–431.

Bajjouk, T., Populus, J., Guillaumont, B., 1998. Quantification of subpixel cover fractions using principal component analysis and a linear programming method: Application to the coastal zone of Roscoff (France). Remote Sensing of Environment 64, 153–165.

Barsi, J.A., Alhammoud, B., Czapla-Myers, J., Gascon, F., Haque, M.O., Kaewmanee, M., Leigh, L., Markham, B.L., 2018. Sentinel-2A MSI and Landsat-8 OLI radiometric cross comparison over desert sites. European Journal of Remote Sensing 51, 822–837.

Bender, R.R., Haegele, J.W., Ruffo, M.L., Below, F.E., 2013. Nutrient uptake, partitioning, and remobilization in modern, transgenic insect-protected maize hybrids. Agronomy Journal 105, 161–170.

Bergamaschi, H., Dalmago, G.A., Comiran, F., Bergonci, J.I., Müller, A.G., França, S., Santos, A.O., Radin, B., Menegassi Bianchi, C.A., Pereira, P.G., 2006. Deficit hídrico e produtividade na cultura do milho. Pesquisa Agropecuaria Brasileira 41, 243–249.

Bertolin, N. de O., Filgueiras, R., Venancio, L.P., Mantovani, E.C., 2017. Predição da produtividade de milho irrigado com auxílio de imagens de satélite. Revista Brasileira de Agricultura Irrigada 11, 1627–1638.

Kalaitzidis, C., Heinzel, V., Zianis, D., 2010. A Review of multispectral vegetation indices for biomass estimation, in: Manakos, I., Kalaitzidis, C. (Eds.), 29th Symposium of the European Association of Remote Sensing Laboratories. IOS Press, Chania, Greece, pp. 201–207.

Campos, I., Neale, C.M.U., Arkebauer, T.J., Suyker, A.E., Gonçalves, I.Z., 2018. Water productivity and crop yield: A simplified remote sensing driven operational approach. Agricultural and Forest Meteorology 249, 501–511.

Campos, I., Neale, C.M.U., Suyker, A.E., Arkebauer, T.J., Gonçalves, I.Z., 2017. Reflectance-based crop coefficients REDUX: For operational evapotranspiration estimates in the age of high producing hybrid varieties. Agricultural Water Management 187, 140–153.

Carmona, F., Rivas, R., Fonnegra, D.C., 2015. Vegetation index to estimate chlorophyll content from multispectral remote sensing data. European Journal of Remote Sensing 48, 319–326.

Caviglia, O.P., Melchiori, R.J.M., Sadras, V.O., 2014. Nitrogen utilization efficiency in maize as affected by hybrid and N rate in late-sown crops. Field Crops Research 168, 27–37.

Chavez, P.S., 1996. Image-Based Atmospheric Corrections - Revisited and Improved. Photogrammetric Engineering and Remote Sensing 62, 1025–1036.

Chavez, P.S., 1988. An improved dark-object subtraction technique for atmospheric scattering correction of multispectral data. Remote Sensing of Environment 24, 459–479.

Chen, P., Fedosejevs, G., Tiscareño-Lopes, M., Arnold, J.G., 2006. Assessment of MODIS-EVI, MODIS-NDVI and vegetation-NDVI composite data using agricultural measurements: an example at corn fields in western Mexico. Environmental Monitoring and Assessment 119, 69–82.

Congedo, L., 2018. Semi-Automatic Classification Plugin Documentation: Release 6.2.0.1. https://media.readthedocs.org/pdf/semiautomaticclassificationmanual/latest/semiautomaticclassificationmanual.pdf. (accessed 8.29.18).

Daughtry, C.S.T., Gallo, K.P., Goward, S.N., Prince, S.D., Kustas, W.P., 1992. Spectral estimates of absorbed radiation and phytomass production in corn and soybean canopies. Remote Sensing of Environment 39, 141–152.

ESA - European Space Agency, 2015. SENTINEL-2: User Handbook. https://doi.org/GMES-S1OP-EOPG-TN-13-0001. (accessed 11.23.18).

Fancelli, A.L., Dourado Neto, D., 2000. Produção de milho. Agropecuária,

Guaíba, RS.
Fang, H., Liang, S., Hoogenboom, G., 2011. Integration of MODIS LAI and vegetation index products with the CSM-CERES-Maize model for corn yield estimation. International Journal of Remote Sensing 32, 1039–1065.

Gallo, K.P., Brooks, C.C., Daughtry, C.S.T., Bauer, M.E., Vanderbilt, V.C., 1982. Spectral estimates of intercepted solar radiation by corn and soybean canopies, in: Symposium on Machine Processing of Remotely Sensed Data. Laboratory for Applications of Remote Sensing, West Lafayette, Indiana, pp. 190–198.

Gates, D.M., Keegan, H.J., Schleter, J.C., Weidner, V.R., 1965. Spectral Properties of Plants. Applied Optics 4, 11.

Gava, G.J.D.C., De Oliveira, M.W., De Almeida Silva, M., Jerônimo, E.M., Cruz, J.C.S., Trivelin, P.C.O., 2010. Produção de fitomassa e acúmulo de nitrogênio em milho cultivado com diferentes doses de ^{15}N-uréia. Semina:Ciencias Agrarias 31, 851–862.

Gitelson, A.A., Kaufman, Y.J., Merzlyak, M.N., 1996. Use of a green channel in remote sensing of global vegetation from EOS- MODIS. Remote Sensing of Environment 58, 289–298.

Gitelson, A.A., Viña, A., Ciganda, V., Rundquist, D.C., Arkebauer, T.J., 2005. Remote estimation of canopy chlorophyll content in crops. Geophysical Research Letters 32, 1–4.

Goward, S.N., Huemmrich, K.E., 1992. Vegetation canopy PAR absorptance and the normalized difference vegetation index 140, 119–140.

Guo, N., Wang, X., Cai, D., Yang, J., 2007. Comparison and evaluation between MODIS vegetation indices in Northwest China. International Geoscience and Remote Sensing Symposium (IGARSS) 3366–3369.

Hanway, J.J., 1966. How a corn plant develops, Iowa State University of Science and Technology, Cooperative Extension Service. Ames, Iowa.

Hatfield, J.L., Prueger, J.H., 2010. Value of using different vegetative indices to quantify agricultural crop characteristics at different growth stages under varying management practices. Remote Sensing 2, 562–578.

Huemmrich, K.F., 1996. Effects of shadows on vegetation indices, in: IGARSS ’96. 1996 International Geoscience and Remote Sensing Symposium. IEEE, Lincoln, Nebraska, pp. 2372–2374.

Huete, A., Didan, K., Miura, T., Rodriguez, E.P., Gao, X., Ferreira, L.G., 2002. Overview of the radiometric and biophysical performance of the MODIS vegetation indices. Remote Sensing of Environment 83, 195–213.

Huete, A.R., 1988. A soil-adjusted vegetation index (SAVI). Remote Sensing of Environment 25, 295–309.

Hütsch, B.W., Schubert, S., 2018. Maize harvest index and water use efficiency can be improved by inhibition of gibberellin biosynthesis. Journal of Agronomy and Crop Science 204, 209–218.

Ji, L., Peters, A.J., 2007. Performance evaluation of spectral vegetation indices using a statistical sensitivity function. Remote Sensing of Environment 106, 59–65.

Jiang, Z., Huete, A.R., Chen, J., Chen, Y., Li, J., Yan, G., Zhang, X., 2006. Analysis of NDVI and scaled difference vegetation index retrievals of vegetation fraction. Remote Sensing of Environment 101, 366–378.

Jiménez-Muñoz, J.C., Sobrino, J.A., Plaza, A., Guanter, L., Moreno, J., Martínez, P., 2009. Comparison between fractional vegetation cover retrievals from vegetation indices and spectral mixture analysis: Case study of PROBA/CHRIS data over an agricultural area. Sensors 9, 768–793.

Jordan, C.F., 1969. Derivation of leaf-area index from quality of light on the forest floor. Ecology 50, 663–666.

Kao, H., Ren, H., Lee, C., 2014. Calibrated ratio approach for vegetation detection in shaded areas. Journal of Applied Remote Sensing 8, 083543.

Knipling, E.B., 1970. Physical and physiological basis for the reflectance of visible and near-infrared radiation from vegetation. Remote Sensing Environment 1, 155–159.

Djaman, K., Irmak, S., Rathje, W.R., Martin, D.L., Eisenhauer, D.E., 2013. Maize evapotranspiration, yield production functions, biomass, grain yield, harvest index, and yield response factors under full and limited irrigation. Transactions of the ASABE 56, 273–293.

Kross, A., McNairn, H., Lapen, D., Sunohara, M., Champagne, C., 2015. Assessment of RapidEye vegetation indices for estimation of leaf area index and biomass in corn and soybean crops. International Journal of Applied Earth Observation and Geoinformation 34, 235–248.

Li, Z., Guo, X., 2015. Remote sensing of terrestrial non-photosynthetic vegetation using hyperspectral, multispectral, SAR, and LiDAR data. Progress in Physical Geography 40, 276–304.

Liu, J., Miller, J.R., Pattey, E., Haboudane, D., Strachan, I.B., Hinther, M., 2004. Monitoring crop biomass accumulation using multi-temporal hyperspectral remote sensing data, in: IGARSS 2004. 2004 IEEE International Geoscience and Remote Sensing Symposium. IEEE, Anchorage, Alaska, pp. 1637–1640.

Liu, J., Pattey, E., Miller, J.R., McNairn, H., Smith, A., Hu, B., 2010. Estimating crop stresses, aboveground dry biomass and yield of corn using multi-temporal optical data combined with a radiation use efficiency model. Remote Sensing of Environment 114, 1167–1177.

Lizaso, J.I., Batchelor, W.D., Boote, K.J., Westgate, M.E., 2005. Development of a leaf-level canopy assimilation model for CERES-Maize. Agronomy Journal 97, 722–733.

Lukeba, J.L., Vumilia, R.K., Nkongolo, K.C.K., Mwabila, M.L., Tsumbu, M., 2013. Growth and leaf area index simulation in maize (*Zea mays* L.) under small-scale farm conditions in a Sub-Saharan African region. American Journal of Plant Sciences 04, 575–583.

Maresma, Á., Ariza, M., Martínez, E., Lloveras, J., Martínez-Casasnovas, J.A., 2016. Analysis of vegetation indices to determine nitrogen application and yield prediction in maize (*Zea mays* L.) from a standard UAV service. Remote Sensing 8, 973-988.

Matsushita, B., Yang, W., Chen, J., Onda, Y., Qiu, G., 2007. Sensitivity of the Enhanced Vegetation Index (EVI) and Normalized Difference Vegetation Index (NDVI) to Topographic Effects: A case study in high-density cypress forest. Sensors 7, 2636–2651.

Monteith, J.L., 1972. Solar radiation and productivity in tropical ecosystems. Journal of Applied Ecology 9, 947–966.

Myneni, R.B., Williams, D.L., 1994. On the relationship between FAPAR and NDVI. Remote Sensing of Environment 49, 200–211.

Navarro, G., Caballero, I., Silva, G., Parra, P.-C., Vázquez, Á., Caldeira, R., 2017. Evaluation of forest fire on Madeira Island using Sentinel-2A MSI imagery. International Journal of Applied Earth Observation and Geoinformation 58, 97–106.

Peña, M.A., Brenning, A., 2015. Assessing fruit-tree crop classification from Landsat-8 time series for the Maipo Valley, Chile. Remote Sensing of Environment 171, 234–244.

Pinto, D.G., Fontana, D.C., Dalmago, G.A., Cunha, G.R. da, Fochesato, E., Vicari, M.B., Gouvêa, J.A. de, Santi, A., 2017. Temporal dynamics of spectral reflectance and vegetation indices during canola crop cycle in southern Brazil. Ciência Rural 47, 1–8.

Plaza, A., Martínez, P., Pérez, R., Plaza, J., 2004. A quantitative and comparative analysis of endmember extraction algorithms from hyperspectral data. IEEE Transactions on Geoscience and Remote Sensing 42, 650–663.

Qin, H., Wang, C., Zhao, K., Xi, X., 2018. Estimation of the fraction of absorbed photosynthetically active radiation (fPAR) in maize canopies using LiDAR data and hyperspectral imagery. PLoS ONE 13, 1–20.

Keshava, N., Mustard, J.F., 2002. Spectral unmixing. IEEE Signal Processing Magazine 19, 44–57.

Roberts, D., Halligan, K., Dennison, P., 2007. VIPER Tools User Manual Version 1.5, University of Califórnia. San Francisco, California.

Roberts, D.A., Gardner, M., Church, R., Ustin, S., Scheer, G., Green, R.O., 1998. Mapping chaparral in the Santa Monica Mountains using multiple endmember spectral mixture models. Remote Sensing of Environment 65, 267–279.

Rondeaux, G., Steven, M., Baret, F., 1996. Optimization of soil-adjusted vegetation indices. Remote Sensing of Environment 55, 95–107.

Rouse, J.W., Hass, R.H., Schell, J.A., Deering, D.W., 1973. Monitoring vegetation systems in the great plains with ERTS, in: Third ERTS Symposium. NASA, Washington, DC, pp. 309-317.

Roy, D.P., Wulder, M.A., Loveland, T.R., C.E., W., Allen, R.G., Anderson, M.C., Helder, D., Irons, J.R., Johnson, D.M., Kennedy, R., Scambos, T.A., Schaaf, C.B., Schott, J.R., Sheng, Y., Vermote, E.F., Belward, A.S., Bindschadler, R., Cohen, W.B., Gao, F., Hipple, J.D., Hostert, P., Huntington, J., Justice, C.O., Kilic, A., Kovalskyy, V., Lee, Z.P., Lymburner, L., Masek, J.G., McCorkel, J., Shuai, Y., Trezza, R., Vogelmann, J., Wynne, R.H., Zhu, Z., 2014. Landsat-8: Science and product vision for terrestrial global change research. Remote Sensing of Environment 145, 154–172.

Rundquist, B.C., 2002. The influence of canopy green vegetation fraction on spectral measurements over native tallgrass prairie. Remote Sensing of Environment 81, 129–135.

Santos, H.G. dos, Carvalho-Júnior, W. de, Dart, R. de O., Áglio, M.L.D., Sousa, J.S. de., Pares, J.G., Fontana, A., Martins, A.L. da S., Oliveira, A.P. de O., 2011. O novo mapa de solos do Brasil: Legenda atualizada, Embrapa. Rio de Janeiro.

Schneider, S.C., Gupta, E.C.., 1985. Corn emergence as influenced by soil temperature, matric potential, and aggregate size distribution. Society of America Journal 49, 415–422.

Shafian, S., Rajan, N., Schnell, R., Bagavathiannan, M., Valasek, J., Shi, Y., Olsenholler, J., 2018. Unmanned aerial systems-based remote sensing for monitoring sorghum growth and development. PLoS ONE 13, 1-15.

Shimabukuro, Y., Ponzoni, F., 2017. Mistura espctral: modelo linear e aplicações.

Oficina de Textos, São Paulo.

Shimabukuro, Y.E., Novo, E.M., Ponzoni, F.J., 1998. Índice de vegetação e modelo linear de mistura espectral no monitoramento da região do Pantanal. Pesquisa Agropecuaria Brasileira 33, 1729–1737.

Shimabukuro, Y.E., Smith, J.A., 1991. The least-squares mixing models to generate fraction images derived from remote sensing multispectral data. IEEE Transactions on Geoscience and Remote Sensing 29, 16–20.

hrivastava, D., Kumar, V., Sharma, R.U., 2016. Automated endmember extraction for subpixel classification of multispectral and hyperspectral data, in: Larar, A.M., Chauhan, P., Suzuki, M., Wang, J. (Eds.), Proc. SPIE 9880, Multispectral, Hyperspectral, and Ultraspectral Remote Sensing Technology, Techniques and Applications VI. New Delhi, India, p. 988012.

Soleymani, A., 2018. Corn (*Zea mays* L.) yield and yield components as affected by light properties in response to plant parameters and N fertilization. Biocatalysis and Agricultural Biotechnology 15, 173–180.

Somers, B., Asner, G.P., Tits, L., Coppin, P., 2011. Endmember variability in Spectral Mixture Analysis: A review. Remote Sensing of Environment 115, 1603–1616.

Soufizadeh, S., Munaro, E., McLean, G., Massignam, A., van Oosterom, E.J., Chapman, S.C., Messina, C., Cooper, M., Hammer, G.L., 2018. Modelling the nitrogen dynamics of maize crops - Enhancing the APSIM maize model. European Journal of Agronomy 100, 118–131.

Sultana, S.R., Ali, A., Ahmad, A., Mubeen, M., Zia-Ul-Haq, M., Ahmad, S., Ercisli, S., Jaafar, H.Z.E., 2014. Normalized difference vegetation index as a tool for wheat yield estimation: A case study from Faisalabad, Pakistan. The Scientific World Journal 2014, 1–8.

Sun, G., Chen, X., Ren, J., Zhang, A., Jia, X., 2017. Stratified spectral mixture analysis of medium resolution imagery for impervious surface mapping. International Journal of Applied Earth Observation and Geoinformation 60, 38–48.

Tagarakis, A.C., Ketterings, Q.M., 2017. In-season estimation of corn yield potential using proximal sensing. Agronomy Journal 109, 1323–1330.

Tan, C., Samanta, A., Jin, X., Tong, L., Ma, C., Guo, W., Knyazikhin, Y., Myneni, R.B., 2013. Using hyperspectral vegetation indices to estimate the fraction of photosynthetically active radiation absorbed by corn canopies. International Journal of Remote Sensing 34, 8789–8802.

USGS - United States Geological Survey, 2016. Landsat 8 (L8): Data Users Handbook, USGS.

https://landsat.usgs.gov/sites/default/files/documents/Landsat8DataUsersHandbook.pdf (accessed 10.17.18).

Vincini, M., Frazzi, E., D'Alessio, P., 2008. A broad-band leaf chlorophyll vegetation index at the canopy scale. Precision Agriculture 9, 303–319.

Wang, K., Liu, C., Zheng, X., Pihlatie, M., Li, B., Haapanala, S., Vesala, T., Liu, H., Wang, Y., Liu, G., Hu, F., 2013. Comparison between eddy covariance and automatic chamber techniques for measuring net ecosystem exchange of carbon dioxide in cotton and wheat fields. Biogeosciences 10, 6865–6877.

Wang, R., Cherkauer, K., Bowling, L., 2016. Corn response to climate stress detected with satellite-based NDVI time series. Remote Sensing 8, 1–22.

Willmott, C.J., 1982. Some comments on the evaluation of model performance. Meteorological Society 63, 1309–1313.

Wolschick, D., Carlesso, R., Petry, M.T., Jadoski, S.O., 2003. Adubação nitrogenada na cultura do milho no sistema plantio direto em ano com precipitação pluvial normal e com "El Niño." Revista Brasileira de Ciência do Solo 27, 461–468.

Xiao, J., Moody, A., 2005. A comparison of methods for estimating fractional green vegetation cover within a desert-to-upland transition zone in central New Mexico, USA. Remote Sensing of Environment 98, 237–250.

Yang, J., He, Y., Oguchi, T., 2014. An endmember optimization approach for linear spectral unmixing of fine-scale urban imagery. International Journal of Applied Earth Observation and Geoinformation 27, 137–146.

Yin, J., Huang, C., Luo, X., Du, Q., 2019. Automatic endmember bundle unmixing methodology for lunar regional area mineral mapping. Icarus 319, 349–362.

Zhang, T.W., Huang, C., 2015. An analysis of shadow effects on spectral vegetation indices using a ground-based imaging spectrometer, in: 7th Workshop on Hyperspectral Image and Signal Processing: Evolution in Remote Sensing (WHISPERS). IEEE, Tokyo, Japan, pp. 1–4.

Zhou, K., Deng, X., Yao, X., Tian, Y., Cao, W., Zhu, Y., Ustin, S.L., Cheng, T., 2017. Assessing the spectral properties of sunlit and shaded components in rice canopies with near-ground imaging spectroscopy data. Sensors 17, 1–17.

GENERAL CONCLUSIONS

This work shows the great potential of remote sensing (RS) data and approaches in agriculture, by means of evapotranspiration and yield estimation on irrigated corn fields in the western region of Bahia state, Brazil. RS data and approaches allow knowing physical phenomena (e.g., evapotranspiration) and biophysical parameters of vegetation (e.g., leaf area index, aboveground dry biomass, yield, among others) in a specialized way, with accuracy and low cost, especially in large-scale agriculture (e.g., farms with many central pivots). In the agriculture which aims at highly efficient use of water and inputs, saving of labor and continuous monitoring, it is essential to use RS.

This is the first scientific study that investigates the performance of SAFER algorithm for ET estimation over large areas of corn fully irrigated and suggests new coefficients for it, after calibration and validation. The investigation showed the low accuracy of SAFER for corn ET estimation if the original coefficients of the algorithm are used (a = 1.8 and b = -0.008). Thus, care must be taken in using SAFER to estimate the ET of corn or similar crops in large areas fully irrigated. On the other hand, after calibration and validation, new coefficients were recommended (a = 0.32 and b = -0.0013), and the SAFER showed a very good accuracy in corn ET estimation.

Yield estimation, even in large commercial farms which adopt a relatively high level of production technology, is still performed by means of field observation and empirical methods (e.g. estimating corn yields by the kernel count method), which in turn normally have low representativeness and low accuracy. RS may overcome these drawbacks. A new and simplified remote sensing approach tested for corn yield estimation at farm level in Brazil was very promising, and the difference between measured and estimated data remained between -5 and 5% for Pioneer hybrids and -10 and 10% for Status Viptera 3. On the other hand, future research should investigate the best harvest index value for each hybrid and losses during harvest, because these are data which generated uncertainties in the present study.

In the third chapter, the performance of nine VI for estimation of corn aboveground dry biomass was investigated, and among the analyzed VI, EVI,

SAVI and OSAVI were considered the first, second and third best for this purpose, respectively. The intervals that extended up to 120 days after sowing were the best.

Finally, this study presented some challenges as working with data of commercial farm and also with a great number of corn hybrids, but which were overcame. This work brings results interesting for scientific community, but also for the farmers of Brazil, which is constant due to improvements in production processes, mainly in the water use. This work was a great challenge, especially due to use of data of commercial farm and also with a great number of corn hybrids, on the other hand, it brings results interesting for scientific community, but also for the farmers of Brazil, which is constant due to improvements in production processes, mainly in the water use.